國立交通大學

材料科學與工程學系

博士論文

層狀二維材料製備-由電漿電化學製備石墨氧化物、石墨烯及由焠火製備奈米片狀二硫化鉬

Production of two-dimensional layered materials－graphite oxide and graphene by plasma electrochemistry and MoS_2 nanosheets by quenching method

姓　名：　鄧文成

指導教授：　韋光華

中華民國 一百零三年四月

國立交通大學

National Chiao Tung University

博士論文

Doctoral Dissertation

層狀二維材料製備-由電漿電化學製備石墨氧化物、石墨烯及由焠火製備奈米片狀二硫化鉬

Production of two-dimensional layeredmaterials－graphite oxide and grapheneby plasma electrochemistry and MoS_2 nanosheets by quenching method

系　　所：　Department of Materials Science and Engineering

學　　號：　9818843

姓　　名：　DANG VAN THANH

指導教授：　Prof. KUNG-HWA WEI

Hsinchu, April 17, 2014

層狀二維材料製備-由電漿電化學製備石墨氧化物、石墨烯及由焠火製備奈米片狀二硫化鉬

Production of two-dimensional layered materials－graphite oxide and graphene by plasma electrochemistry and MoS_2 nanosheets by quenching method

研究生：Dang Van Thanh　　Student: Dang Van Thanh

指導教授：**韋光華**　　Advisor: Prof. Kung-Hwa Wei

國立交通大學

材料科學與工程學系

博士論文

A thesis
Submitted to Department of Materials Science and Engineering
College of Engineering
National Chiao Tung University
in partial Fulfillment of Requirements
for the Degree of Doctor of Philosophy
in
Materials Science and Engineering

April 2014
Hsinchu, Taiwan, Republic of China

中華民國 一百零三年四月

Abbreviations

HOPG: highly ordered pyrolytic graphite

GE: recycled graphite

HG: high purity graphite

CP: cathodic plasma process

VPE: vapor plasma envelope

EG: expandable graphite

PEGO: plasma-expanded graphite oxide

PEEG: Plasma electrochemically exfoliated graphene

DI: deionized water

EPEGO: exfoliated PEGO

NMP: N-methyl-2-pyrrolidone

MB: Methylene Blue

GSs: Graphene sheets

MoS_2-DI: Exfoliation of solution of MoS_2 in DI water, without quenching.

MoS_2-DIQ: Exfoliation of solution of MoS_2 in DI water, with quenching.

MoS_2-KOH: Exfoliation of solution of MoS_2 in aqueous KOH, without quenching.

MoS_2-KOHQ: Exfoliation of solution of MoS_2 in aqueous KOH, with quenching.

Table of Contents

Abstract

The purpose of this work is to find out new approaches for one-pot synthesis of graphite oxide and graphene by plasma electrochemical exfoliation of graphite in a basic electrolyte solution in a short-reaction time with regards of environmental friendliness, energy/time saving, and low cost. First of all, we adopted a highly efficient cathodic plasma (CP) process in which the vapor plasma envelope calorific effect provides instant oxidation and expansion of graphite for producing plasma-expanded graphite oxides (PEGOs) from recycled graphite electrodes (GEs) or high purity graphite (HG), within a reaction time of 10 min without the need for strong oxidants or concentrated acids. X-ray diffraction, X-ray photoelectron spectroscopy and Raman spectroscopy confirmed the dramatic structural change from GEs or HG to graphite oxides after the CP process. Furthermore, scanning electron microscopy and transmission electron microscopy revealed that the graphite oxide possessed a spheroidal morphology, with dimensions of 1–3 μm, as a result of melting and subsequent quenching during the plasma electrolysis process. We obtained a stable, homogeneous dispersion of PEGOs in N-methyl-2-pyrrolidone after sonication and filtering of the centrifuged PEGOs. We used these spheroidal graphite oxide particles as effective adsorbents for the removal of pollutants (e.g., Methylene Blue) from aqueous solutions. These PEGOs also served as good precursors for the preparation of graphite nanopletets.

Sequently, we have demonstrated a new and highly efficient plasma-assisted electrochemical exfoliation method, involving a plasma-generated graphite cathode and a graphite anode, for the production of graphene sheets from electrodes in a basic electrolyte solution in a short reaction time. The AFM images revealed a lateral dimension of approximately 0.5–2.5 μm and a thickness of approximately 2.5 nm, corresponding to approximately seven layers of graphene, based on an interlayer spacing of 0.34 nm. Additively, the influence of electrolytic concentration on morphological and structural properties of plasma-electrochemically exfoliated graphene is investigated and presented. Finally, we developed an efficient solution-based method for the production of few-layer MoS_2 nanosheets through exfoliation of bulk MoS_2 compounds that were subject to quenching in liquid N_2 and subsequent ultrasonication. AFM images of individual nanosheets revealed that the thickness varied from 1.5 to 3.5 nm and the lateral dimensions from 0.5 to 3.5 μm.

摘要:

此實驗的目的是要找出在相對基本的電解液中，能夠快速用電漿電化學剝離法製造出石墨氧化物及石墨烯並且達到對環境友善、節省能源及時間與低成本的效果。首先，我們在回收的石墨電極或高純度石墨採用高效率陽極電漿法以蒸汽熱電漿反應對石磨產生即時氧化及擴張隨後產出展開電漿石墨氧化物，而此法可在不需要強氧化劑或高濃酸的條件下，十分鐘的反應時間內完成。X-RAY 繞射分析、X-RAY 光電子圖譜或拉曼圖譜可檢測出在經過陽極電漿法後，從石墨電極或高純度石墨到石磨氧化物的劇烈結構改變。此外，掃描式電子顯微鏡與穿透式電子顯微鏡更可顯示出石墨氧化物擁有類似圓球狀的型態，範圍尺度在 1-3μm 間，這是在電漿電解法中融化並隨後冷卻的結果。聲裂法及離心過濾石墨氧化物後，我們得到在 N-甲基吡咯烷酮中有穩定且同質均勻分布的展開石墨氧化物。應用上可將類圓球狀的石墨氧化物當作強吸收劑用來去除水溶液中的髒汙(例如:亞甲基藍)。他也是個好的製造石墨奈米小板之前驅物。隨後，我們也說明如何由石墨陰陽極電漿電解剝離法在短時間內與簡單電解液的條件下產出石墨烯。原子力顯微鏡影像顯示出，橫向尺度大約 0.5-2.5μm 及厚度約 2.5nm，相當於七層石墨烯(每層約 0.34nm)的厚度。最後，我們研究電解液的濃度如何影響電漿電化學剝離石墨烯的表面形態及結構最後我們發展出一個高效率液相製法使用 N_2 將塊狀 MoS_2 製備成 MoS_2 nanosheets，由 AFM 的圖可以看出分開的 MoS_2 nanosheets 的厚度由 1.5 nm ~3.5 nm 且尺寸大小在 0.5μm ~3.5 μm 之間。。

Acknowledgment

First and foremost, I gladly acknowledge my debt to Prof.Kung-Hwa Wei. Without his constant friendship, generous encouragement and concise advice, this thesis would never have been completed. Additionally, I am grateful to Prof. Chih-Wei Chu, Prof. Lain-Jong Li, and Prof. Yao-Jane Hsu because they kindly gave me much comments and suggestions relating to my research direction. I would also especially like to recognize Prof. Chih-Wei Chu for permitting me to use his facilities and equipment.

I would also like to thank Dr. Jian-Ming Jiang, Mr. Hsiu-Cheng Chen, and Mr. Chien-Chung Pan. They kindly taught me all of equipment in my lab and helped order facilities, and chemicals equipment for my research setup. Four years ago, when I started Ph.D. program, my life in the Taiwan was complicated by language and cultural differences. Many people have helped me in the course of my research, and any merit on its behalf is in large measure due to them.

Finally, special thanks go to my parents, my wife, and my son. Your love always made it possible for me to go through tough trails. Thank you for being there, smiling at me with love, good days or bad days

Dang Van Thanh

Hsinchu, Taiwan

March 2014

Figure List

Table List

Chapter 1: Introduction

Graphene (GNs), a single layer of carbon atoms bound together in a hexagonal lattice (i.e., a two-dimensional form of graphite),[1] has many potential applications in, for example, energy-storage materials,[2-6] polymer composites,[7-9] transparent conductive electrodes,[10-13] memory devices,[14-16] and sensors.[17-20] To meet the demand, large-scale production of graphene is required. Several methods have been developed for the preparation of GNs, such as: electrochemical exfoliation,[21,22] arc discharging,[23,24] mechanical milling [25,26], expanded graphite-based exfoliation [8,27-30] and chemical reduction of exfoliated graphite oxide (GO).[31-34] Among these methods, chemical oxidation of graphite, conversion of the resulting graphite oxide to graphene oxide, and the subsequent reduction of graphene oxide is widely considered as one of most commonly approach for the large-scale production of GNs. Unfortunately, the mixtures of strong oxidants and concentrated acids, which is used to prepare GOs, are highly toxic and dangerously unstable, so extra safety precautions are required.[35,36] In addition, the GO production via oxidation of graphite usually consumes long time. Therefore, an alternative approach for producing GO or graphene from available graphite-based sources with simple, low cost equipments and rapid throughput processing are highly desirable. The key for such a process is the exfoliation of graphite via fast and controlled electrochemical exfoliation of graphite. In fact, electrochemical exfoliation of graphite has been reported to be a green and cost-effective approach for producing graphite oxides and high-quality few-layer graphene flakes in high yield using simple equipment. *Cui et al*.[37] reported the preparation of graphite oxide nanoparticles and graphene by electrochemical oxidation of graphite anode in deionized water at galvanostatic mode. These facts suggest that it is possible to

disaggregate graphite into graphite oxide or individual graphene sheets using controlled electrochemical exfoliation approach.

In this dissertation, a new and highly efficient plasma electrochemical exfoliation method will be described consisting of a plasma-generated graphite cathode and a stainless steel anode or graphite anode for the production of graphite oxide or graphene sheets. The purpose of this work is to find out new approaches for one-pot synthesis of graphite oxide and graphene by the plasma electrochemical exfoliation of graphite in a basic electrolyte solution in a short-reaction time with regards of environmental friendliness, energy/time saving, and low cost. In addition, we also demonstrate a new and simple solution-based method for the production of few-layer MoS_2 nanosheets through exfoliation of bulk MoS_2 compounds through quenching in liquid N_2.

After the introduction, a brief overview of methods for preparation of graphene, particularly the electrochemical method and plasma electrolysis processing, is presented in chapter 2. Chapter 3 describes our proposed method to synthesize graphite oxide using plasma electrolysis. The oxidized mechanism of graphite into graphite oxide will be discussed. The as-synthesized graphite oxide produced through this process is demonstrated as an effective adsorbent for a removal of Methylene Blue from aqueous solutions and can serve as a suitable precursor for the preparation of graphite nanoplatelets. Chapter 4 contains a highly efficient and green method for the production of graphene sheets from both graphite electrodes in a basic electrolyte solution through an electrochemical process involving a plasma-generated graphite cathode. The influence of electrolytic concentration on morphological and structural properties of plasma-electrochemically exfoliated graphene is investigated and presented in chapter 5. Chapter 6 develops and applies further the exfoliated mechanism in chapter 3-4 for

the production of few-layer MoS_2 nanosheets through exfoliation of bulk MoS_2 compounds through quenching in liquid N_2. Finally, the features of this dissertation and outlook for further studies will be discussed in chapter 7.

Chapter 2: Overview of electrochemical exfoliation and plasma electrolysis

2-1. Introduction to graphene

Graphene (GNs), a single layer of carbon atoms bonded together in a hexagonal lattice or two-dimensional graphite, has recently emerged as a rising star in materials science. The excellent properties of graphene were reported by high values of its Young's modulus (~ 1100 GPa), fracture strength (125 GPa) [1],[1] thermal conductivity (~ 5000 W m^{-1} K^{-1}),[2] mobility of charge carriers (200 000 cm^2 V^{-1} s^{-1}) [3][3] and specific surface area (2630 m^2 g^{-1}) [4].[3,4] Several methods have been developed for preparing graphene sheet since it was firstly isolated by Novoselov and Geim using Scotch tape in 2004, such as: electrochemical exfoliation,[5,6] arc discharging,[7,8] mechanical milling [9,10], expanded graphite-based exfoliation [11-15] and chemical reduction of exfoliated graphite oxide.[16-19]. A summary of different preparing processes of GN is shown in Fig.2-1.[20] More detail of preparation methods, properties of graphene and its application can be found in previous literatures [16-20].

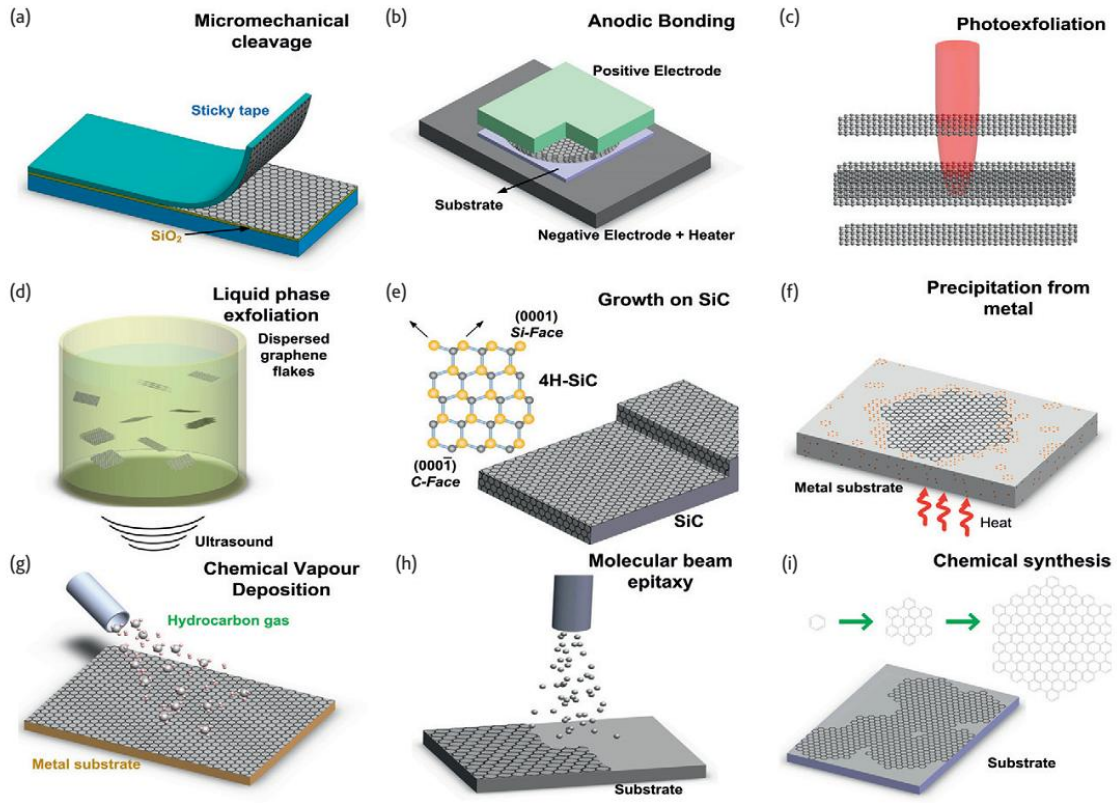

Figure 2-1. Schematic illustration of current graphene production techniques.[20] (a) Micromechanical cleavage. (b) Anodic bonding. (c) Photoexfoliation. (d) Liquid phase exfoliation. (e) Growth on SiC. Gold and grey spheres represent Si and C atoms, respectively. At elevated T, Si atoms evaporate (arrows), leaving a carbon-rich surface that forms graphene sheets. (f) Segregation/precipitation from carbon containing metal substrate. (g) Chemical vapor deposition. (h) Molecular Beam epitaxy. (i) Chemical synthesis using benzene as building block.

2-2. Electrochemical approach to produce graphene

Electrochemical methods have been used for the synthesis of graphite

intercalation compounds (GICs) in the past decades.[21] A recent review indicates that this technique was employed as early as 1840.[22] The consequent efforts, successes and developments of this method for production of graphite oxide and graphene is presented in Fig.2-2.[22]

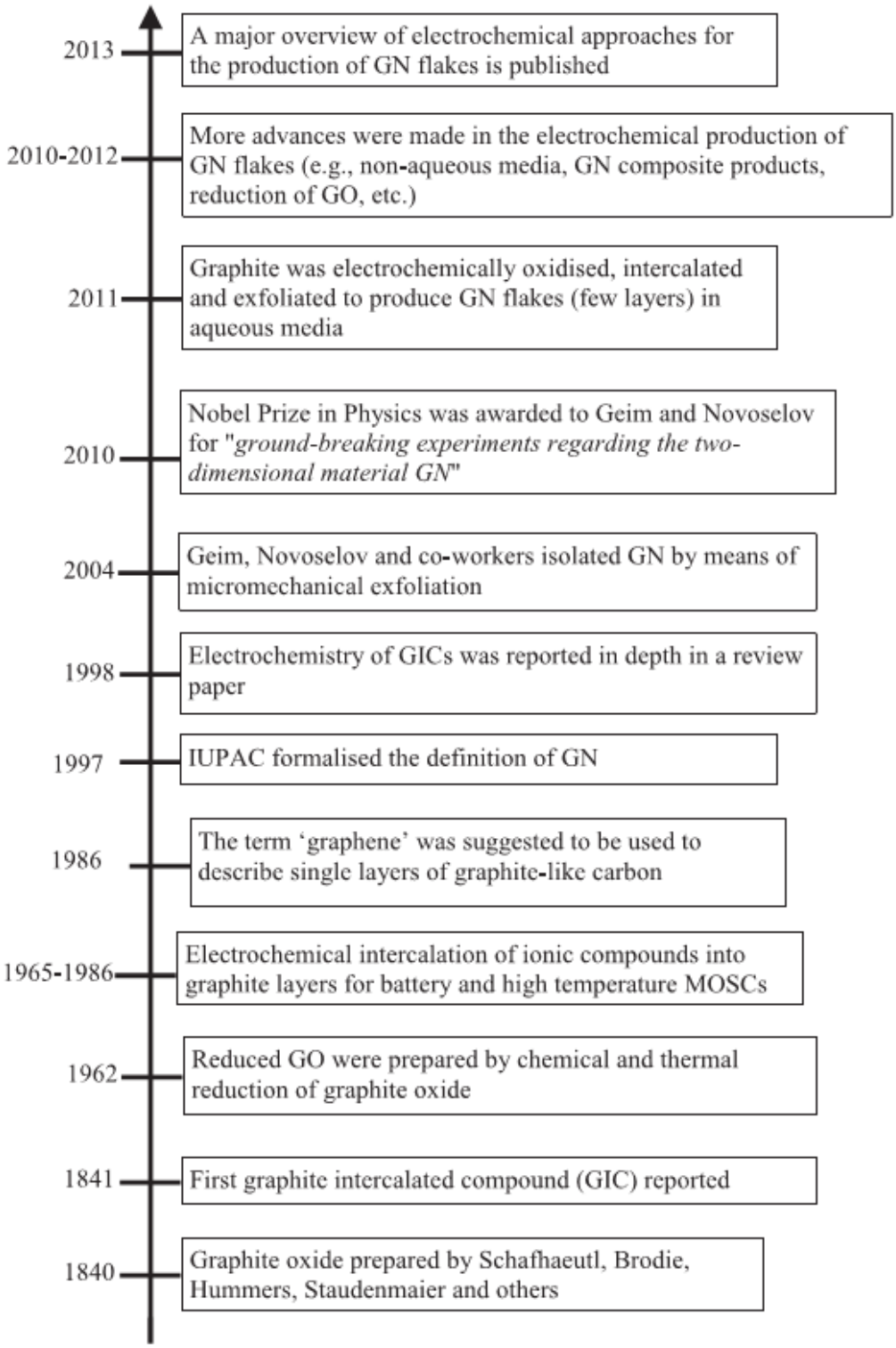

Figure 2-2. Timeline for the development of GN using electrochemical technique.[22]

Basically, electrochemical exfoliation employs an ionically conductive solution (electrolyte) and a direct current (DC) power source to prompt the structural changes within the graphitic precursor (e.g. rod, plate, or wire) used as the electrode. The schematic of a conventional parallel two-electrode electrochemical cell used for the batch production of GN flakes is displayed in Fig.2-3.[23] The principle of preparing GN flakes by electrochemical method (Fig. 2-4) involves the intercalation processes where guest anions X^-, such as BF_4^- and SO_4^{2-} (anodic exfoliation)[24,25], or cations M^+, such as Li^+ and TBA^+, EA^+ (cathodic exfoliation)[5,26-28], penetrate into the Van der Waals gaps between the carbon layers and enlarge the interlayer distance of the host graphite working electrode (WE) resulting in the intercalation of a cation or anion from the electrolyte.[22] A post-treatment step is then required to effectively exfoliate the graphite intercalation compounds/expanded graphite either by ultrasonication or electrochemical and thermal decomposition of the intercalants at elevated voltage (5–20V) and temperatures.[27-31] By using various electrolytes, likes: HBr, HCl, HNO_3, and H_2SO_4, a high-quality graphene thin films from electrochemical exfoliation of highly oriented pyrolytic graphite can be achieved.[25] The exfoliated graphene sheets exhibit lateral size up to 30μm, and more than 65% of the sheets have the thickness less than 2 nm. Over 60% of the sheets are bilayers with AB stacking, and though oxidized, they have significantly higher electron mobility than most of reduced graphene oxide.[25] The detail process of electrochemical synthesis of GNs was described in Ref. 22-28.

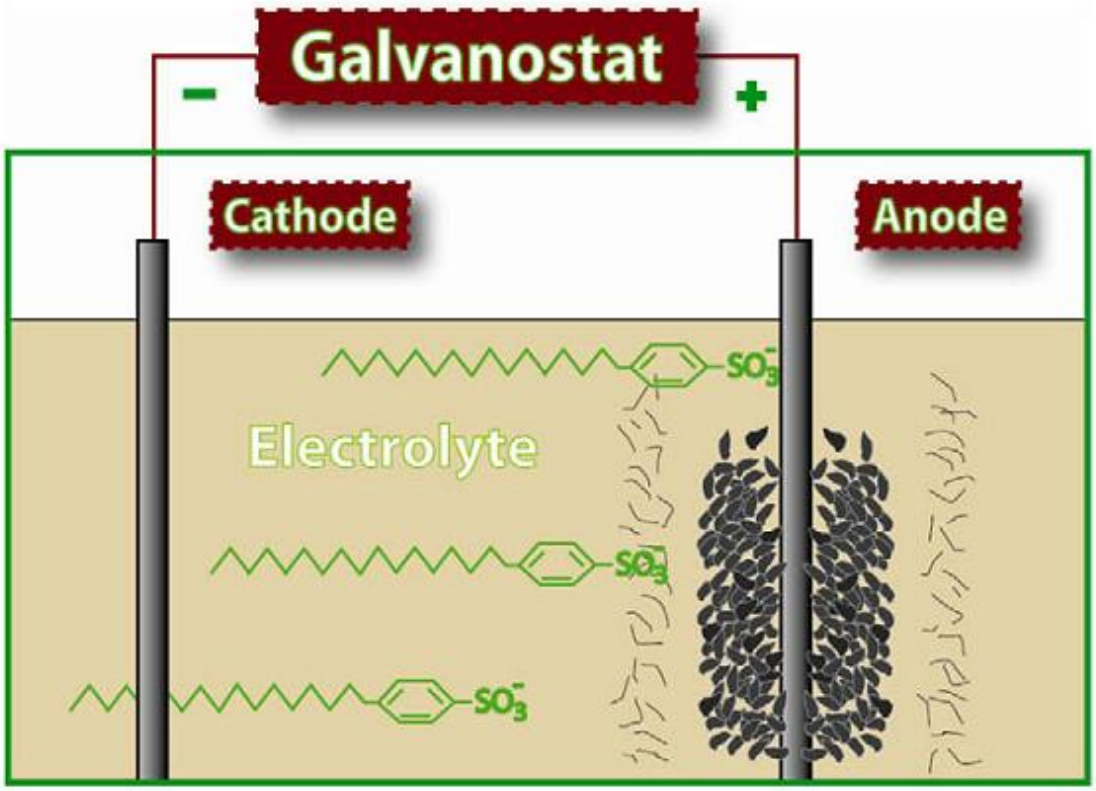

Figure 2-3. Diagram of the apparatus for synthesis of graphene via electrolytic exfoliation.[23]

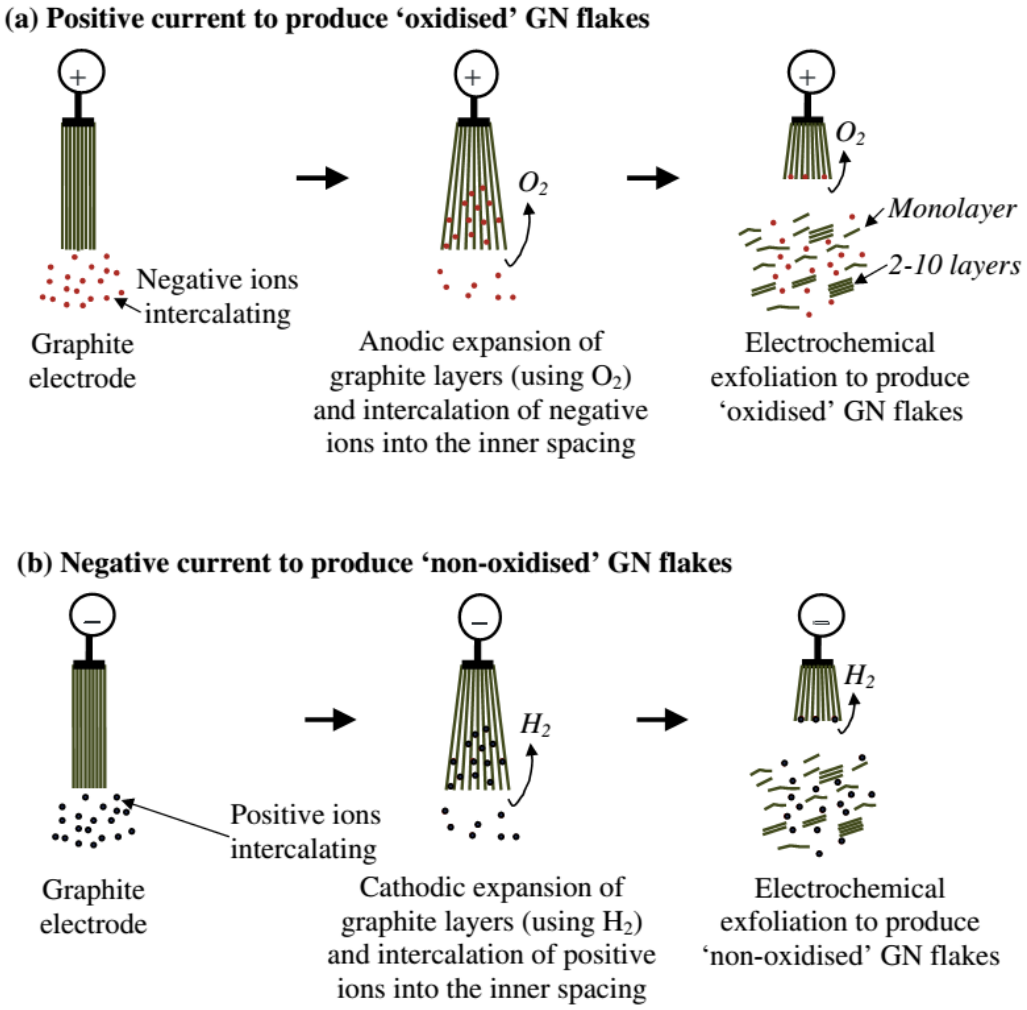

Figure 2-4. Electrochemical approaches (a) oxidation, intercalation and exfoliation (negative ions are shown in red color) and (b) reduction, intercalation and exfoliation to produce single and multilayer GN flakes. [22]

2-3. Cathodic plasma electrolysis to produce nanomaterials

Plasma electrolysis is a hybrid of conventional electrolysis and atmospheric plasma processes. In principle, it employs a voltage that is much higher than it is used at the traditional electrochemical method between two electrodes in an

aqueous media. One of the electrodes must have much smaller surface than the second one or ones, and it is called the active electrode, regardless the anode or the cathode. The active electrode (work-piece) is the object or objects to be treated. Depending on the polarity of applied voltage to the work-piece, this process can be divided into either anodic or cathodic plasma electrolysis processing (CPE). Most studies are concentrated on the anodic regime of plasma electrolysis and very few on the cathodic regime. The schematic division for this plasma electrolysis process is shown in the Fig 2-4. [32]

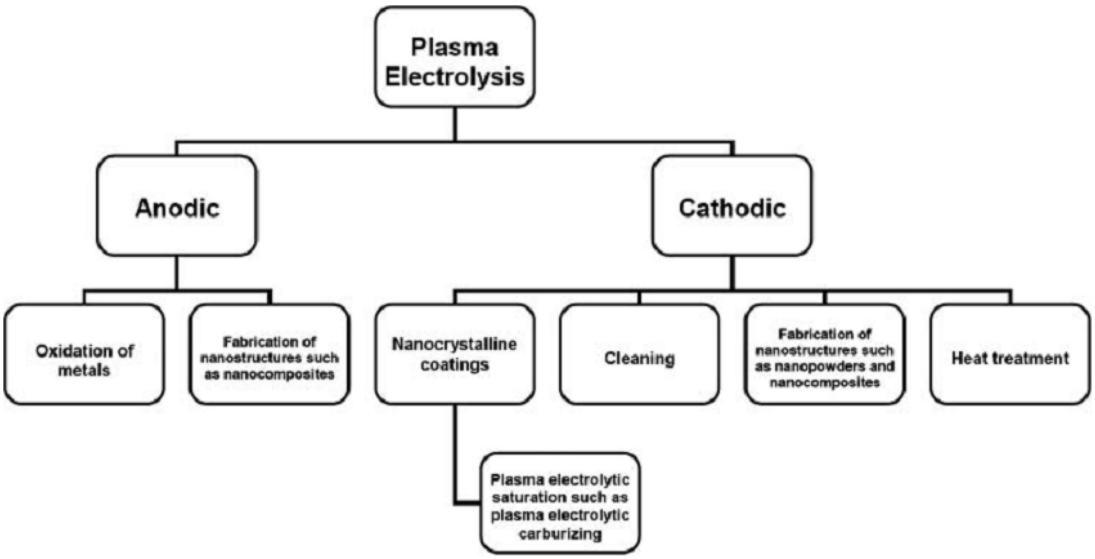

Figure 2-4. Typical classification of plasma electrolysis and its applications.[32]

The mechanism of CPE is based on the evaporation or reaction of electrolyte and then electrical break down of the gaseous envelope around the active electrode resulting in the formation of sparks around the processed electrode.[33] The main factors, that influence the formation of the continuous plasma envelope, include: applied potential, temperature of the electrolyte, electrode geometry, nature and

properties of the electrolyte, and flow dynamics. [34,35] Good reviews of detail mechanism for plasma electrolysis and its application could be found in Ref 33-35.

In cathodic configuration, this processing used for producing of nitride, carbon, titanium, molybdenum, zinc and zinc-aluminium based coatings on metal substrate.[33,34,36,37] The nano-crystalline graphite films on titanium substrate prepared from a predominantly ethanol liquid phase have been deposited by the cathodic plasma electrolysis.[38 39] It has been observed that the properties of obtained layers depend on the characteristics of achieved nanostructures, such as: average size, distribution and average coordination number of nanocrystallites. Furthermore, the properties of the processed surface can be tailored by tailoring the nanostructure characteristics.[38 39] In fact, each layer of graphene in the bulk graphite is sandwiched between two layers of hexagonally close-packed C atoms, with the adjacent layers, bound by weak van der Waals interactions, readily exfoliating into individual graphene nanosheets upon the impacting on the surface, such as ultrasonication or thermal extension; as a result, we suspected that the plasma electrolysis phenomenon on the surface of graphitic electrode might be involved in breaking van der Waals force bonded graphene layers in the bulk state to controlled produce GO or graphene flakes. To address the above-mentioned issues, we have utilized cathodic plasma electrolysis as a part of the graphite oxide or graphene controlled fabrication process. The detail motivation and experimental of this assumption will be presented in next chapter.

2-4. Solution-based exfoliation approach to produce MoS_2

Siminar to graphene, the transition metal dichalcogenides that consist of hexagonal layers of metal atoms (M) sandwiched between two layers of chalcogen atoms (X) with a MX_2 stoichiometry, such as MoS_2 also involve van der Waals

interactions between adjacent sheets with strong covalent bonding within each sheet. [40-42] Thus, they can be synthesized by methods commonly employed in the production of graphene.[43,44] The excellent review on synthesis, properties, and its applications could be found reference 40-44.

Chapter 3: Plasma electrolysis allows the facile and efficient production of graphite oxide from recycled graphite

Graphene, a single layer of carbon atoms bound together in a hexagonal lattice, has many potential applications in energy-storage devices such as super capacitors and batteries. Among several methods for preparing graphene, the chemical reduction of graphene oxide that are obtained from oxidation of graphite and subsequent exfoliation is widely considered to be the most promising approach for the large-scale production of graphene. The oxidation of graphite to graphite oxide involves concentrated mineral acids that are highly toxic and poses an environmental risk when they are discharged after use. In this chapter, we adopted a highly efficient cathodic plasma process in which the vapor plasma envelope calorific effect provides instant oxidation and expansion of graphite for producing plasma-expanded graphite oxides from recycled graphite electrodes or high purity graphite, providing a first green step toward the mass production of graphene.

3-1.Introduction

Graphene, a single layer of carbon atoms bound together in a hexagonal lattice (i.e., a two-dimensional form of graphite), [45] has many potential applications in, for example, energy-storage materials, [4,46-49] polymer composites, [12,50,51] transparent conductive electrodes, [52-55] memory devices, [56-58] and sensors. [59-62] Several methods are available for preparing graphene: chemical vapor deposition (CVD), [63-65] epitaxial,[22, 23] unzipping of carbon nanotubes,[24, 25] electrochemical exfoliation, [23,25,30,66] liquid-phase exfoliation of graphite, [67,68] and chemical reduction of graphite oxide (GO).[69,70] Among these methods, the chemical reduction of GO is one of the most promising approaches for the large-scale production of graphene; it involves (i) oxidation of graphite to GO using the

methods developed by Staudenmeier, [71] U. Hofmann, [72] or Hummers, [73] (ii) exfoliation of GO through ultrasonication or thermal treatment to yield graphene oxide; and (iii) chemical reduction of graphene oxide to a graphene or graphitic network of sp^2-hybridized carbon atoms. The mixtures of strong oxidants and concentrated acids used to prepare GO are, however, highly toxic and dangerously unstable, requiring additional safety precautions. [74,75] Moreover, the discharge of large quantities of acidic waste poses an environmental risk. Thus, new methods for the preparation of GO, without the need for toxic chemical agents or the harsh oxidation of graphite, would be of great interest from the perspectives of science, technology, and environmental protection. Hudson et al. [76] reported the preparation of GO from graphite using an electrochemical method with a reaction time on the order of several weeks; it would require further improvements if it were to become as effective as the chemical methods described above. Several other studies based on the electrochemical activation of glassy carbon (GC) or highly ordered pyrolytic graphite (HOPG) have also been reported for the successful formation of GO. [77,78] For each of these methods, however, graphite of relatively high purity (e.g. purified natural graphite, glassy carbon, or HOPG) is used as the starting material. To date, the preparation of GO using low-purity graphite such as graphite electrodes (GEs) that have been recycled from used batteries as the starting material has not yet been reported. Herein, we demonstrate a highly efficient, green, and facile approach—involving cathodic plasma (CP) processing and subsequent ultrasonication—for the synthesis of GO from GEs recycled from batteries.

A classic electrolysis reaction involves either an anode oxidation or a cathode reduction process in an electrolyte bath. In an electrolytic process, the onset of plasma can be triggered around the working electrode—so-called plasma

electrolysis—when the applied voltage is larger than the threshold voltage, with a strong electric field generated near the working electrode (either the anode or cathode). [34,35,38] The plasma near the working electrode induces strong Joule heating in the vicinity of the submerged part of this electrode, resulting in the formation of a vapor plasma envelope (VPE) with a surrounding temperature exceeding 2000 °C. [34] Plasma electrolysis can, therefore, be used to enhance chemical or physical processes occurring on the electrodes. For example, plasma electrolytic oxidation in an electrolyte bath, where the working electrode is an anode having a surface area much smaller than that of the cathode, is widely used industrially for oxidizing metal surfaces to form metal oxide coatings.

In the present study, however, we applied a highly negative voltage (–60 V) from a DC power supply to a graphite working electrode, which we used as the cathode; when this graphite cathode approached, but barely reached, the surface of the electrolyte, plasma was generated instantly on the cathode (see the demonstration movies in the Supporting Information). If the graphite working cathode were submerged into the electrolyte at shallow depths (e.g., 1 cm), no plasma was generated. We, therefore, term this plasma electrolysis process as a cathodic plasma (CP) process. Figure 1 presents schematic representations of the equipment set-up that we used for the CP process in conjunction with an ultrasonication bath. Surprisingly, the surface of the graphite electrode tip that was covered by the generated plasma could be oxidized and exfoliated into the electrolyte in a controllable manner. One possible explanation for the mechanism in this CP process is that the enormous amount of heat generated from the VPE calorific effect supplied the thermal energy required for the local oxidation of the surface of the GE. Hence, this process could be used for oxidation of the GE or HG to produce graphite oxide without the need for a mixture of strong oxidants and

concentrated acids; we term the material produced as plasma-expanded graphite oxide (PEGO). The entire experiment could be performed within 10 min at a temperature below 80 °C when using KOH and $(NH_4)_2SO_4$ in deionized (DI) water as the electrolytic solution. The detailed experimental conditions are described in the experimental section.

With further ultrasonication of a solution of PEGO in NMP, we obtained exfoliated PEGO (EPEGO). In addition, during ultrasonication, a local hot spot of the VPE (spark) could induce instant exfoliation reactions, producing a small portion of graphene sheets or graphene-like materials. The major advantages of this CP approach for producing graphite oxide from graphite are a simple setup, low cost (GO can be derived from a plentiful resource: recycled GEs), rapid processing, and environmental friendliness.

3-2. Experimental

3-2.1. Preparation of PEGO and PEHGO

The electrolytic solution, comprising KOH (10%, 180 mL) and $(NH_4)_2SO_4$ (5%, 20 mL) at a pH of approximately 14, was preheated to an initial temperature of 70 °C. A cylindrical graphite rod (GE) or high purity graphite (HG) was used as the cathode connected to a voltage supply unit (negative voltage output); the cathode diameter and length were 6 and 40 mm, respectively. A stainless-steel grid acted as the anode in the electrochemical system for the plasma expansion process (PEP). The top end of the cathode was placed about 1 mm above the surface of the electrolytic solution, while the anode was submerged in the electrolytic solution. The surface area of the cathode was much smaller than that of the anode as illustrated in Figure 1a. Both electrodes were connected to a regulated DC power supply (TES-6220) with an applied maximum fixed voltage of 60 V and a

maximum current intensity of 3 A, resulting in a discharging plasma in the area adjacent to the GE and the electrolytic solution. As the exfoliation of GE progressed, the tip position of the GE was lowered to maintain a current of approximately 1.75 A. The temperature of the solution within the beaker was measured during the process using a conventional mercury thermometer; it was maintained at approximately 70–80 °C. To enhance exfoliation and the homogeneity of the reaction, the beaker containing the electrolytic bath was submerged partially in an ultrasonication bath maintained at 20 kHz under a power of 150 W. The length of time in which the samples experienced simultaneous treatment was 10 min. Fig.3-1 provides schematic representations of the equipment set-up used in the CP process (also see the demonstration movies in the Supporting Information).

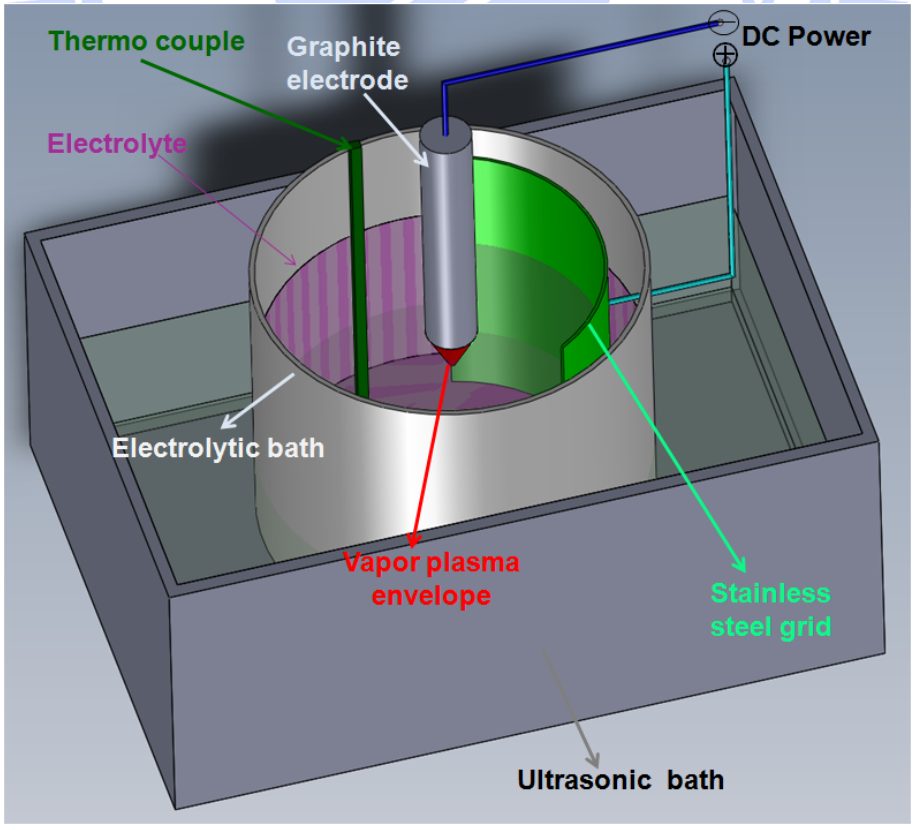

Figure 3-1. Schematic representation of the equipment used for the CP process combined with ultrasonic vibration.

After CP treatment, the products were collected through vacuum filtration of the solution through PVDF membranes (average pore size: 0.2 μm) supported on a fritted glass holder. The resulting mixture was washed sequentially with DI water and 1% HCl and then repeatedly with DI water until the pH reached 8. After drying at room temperature under vacuum for 24 h, the PEGO was obtained. The prepared samples were stored in a drying box at 50 °C until required for use. For comparing to the processing of recycled graphite electrode, we also applied the CP process to high purity graphite (HPG) for demonstrating the generality of the CP process, regardless of the starting graphite materials. The graphite oxides produced from the recycled graphite electrode (GE) and high purity graphite (HPG) are termed PEGO and PEHGO, respectively.

3-2.2. Preparation of EPEGO

The obtained PEGO (10 mg) was added to N-methyl-2-pyrrolidone (NMP, 100 mL) to create PEGO dispersion (0.1 mg/mL), which was subjected to exfoliation for 30 min using a tip ultrasonication apparatus (SONICS, 700 W, 75% amplitude). To remove unwanted large graphite particles produced during the exfoliation process, the resultant mixture was centrifuged for 5 min at 4000 rpm and then for 25 min at 1500 rpm. After centrifugation, the top 10 mL of the dispersion was decanted by pipette; herein, this sample is referred to as CGOD. The other resultant mixture was filtered through an AAO membrane (Anodisc;

diameter: 47 mm, nominal pore size: 0.02 μm); the solids were then dipped in EtOH to remove residual NMP. The flakes that floated on the surface of the EtOH were collected on a Si substrate. After drying under vacuum at 50 °C for 24 h, a powdery product remained on the surface of the Si substrate; herein, it is named EPEGO.

3-2.3. Adsorption of MB on PEGO

The obtained PEGO powder (20 mg) was added to DI water (4 mL) to create a PEGO dispersion (5 mg/mL), which was added to MB solution (10 mg/L, 10 mL) and gently stirred before being left to equilibrate for 3 h. All experiments were performed at room temperature and a pH of approximately 7. After 3 h, a sample of the supernatant (2 mL) was removed by pipette to evaluate the residual MB concentration in the resultant solution. The amount of MB adsorbed was calculated using Beer's law, based on the absorption peak at 665 nm of the sample in a 1-cm quartz cell, as measured using a UV–Vis spectrophotometer.

3-2.4. Measurements and Characterization

The structures of the GE, PEGO, PEHGO and EPEGO were examined using a D2 X-ray diffractometer equipped with a Cu K_α tube and a Ni filter (λ = 0.1542 nm). Surface chemical compositions of PEGO and PEHGO were determined by XPS (Phi V6000). Raman spectra of these samples were recorded using a high-resolution confocal Raman microscope (HOROBA, Lab RAM HR) and a 632.8.5-nm HeNe laser source. UV–Vis spectra were recorded using a Hitachi U-4100 spectrophotometer. SAED patterns and HRTEM images were recorded using a JEOL 2100 apparatus operated at 200 kV; for HRTEM measurement, a few drops of the GE, HG, PEGO, HPEG and EPEGO solution were placed on a Cu grid presenting an ultrathin holey C film. SEM was performed using a JEOL JSM-

6500F scanning electron microscope operated at 15 kV. Prior to SEM measurement, PEGO and HPEGO samples were coated with a thin (ca. 3 nm) layer of Pt. AFM images were obtained using a Digital Instruments Nanoscope III apparatus equipped with a NANOSENSORS Si tip, operated in the tapping mode with a resonance frequency of 130 kHz. AFM samples were prepared by drop-casting CGOD solutions onto the surfaces of Si/SiO_2 substrates and then drying in air.

4-3.Results and discussions

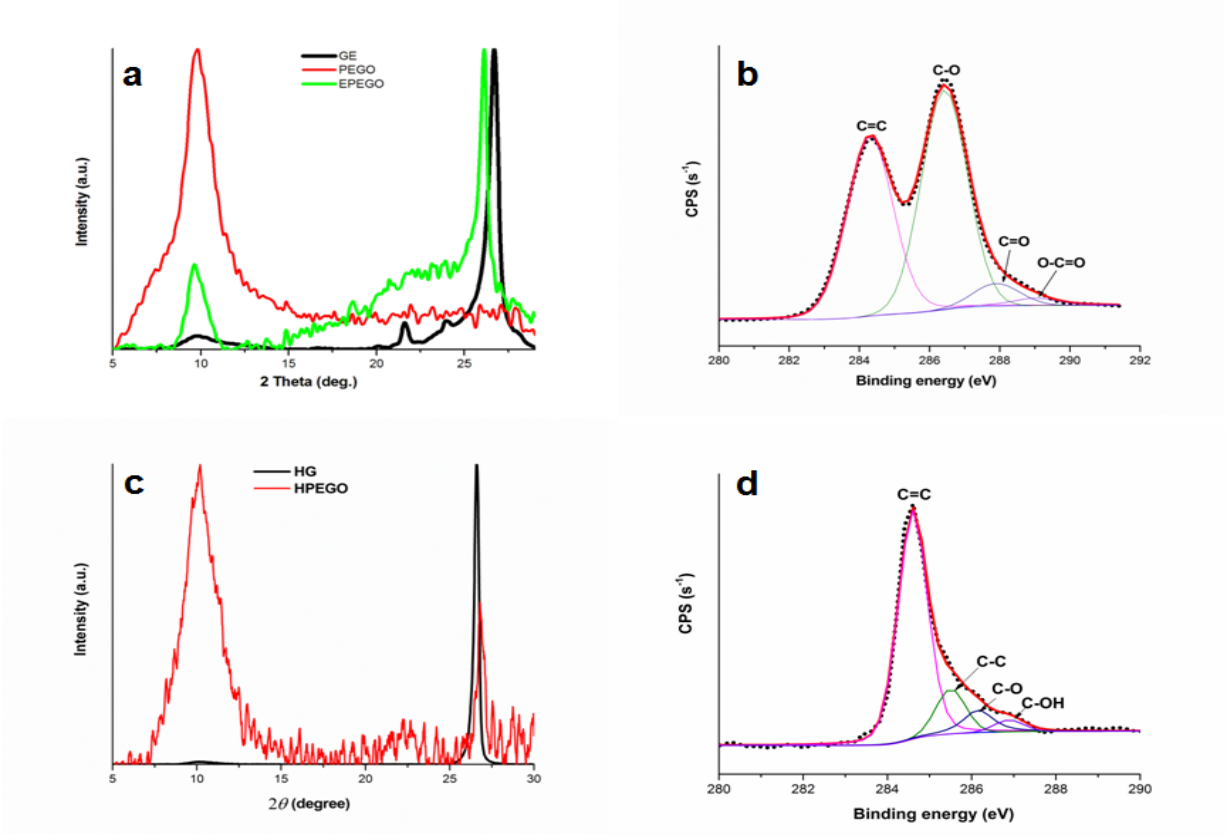

Figure 3-2. (a) X-ray diffraction patterns of the GE, PEGO, and EPEGO samples, (b) X-ray photoelectron spectroscopy of C1s signal of PEGO, (c) XRD patterns of the HGO, HPEGO samples, and (d) X-ray photoelectron spectroscopy of C1s signal of HPEGO.

Fig. 3-2a presents X-ray diffraction (XRD) patterns of the GE, PEGO, and EPEGO samples. The diffraction curve of the GE displays a sharp, high-intensity peak near a value of 2θ of 26.6° that can be assigned to the characteristic peak (002) of graphite; this signal indicates a rather highly ordered crystal structure with a value of d_{002}, which is the spacing between two neighboring atomic planes in graphite, of 0.334 nm. In addition, weak peaks appear at values of 2θ of 21.5 and 23.5°, possibly resulting from some additives or impurities in the GE. After the GE had experienced the CP process, the characteristic (002) peak at a value of 2θ of 26.6° for PEGO almost disappeared completely, whereas the intensity of the diffraction peak at a value of 2θ of 9.8° (corresponding to a value of d_{001} of 0.896 nm), the characteristic (001) peak of GO, increased significantly, implying an increase in the interplanar distance: from 0.334 nm for GE to 0.896 nm for PEGO. This finding indicates that the original graphene layers in GE had lost their periodic arrangement in the z-direction after they had transformed into PEGO, an intercalated graphite compound,[46-48] through this CP process. For the EPEGO, the intensity of the characteristic (001) peak at a value of 2θ of 9.8° (d_{001} = 0.896 nm) decreased significantly, with a large peak appearing at a value of 2θ of approximately 26° (d_{002} = 0.341 nm). This d_{002} spacing for the EPEGO is close to the spacing of the characteristic (002) peak of GE (0.334 nm), indicating that the EPEGO contained exfoliated graphite sheets or graphite nanoplatelets. The presence of a peak for the EPEGO at a value of 2θ of 9.8° indicates, however, that a significant portion of PEGO had not been exfoliated.

Figure 3-2b demonstrates the C 1s XPS spectrum of PEGO, where the peak at ~ 284.4 eV is attributed to the C=C (sp^2-hybridized carbon atoms,) and the large and broad peak at ~ 286.4 eV is caused by C-O (hydroxyl and epoxy,) groups along with two de-convoluted minor components at~ 287.9 eV and at ~ 289.0 eV

that resulted from C=O (carbonyl,) and O-C=O (carboxylate carbon,) groups, respectively, confirming the presence of graphite oxide and being consistent with the results of XRD. [16,79,80] Fig. 2c and 2d presented the XRD pattern and C 1s XPS spectrum of HPEGO, respectively. The peak at 2θ =26.6° in the XRD curve of HPEGO sample confirms the presence of a substantial amount of the graphite phase, suggesting a lower conversion of high purity graphite (HG) into graphite oxide with the CP process than in the case of GE. In addition, the shoulder next to the C 1s XPS peak at 286 eV for the HPEGO samples can also be de-convoluted into four minor peaks at 284.6, 285.5, 286.1and 286.9 eV that were attributed to C=C (sp^2-hybridized carbon atoms), C-C (sp^3-hybridized carbon atoms,), C-O (hydroxyl group) and COOH (alcohol/ether groups), respectively, indicating graphite oxide-like structure. [79] Table 1A lists a quantitative comparison on the amounts of various oxygen containing groups in PEGO and HPEGO bases on the area under the XPS peaks. The atomic percentage of carbon in HPEGO (87%) is higher than that (43%) of PEGO, which translated to a carbon to the oxygen bonded carbon (C/O) ratio of 1.75 and 7.0, respectively, indicating that the CP process is more effective of generating GO from GE than from HG. This can be attributed to the more uniform packing of graphene layers in HG than in GE, as reflected in the much sharper (002) peak, at a value of 2θ of 26.6°, for the HG than that of the GE in the XRD curves.

Table 3-1. The relative atomic percentage of various functional groups in PEGO and HPEGO estimated based on the area under the C 1s peaks

C=C (%)	C-C (%)	C-O (%)	C-OH (%)	C=O (%)	O-C=O (%)

PEGO	43		50		5	2
HPEGO	74	13	9	4		

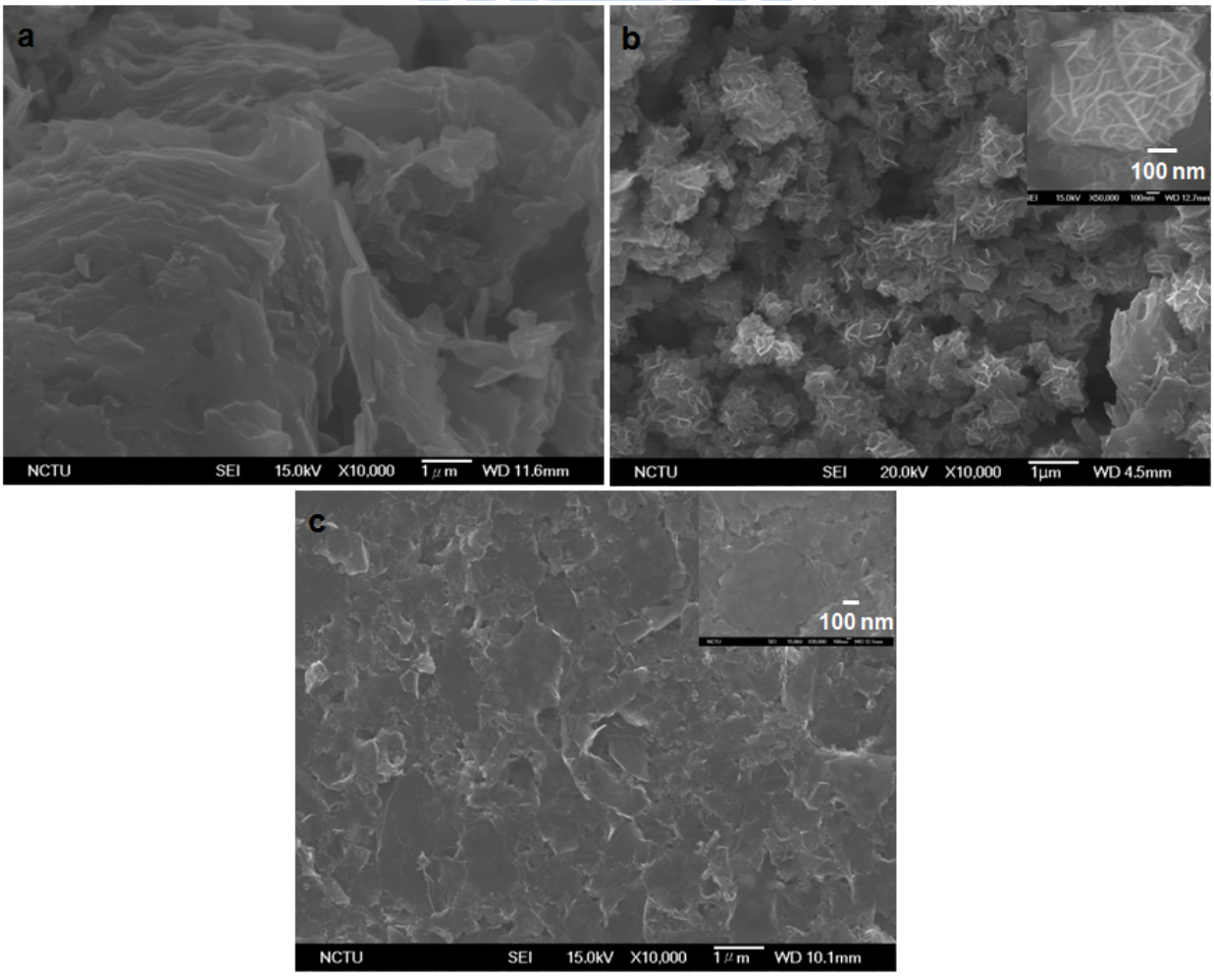

Figure 3-3. SEM images of the (a) GE, (b) PEGO, and (c) EPEGO samples; insets: high-magnification images.

Fig.3-3 presents scanning electron microscopy (SEM) images of the GE, PEGO, and EPEGO samples, revealing their significantly different structures. Fig. 3a indicates that the GE in powder form consisted largely of multilayered graphite clusters. Fig. 3b reveals that the PEGO (see Figure S2 in the supporting information for HPEGO), produced after the GE had been subjected to the CP process, featured crumpled structures and a heterogeneous surface, due to fast quenching; a high-magnification image of the PEGO (inset to Fig. 3b) indicates that it possessed spheroidal features having dimensions of 1–3 μm. The crumpled PEGO comprised many thin graphite oxide sheets, with the interactions among them being rather weak; thus, we expected it to undergo further exfoliation into thinner graphite oxide sheets. Fig.3-3c reveals that the graphite oxide sheets, with lateral width from several hundreds of nanometers to 3 μm, could be produced after subjecting the PEGO to ultrasonication; the inset displays a magnified view of one such exfoliated sheet having a thickness (ca. 10–50 nm) close to the size of a nanoplatelet. [16] Image analysis calculations based on 20–50 EPEGO nanosheets revealed that the average sheet diameter was approximately 1.5 μm with a thickness of approximately 10–30 nm, based on cross-sectional imaging of the folded edges of EPEGO after tilting the sample from 0 to 25°. Notably, the EPEGO could be imaged clearly through SEM without the charging effects that occurred for PEGO. [16]

Fig.3-4 provides a schematic representation of our proposed mechanism for the formation of the PEGO. We considered that its shape was formed through the “melting/quenching” process displayed in Fig. 4a. During the CP process, the high-temperature plasma that existed in the regions close to the interfaces between the GE and the electrolyte supplied thermal energy for the oxidation of the GE. These regions of high-temperature plasma, however, were surrounded by

the near room-temperature (70 °C) electrolyte; therefore, the temperature dropped rapidly across the interfaces, causing freezing of the oxidized features on the surface. The oxidized graphite clusters were then plucked from the surface of the GE and quenched in the electrolyte to form spherical and crumpled platelets that minimized the surface energy. Furthermore, the ultrasonic vibration enhanced the exfoliation of the outer shell of the oxidized GE. To verify this proposed mechanism, we would need to accurately measure the temperature in the plasma region and perform a quantitative investigation of the prepared PEGO samples using various other characterization tools—experiments that are beyond the scope of this manuscript.

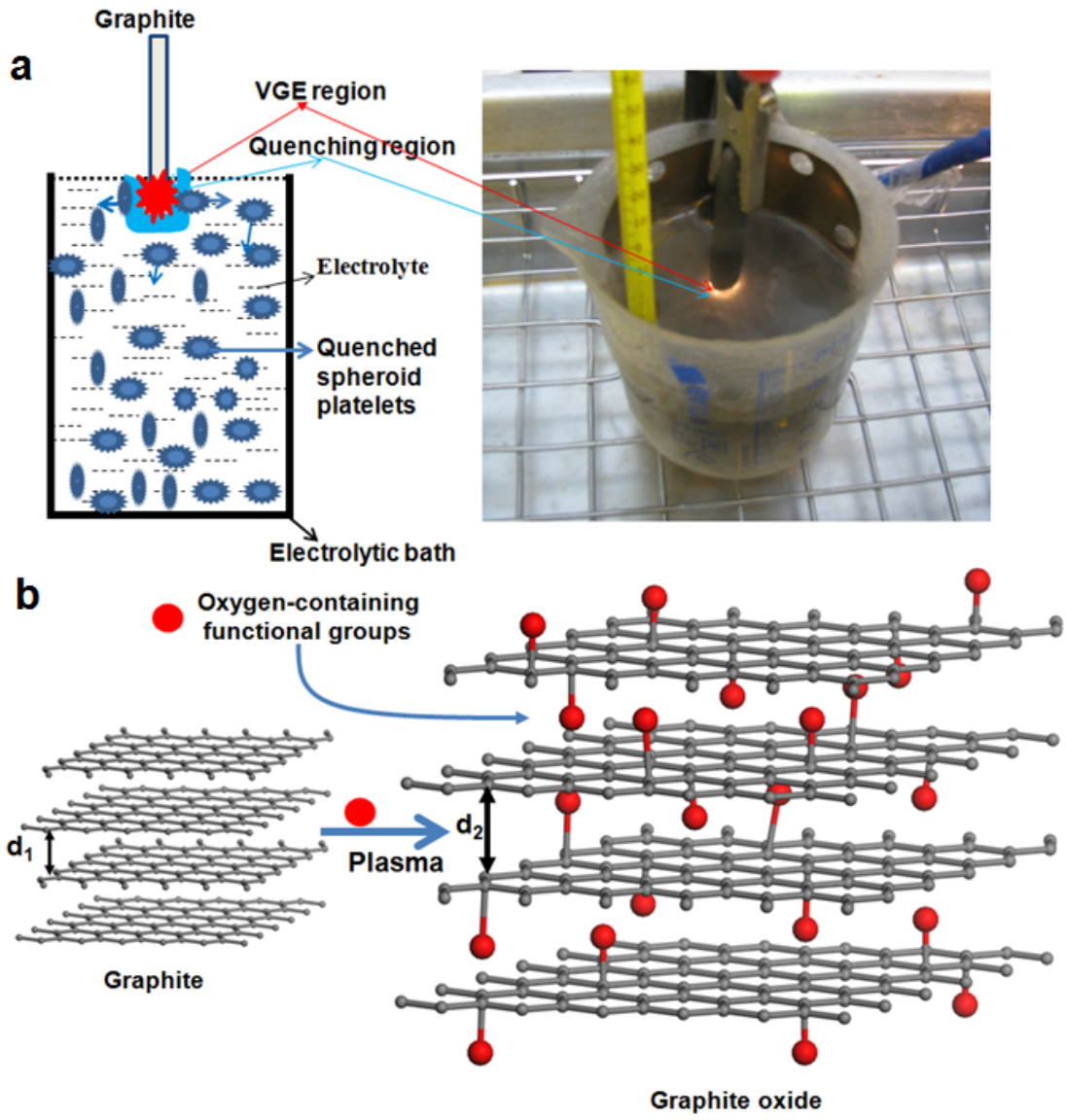

Figure 3-4. (a) Mechanism of formation of PEGO and digital image of VPE.

(b) Mechanism of plasma-mediated expansion of GE.

Fig.3-4 displays a schematic representation of the detailed mechanism for the formation of graphite oxide from graphite when using this CP process. The plasma in the discharge channel can usually reach a very high temperature and pressure within a short period of time time (e.g., $<10^{-6}$ s);[43] therefore, it is quite

possible that when the surface of the GE cathode tip is surrounded by the VPE, which is generated in the interfacial areas between the electrolyte and the GE tip-surface, the GE tip-surface is rapidly heated to a high temperature (see the demonstration movies in the Supporting Information). As a result, the electrolyte in the vicinity of the GE tip-surface that was encompassed by the VPE in the plasma environment would be vaporized instantly, producing a number of active species, such as hydrogen or nitrogen radicals,[35,81,82] or oxygen-containing groups that could penetrate into the spaces between the graphene sheets in the VPE-encompassed GE tip. These radicals then attack the C–C bonds in the graphite to produce GO, resulting in their oxidation and expansion. This simultaneous oxidation and expansion in GE not only produces PEGO but also results in a 30-fold expansion in the spacing between two neighboring atomic planes in PEGO relative to that in the original GE.

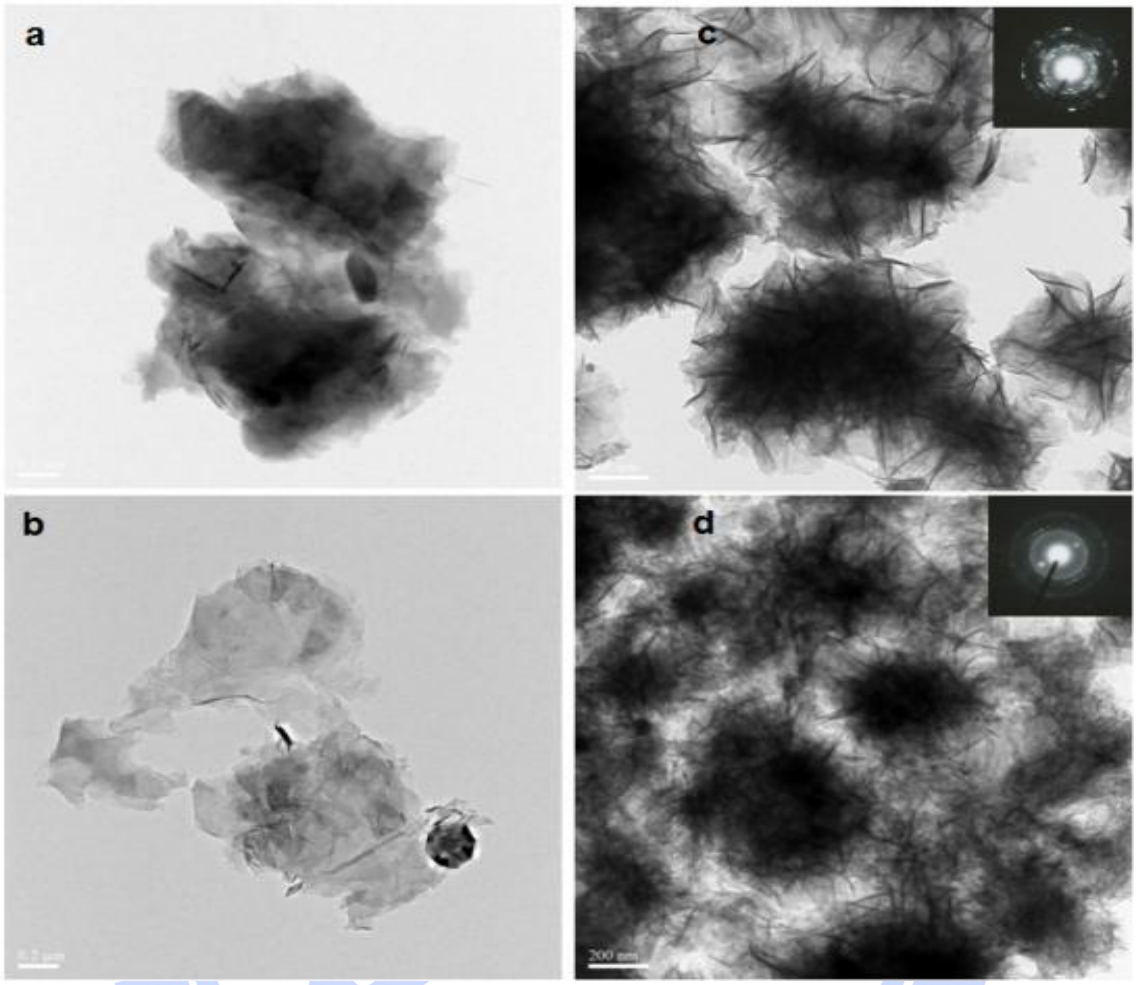

Figure 3-5. TEM images of (a) GE, (b) HG, (c) PEGO, and (d) HPEGO; insets: corresponding SAED pattern.

Figs.3-5 shows TEM images of GE, PEGO, HG, and HPEGO samples. Figs. 5a and 5b display micrometer-sized clusters with relatively thick, stacked aggregates of graphene layers for both GE and HG; Figs.3-5c and 3-5d present images of a crumpled-like structure with inhomogeous surfaces for PEGO and HPEGO after the GE and HG had experienced the CP process, being consistent with the SEM results.

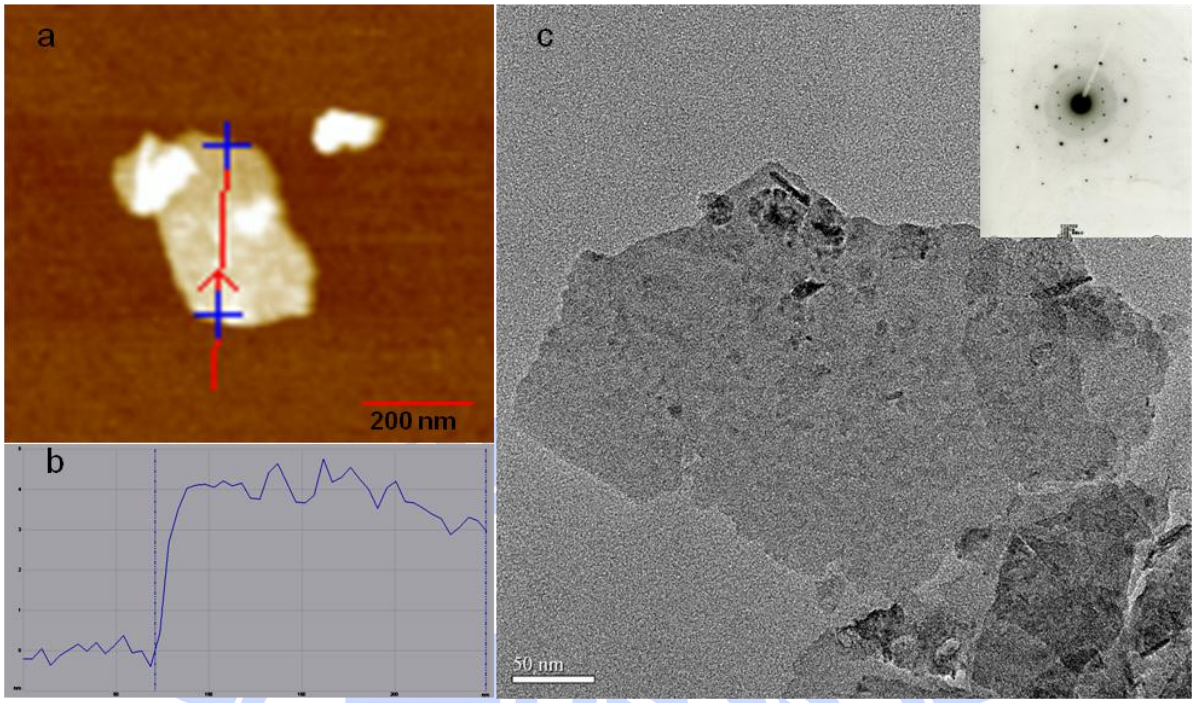

Figure 3-6. (a) AFM image of a nanoplatelet of EPEGO deposited on a Si/SiO_2 substrate. (b) Line scan height profile of the sample in (a). (c) HRTEM image of an EPEGO nanoplatelet; inset: corresponding SAED pattern.

Figs. 3-6a and 3-6b reveals the shapes, thicknesses, and lateral dimensions obtained from typical atomic force microscopy (AFM) images of the EPEGO; this EPEGO sample had a lateral dimension of approximately 250 nm and a thickness of approximately 4 nm, corresponding to approximately four layers of graphene, based on an interlayer spacing of 1 nm. Furthermore, the exfoliated EPEGO could be clearly identified in a high-resolution transmission electron microscopy (HRTEM) image, appearing translucent, with a selected-area-electron-diffraction (SAED) pattern that reveals a typical hexagonally arranged lattice of carbon atoms. Two hexagonal patterns were overlapping each other, suggesting that the EPEGO

samples comprised multi-layered graphene sheets, being consistent with Fig.3-6c The sizes and thicknesses of the nanoplatelets visualized in the HRTEM and AFM images were smaller than those in the SEM images, because the EPEGO samples had been diluted in NMP. These results suggest that PEGO can serve as a potential precursor for the preparation of graphite nanoplatelets. We suspect that optimizing the plasma power and ultrasonication conditions would allow us to control the lateral dimensions and thicknesses of these samples.

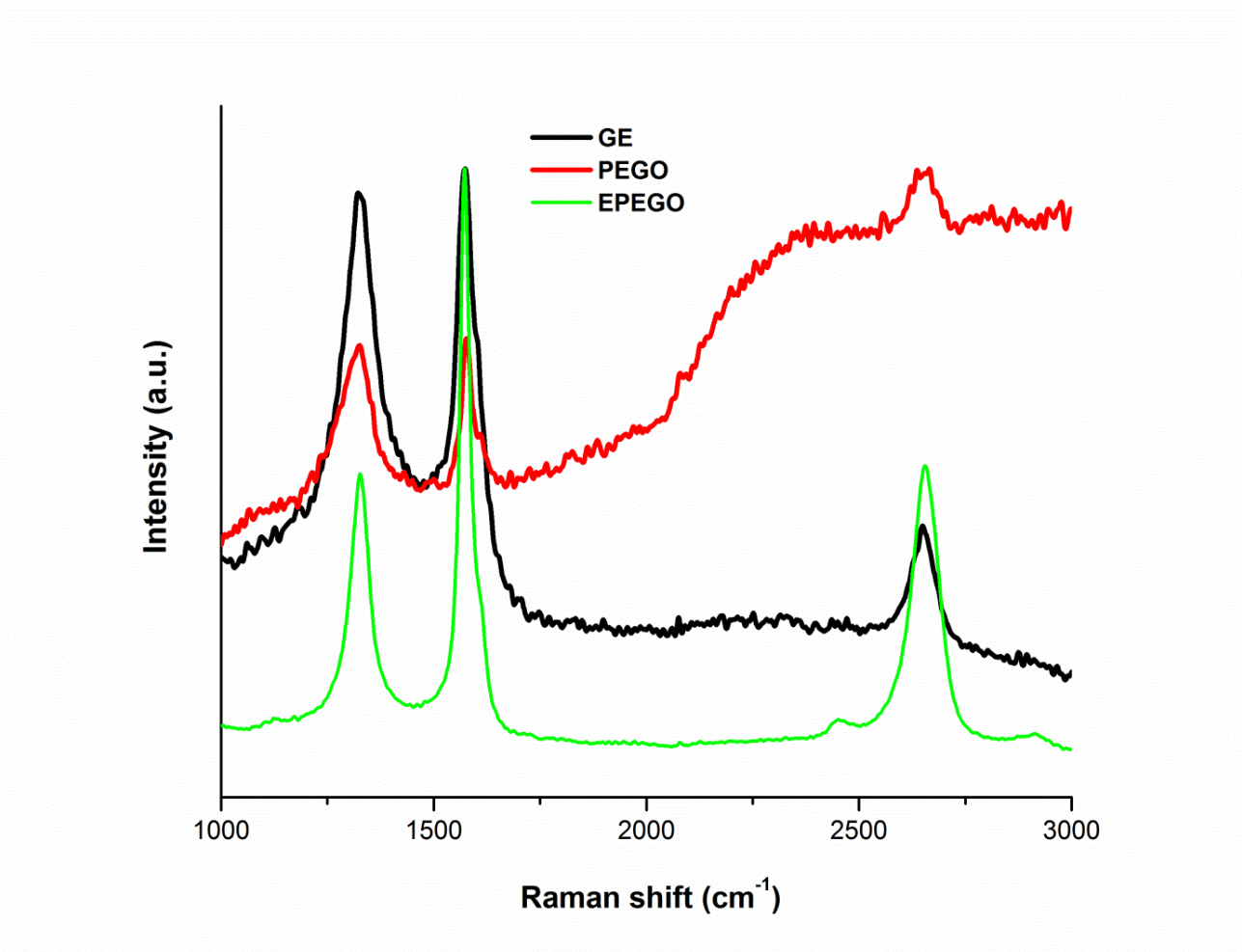

Figure 3-7. Raman spectra of the GE, PEGO, and EPEGO samples.

Fig.3-7 displays Raman spectra of the GE, PEGO, and EPEGO samples, revealing their D (defect), G (graphite), and 2D (doubly generated G) bands at 1325, 1570, and 2658 cm^{-1}, respectively. [83,84] The D band of the GE has relatively high intensity, suggesting that the GE sample featured some defect structures, such as disordered carbon structures or impurities,[85] consistent with the XRD data. The peak positions of the D and G bands of the EPEGO sample are similar to those of the GE and PEGO samples, but the I_D/I_G intensity ratio for the EPEGO (0.53) was significantly lower than those (0.97) for both the GE and PEGO. Moreover, the intensity and sharpness of the G band of the EPEGO both increased significantly relative to those of the GE and PEGO samples, suggesting that disordered C structures, such as sp^3-hybridized C atoms, had been removed partially and that graphitic domains had been restored in the EPEGO sample during the ultrasonication process. In addition, the 2D band for EPEGO consisted of a single-Lorentzian 2D peak; its FWHM of approximately 70 cm^{-1} was, however, almost double that (ca. 35 cm^{-1}) of the 2D peak of graphene, consistent with the multilayer features of turbostratic graphene.[86] These results are consistent with the data from previous SEM and HRTEM studies.

The XRD, SEM, AFM, TEM and Raman data suggested that the PEGO served as a good precursor for the preparation of graphite nanoplatelets. Notably, when using VPE we could oxidize graphite without prior purification to remove additives or impurities, into GO within approximately 10 min, in contrast to the typically long treatment times (ca. 100 h) required when using concentrated acid and strong oxidizing agents. Taking into consideration the aspects of user-friendliness and recyclability, this VPE calorific process appears to be a very efficient means of synthesizing GO.

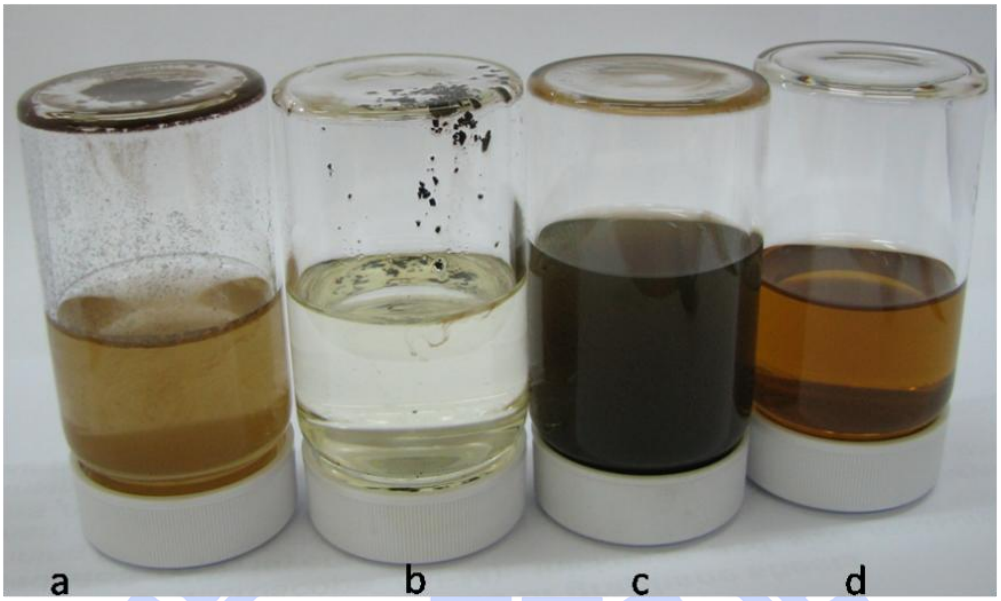

Figure 3-8. Photograph of (a) the dispersion of PEGO in the electrolytic solution, (b) the sample obtained after filtering the sample in (a) through PVDF (pore size: 0.2 μm) and re-dispersion in NMP, (c) the sample obtained after ultrasonication of the sample in (b), and (d) the centrifuged dispersion of PEGO in NMP.

Fig.3-8 displays photographs of dispersions of the PEGO in various solvents after performing the CP process. Fig.3-8a reveals that some of the PEGO obtained from the CP process in the electrolyte solution precipitated to the bottom of the glass vial; Fig.3-8b displays the PEGO sample obtained after filtering and re-dispersing in NMP without ultrasonication; Fig. 3-8c indicates that ultrasonication enabled the dispersion of PEGO in the NMP; and Fig. 8d reveals the clear PEGO/NMP solution obtained after centrifugation. Figs. 8c and 8d indicate that the PEGO solutions were rather homogeneous; they remained stable for long periods of time (12 weeks) with almost no precipitation.

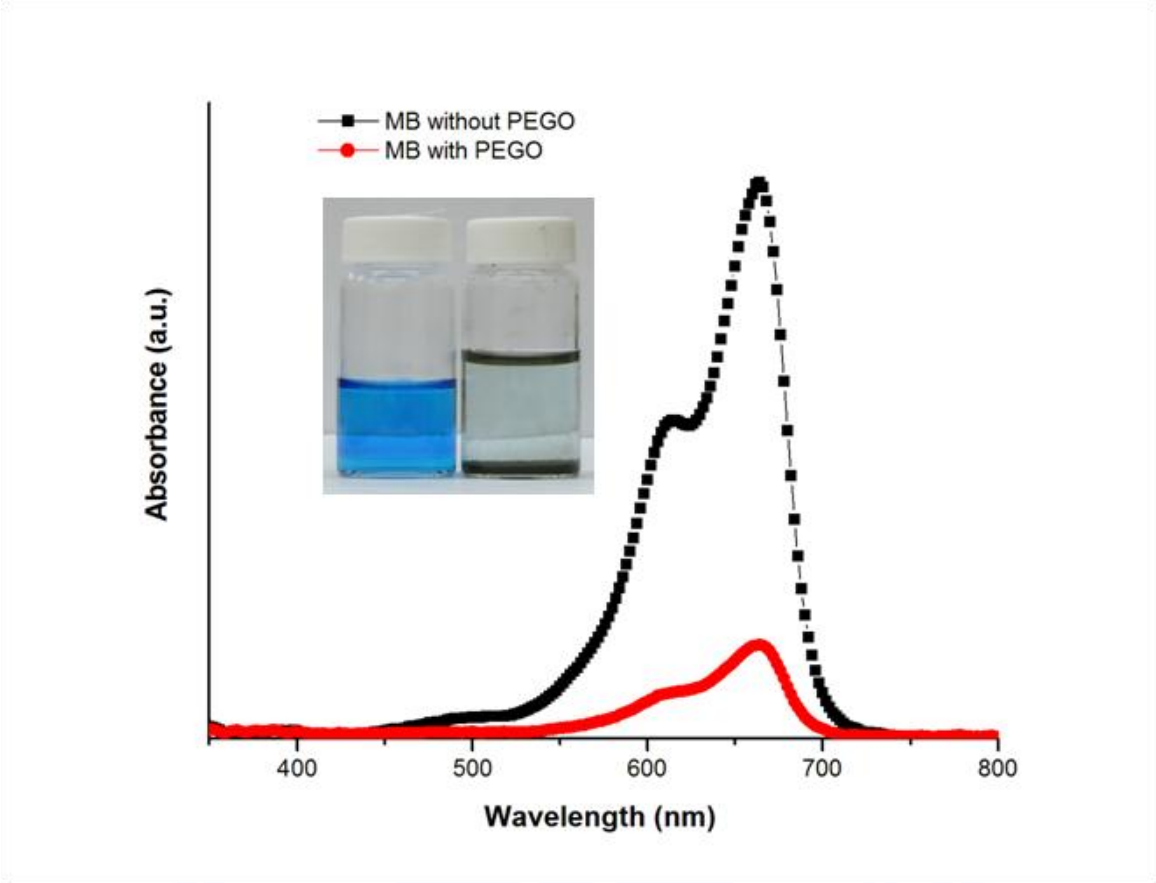

Figure 3-9. UV–Vis spectra of MB solutions in the (red) presence and (black) absence of PEGO; inset: photograph of the (left) original MB solution and (right) MB-adsorbed PEGO solution.

To demonstrate the potential applications of PEGO materials, we applied the PEGO for the removal of Methylene Blue (MB) from aqueous solutions. Because the PEGO had a spheroidal structure, it could form 3D agglomerates with a large surface area,[57] making it a potentially useful absorbent. The inset to Fig.3-9 reveals that an MB solution (10 mg/L, 10 mL), initially displaying a typical blue color, became a pale blue solution 3 h after addition of the PEGO solution (5 mg/mL, 4 mL), revealing that PEGO could remove MB efficiently with most of the MB-

adsorbed PEGO having precipitated to the bottom of the glass container. After decanting the supernatant solution via pipette, we collected the aggregate and dried it at room temperature for 24 h. Notably, we applied the initial PEGO sample without any pretreatment. Fig.3-9 displays UV–Vis spectra of the MB solution in the presence and absence of PEGO. We used the absorbance in each case to calculate the percentage adsorption of MB on the PEGO:

$$\text{Adsorption efficiency} = \left[\left[\frac{(A_i - A_f)}{A_i}\right] \times 100\right] \ [\%] \quad (1)$$

where A_i and A_f are the initial and the final absorbances, respectively. The intensity of the characteristic peak at 665 nm for the MB solution that had been treated with the PEGO was dramatically lower than that of the pristine MB solution, indicating a significant drop in the concentration of MB in the solution; the removal efficiency, determined using equation (1), was 97%. Therefore, our PEGO material appears to be a promising adsorbent for the removal of dyes or pigments, such as MB, from aqueous solutions.

3-4. Conclusions

Our characterization data reveal that swelled graphite oxide can be obtained from recycled graphite electrodes or even high purity graphite through a combination of cathodic plasma processing and ultrasonication at relatively low temperature, under atmospheric pressure, within a very short period of time, without the need for concentrated acids or strong oxidizing agents. The cathodic plasma process is a very efficient means of producing graphite oxide because it takes advantage of the vapor plasma envelope calorific effect that provides instant

oxidation and expansion of graphite and appears to have great promise because it can be performed using various starting materials (e.g., recycled graphites), at low cost, in a simple setup, and with high efficiency and environmental friendliness. The graphite oxide produced through this process can be used as an effective adsorbent for a removal of Methylene Blue from aqueous solutions and can serve as a suitable precursor for the preparation of graphite nanoplatelets.

Chapter 4: Plasma-assisted electrochemical exfoliation of graphite for rapid production of graphene sheets

Plasma electrolysis can be used to enhance the chemical or physical processes occurring at the electrodes. In this chapter, we describe a new plasma-assisted electrochemical exfoliation method, involving a plasma-generated graphite cathode and a graphite anode, for the production of graphene sheets from graphite electrodes in a basic electrolyte solution in a short reaction time. This method provides a green and fast step toward the mass production of two dimension materials such as graphene.

4-1. Introduction

Graphene sheets (GSs), including graphite nanoplatelets (GNPs), graphite nanosheets (GNs), exfoliated graphite (EG), and multiple-layer graphene, are nanometer-scale platelets that comprise of a few layers of planar graphene with platelet thicknesses ranging from 0.34 to 100 nm.[16,18,87] Recently, GSs have attracted great interest because of their extraordinary properties and their potential applications in energy storage,[4,46-49] composites materials,[12,50,51,55,88] and polymer/GNP nanocomposites.[59,89-91] The methods through which GSs are synthesized determine their structures and, therefore, can influence their practical applications.[12,88,92-94] Several methods have been developed for the preparation of GSs, including chemical vapor deposition,[62] discharging,[7,8] mechanical milling,[9,10] liquid-phase exfoliation of graphite,[68,95] chemical reduction of exfoliated graphite oxide (GO),[69,96] and electrochemical exfoliation.[5,6,22,30,97-101] Among them, the electrochemical exfoliation of graphite is one of the simplest and most convenient methods for the large-scale production of GSs.

Plasma electrolysis, when the applied voltage is greater than the threshold voltage in electrochemical reactions, a strong electric field was generated near the working electrode, can be used to enhance the chemical or physical processes occurring at the electrodes. Herein, we describe a highly efficient plasma-assisted electrochemical exfoliation method, involving a plasma-generated graphite cathode and a graphite anode, for the production of graphene sheets from electrodes in a basic electrolyte solution in a short reaction time. This method provides a greener step toward the mass production of graphene. Up to now, we are unaware of any previous reports of the preparation of graphene sheets through electrochemical exfoliation involving plasma.

In the present study, a much larger potential, 60V, as compared to 5-10V in the case of conventional electrochemical method, is applied to the high-purity graphite (HG) cathode that maintain its tip barely above the basic electrolyte, a solution containing a mixture of KOH and $(NH_4)_2SO_4$, different from conventional electrochemical cells,[6,22,25] while the rod-HG anode is submerged in the electrolyte. Discharge can be initiated by lowering the cathode to touch the surface of the electrolyte. Because the surface contact area of cathode in the electrolyte is much smaller than that of the anode, an extremely high electric field is generated near the cathode surface that is in contact with the electrolyte. Simultaneously, hydrogen gas bubbles evolved from the hydrolysis of the water in the electrolyte near the surface contact area of the cathode tip. As a result of an instant ionization of hydrogen gas bubbles by the presence the high electric field near the cathode tip, the onset of plasma around the cathode tip takes place (see experimental section).

4-2. Experimental

4-2.1. Preparation of plasma- electrochemically exfoliated graphene (PEEG)

The electrolytic solution, comprising KOH (5%, 200 mL) and $(NH_4)_2SO_4$ (2.5%, 40 mL) at a pH of approximately 12, was preheated to an initial temperature of 70 °C. A cylindrical high-purity graphite rod (HG) was used as the cathode connected to a voltage supply unit (negative voltage output); the cathode diameter and length were 6 and 100 mm, respectively. Another HG rod (diameter: 6 mm; length: 150 mm) was used as the anode in the electrochemical system for the plasma-assisted electrochemical exfoliation process (PEEP). The HG tip surface cathode was placed about 1 mm above the surface of the electrolytic solution, while the anode was submerged in the electrolytic solution. Both electrodes were connected to a regulated DC power supply (TES-6220) with the bias voltage increased gradually to 60 V, resulting in discharging plasma in the area adjacent to the HG tip surface cathode and the electrolytic solution. The temperature of the solution within the beaker was measured during the process using a conventional mercury thermometer; it was maintained at approximately 70–80 °C. To enhance exfoliation and the homogeneity of the reaction, a magnetic stirrer was placed in the beaker with its rate of spinning maintained at 200 rpm. When a sufficiently high potential of 60 V was applied across the two electrodes, electrochemical oxidation reactions were triggered with the simultaneous release of gases on the surface of anode and the generation of plasma on the HG tip surface cathode (see movie in SI); as a result, the surface of the graphite electrodes slowly disintegrated into micrometer-sized sheets and dispersed into the electrolyte. The tip position of the cathode was lowered to maintain an approximate current range from 0.6 to 1.2 A. The length of time in which the samples experienced simultaneous treatment was 5 min. Fig.4-1a provides a schematic representation of the equipment setup. After cooling to room temperature, the resulting exfoliated graphite flakes were collected through vacuum filtration of the solution through PVDF membranes (average pore size: 0.2 μm) supported on a fritted glass holder. The prepared

products were washed with DI water and dried at 50 °C under vacuum for 24 h. After peeling off the PVDF membrane, the powder prepared from PEEP, described herein as plasma- electrochemically exfoliated graphene (PEEG) was stored in a drying box at 50 °C until required for use. For conventional electrochemical method, two HG rod is dipped into electrolyte, one electrode is biased positively, and other electrode is biased negatively. The graphene sheets produced from this mode named EEG.

4-2.2. Preparation of PEEG dispersion

The obtained PEEG (15 mg) was added to N-methyl-2-pyrrolidone (NMP, 15 mL) to create PEEG dispersion (1 mg/mL) when treated with an ultrasonic cleaning bath, operated at 20 kHz and a power of 130 W for 10 min.

4-2.3. Measurements and Characterization

The structures of the HG and the PEEG powders were examined using a D2 X-ray diffractometer equipped with a Cu K_α tube and a Ni filter (λ = 0.1542 nm). Raman spectra of these samples were recorded using a high-resolution confocal Raman microscope (HOROBA, Lab RAM HR) and a 514.5 nm Ar laser source. High-resolution transmission electron microscopy (HRTEM) images were recorded using a JEOL 2100F apparatus operated at 200 kV; for HRTEM measurement, a few drops of the HG or PEEG dispersion were placed on a Cu grid presenting an ultrathin holey C film. Scanning electron microscopy (SEM) was performed using a JEOL JSM-6500F scanning electron microscope operated at 15 kV. For preparation of the SEM sample, a PEEG dispersion was filtered through an AAO membrane (Anodisc; diameter: 47 mm; nominal pore size: 0.02 μm); the solids were then dipped in EtOH to remove residual NMP; the flakes that floated on the surface of the EtOH were collected on a Si substrate for SEM measurement.

4-2.3. Results and discussion

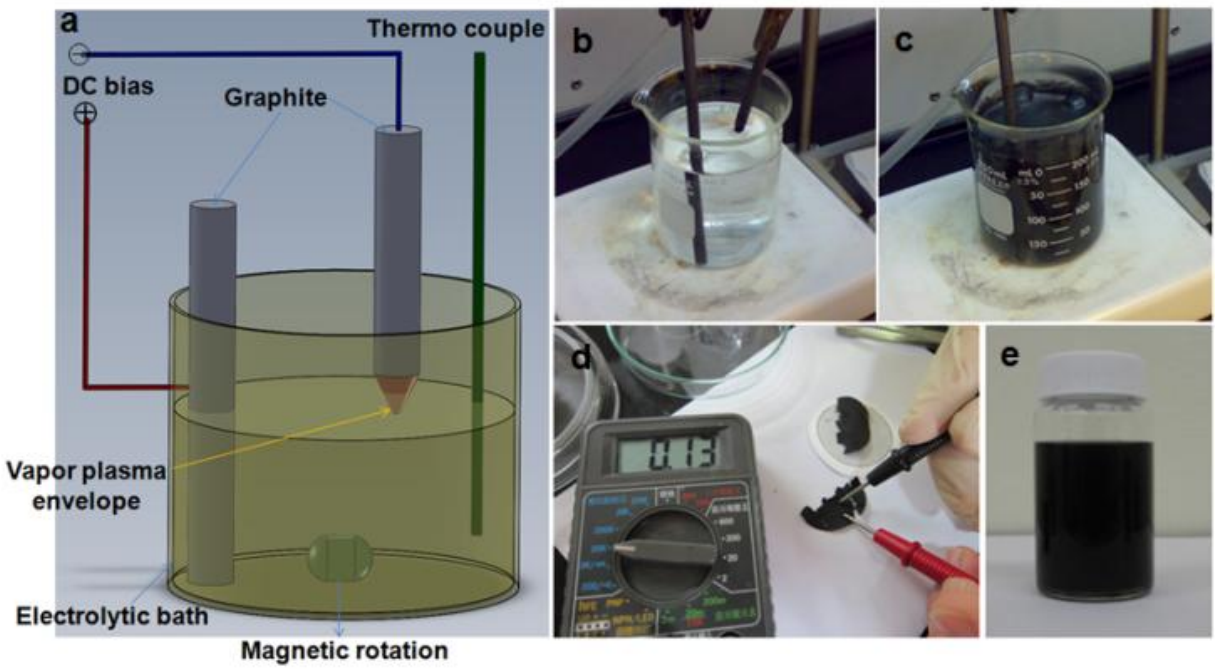

Figure 4-1. (a) Schematic representation of the equipment used for PEEG. (b–e) Photographs of (b, c) the electrolytic solution (b) before and (c) after plasma-assisted electrochemical exfoliation process; (d) the PEEG-based graphene film prepared through vacuum filtering of the electrolyte after plasma-assisted electrochemical exfoliation process; and (e) a dispersion of PEEG in an NMP solution.

Fig. 4-1(a) show a schematic representation of the equipment used for production of the plasma-electrochemically exfoliated graphene sheets (PEEG). Figs. 4-1b and 4-1c display images of the electrolyte at various times during the PEEG, revealing a change in color, from colorless to dark, after only 5 min (see movie in the SI), suggesting a high exfoliation rate when using this method. Fig. 4-1e displays a photograph of the PEEG dispersion in NMP after settling for 6 h; this sample exhibited good dispersion and homogeneity and was stable for a period of

72 h. In addition, the PEEG-based graphene film prepared through vacuum-filtering of the electrolyte after plasma-assisted electrochemical exfoliation process exhibited good conductive properties with resistance of 130 Ω (Fig.4-1d) and sheet resistance of 121 Ω. per square area with a four-probe method. This graphene film might have been compressed during filtration, resulting in re-agglomeration of graphene nanosheets.

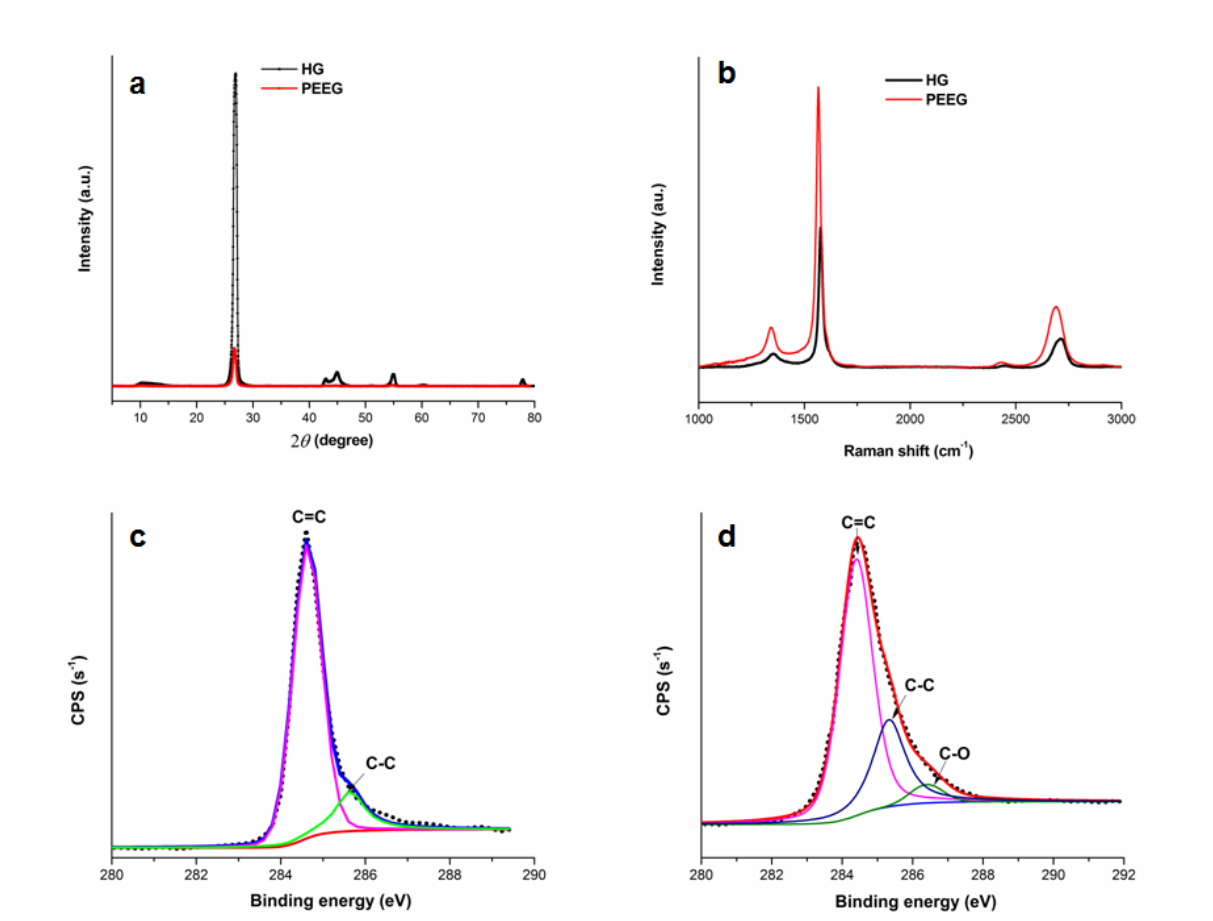

Figure 4-2. (a) XRD patterns and (b) Raman spectra of HG and PEEG and (c, d) XPS spectra (C 1s signal) of (c) HG and (d) PEEG.

Fig. 4-2a displays X-ray diffraction (XRD) patterns of the high purity graphite (HG) and PEEG; that of the HG displays a characteristic sharp, high-intensity (002) peak at a value of 2θ of 26.6° and three small peaks at values of 2θ of 42.8, 44.6, and 54.6°, corresponding to the 100, 101, and 004 reflections, respectively. After the HG had experienced plasma-assisted electrochemical exfoliation process, the intensity of the characteristic (002) peak at 26.6° decreased significantly, suggesting that the graphitic lattice of HG had changed its periodic arrangement in the *z*-direction after exfoliation into graphite flakes. Additionally, the Raman spectra of HG and PEEG (Fig. 4-2b) reveal a structural change from HG to PEEG. The Raman spectrum of HG features a weak D (defect) band, a prominent G (graphite) band, and a broad 2D (doubly generated G) band at 1353, 1579, and 2706 cm^{-1}, respectively, which are characteristic bands of graphite.[83,84] In the Raman spectrum of PEEG, the G band was broader and had shifted to a lower frequency and the D band was more pronounced than that in the spectrum of HG, implying that defects or structural disorder had occurred in the graphitic lattice of PEEG after PEEP. Notably, the 2D band of PEEG had shifted to a lower frequency with a significant increase in intensity relative to that of HG, indicating the formation of graphene structures in PEEG after PEEP.[24,95,99,102,103]

Fig. 4-2c displays the C 1s XPS spectrum of HG; we de-convoluted the C 1s XPS signal into one major peak at 284.4 eV representing C=C bonds (sp^2-hybridized carbon atoms) and a minor peak at 285.5 eV representing C–C bonds (sp^3-hybridized carbon atoms).[79] Fig. 4-2d presents the C 1s XPS spectrum for PEEG; we could de-convolute it into three peaks: the signals of PEEG at binding energies of 284.4 and 285.5 eV represent non-oxygenated carbon components—C=C (sp^2-hybridized carbon atoms) and C–C (sp^3-hybridized carbon atoms) bonds, respectively—while the other at 286.4 eV represents oxygenated C–O components

(i.e., hydroxyl and epoxy units). The intensity and sharpness of the graphitic C=C/C–C signals decreased and widened significantly relative to those of the HG sample, implying that some oxygen-containing functional groups had attacked the C=C bonds in the graphite to generate C–O bonds, resulting in their partial oxidation.[79]

Table 4-1 lists the calculated amounts of the various functional groups in the HG and PEEG samples, based on the areas under these XPS peaks. The atomic percentage ratio of oxygen to carbon atoms in the PEEG [as determined from the small content of C–O bonds (ca. 4.2%)] was approximately 1:22.8, confirming that very slight oxidation occurred during our PEEP process. Notably, strong oxidation could yield graphite oxide–like structures when increasing concentration of electrolyte, changing HG anode into a stainless-steel grid with much higher surface area than that of cathode in which the vapor plasma envelope calorific effect provided instant oxidation and expansion of graphite for producing plasma-expanded graphite oxides from HG.[104]

Table 4-1. Relative atomic percentages of carbon atoms in various functional groups in HG and PEEG, estimated based on the areas under the C 1s peaks.

	C=C (%)	C–C (%)	C–O (%)
HG	84	16	
PEEG	68	27.8	4.2

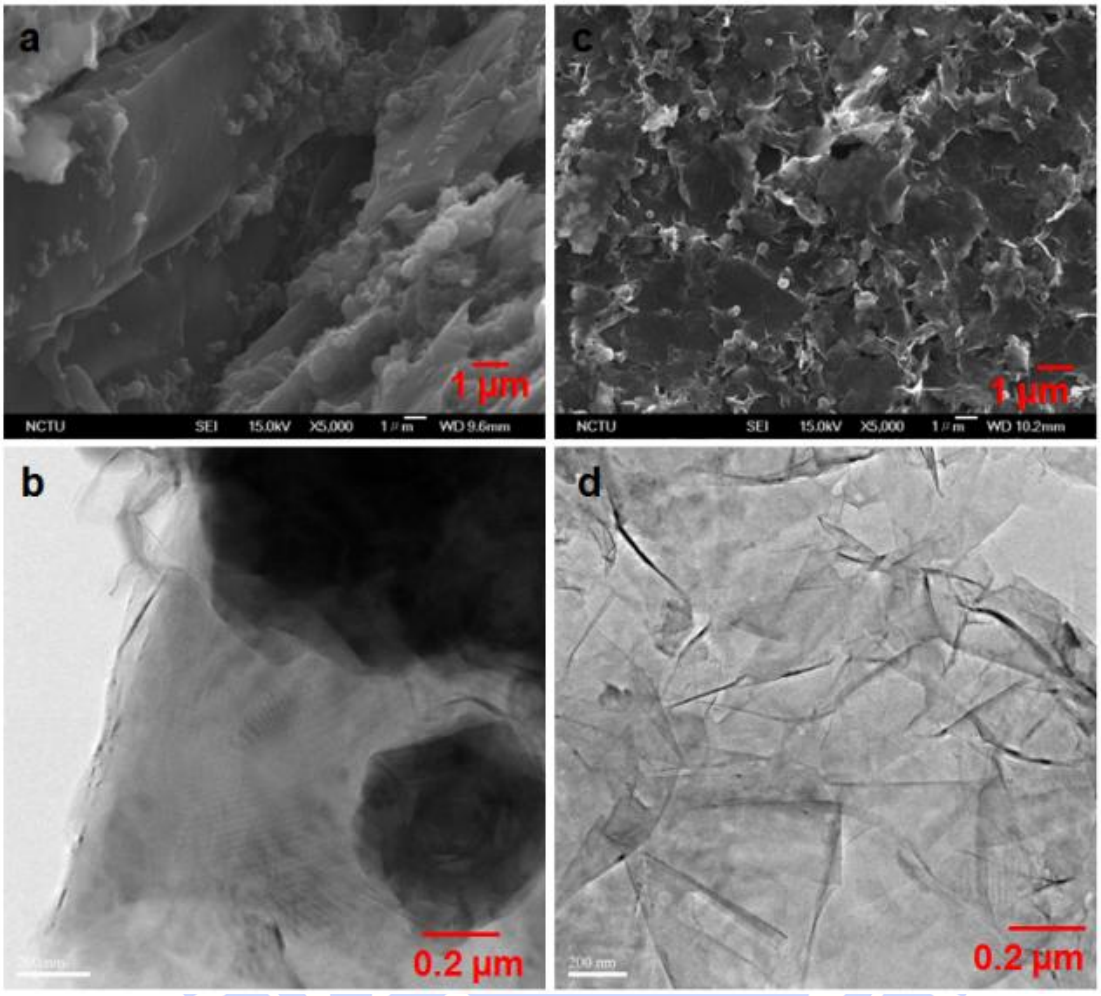

Figure 4-3. SEM (a, c) and TEM (b, d) images of (a, b) HG and (c, d) PEEG.

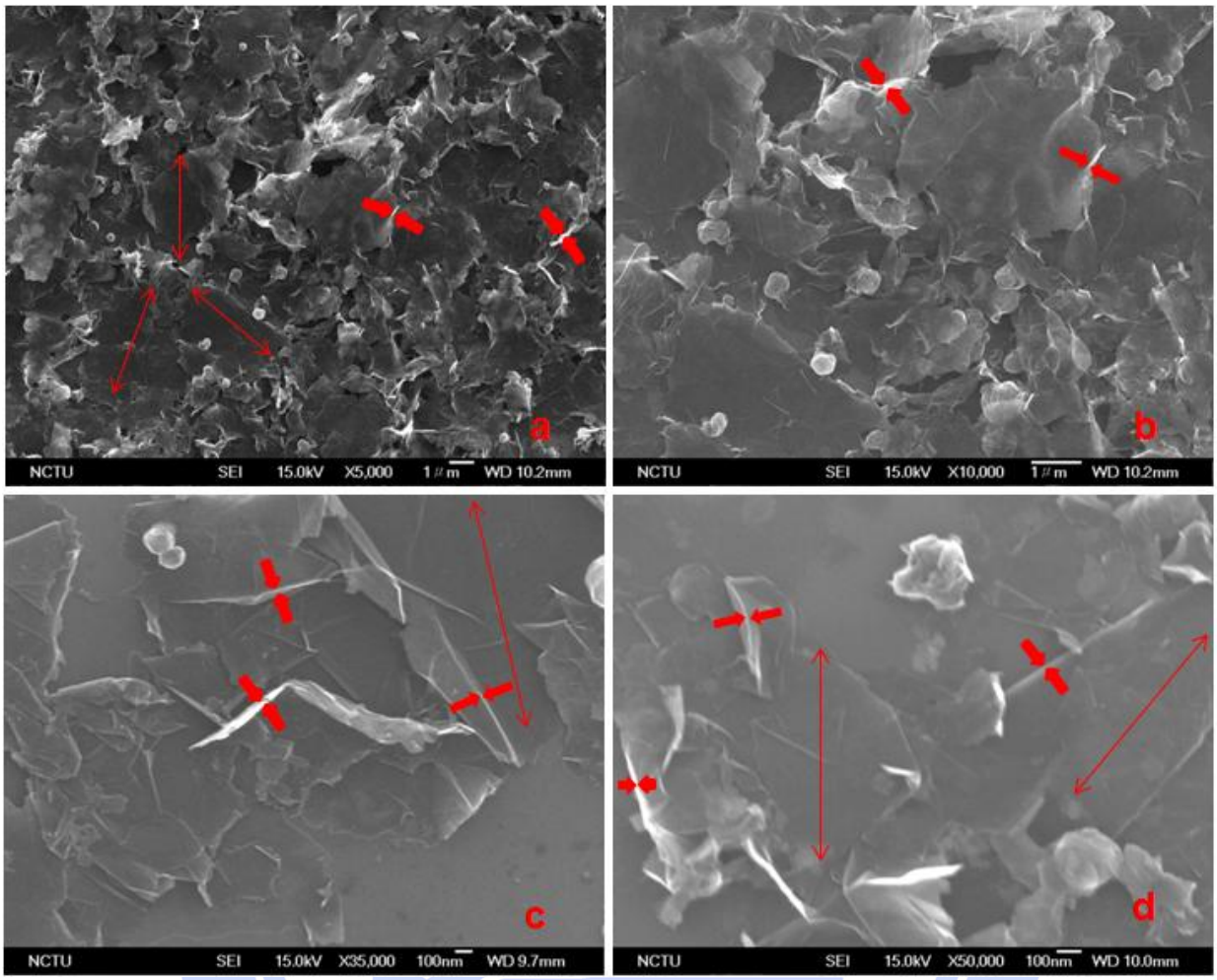

Figure 4-4. SEM images of flattened or scrolled PEEG (b, c, d) high-magnification images; Two arrows pointing in opposite directions indicate the thickness of PEEG that was on the surface of the Si/SiO_2 substrate.

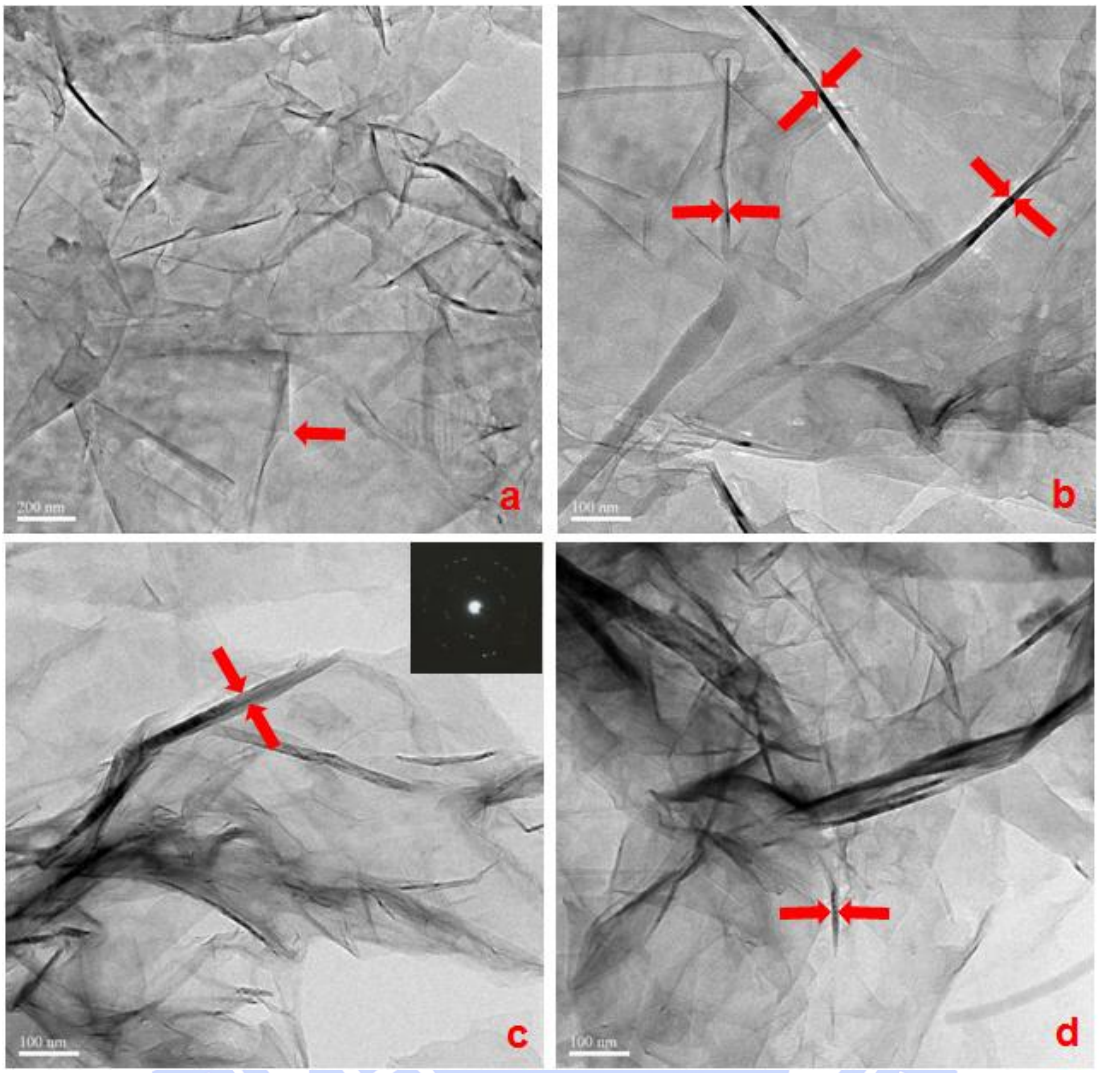

Figure 4-5. TEM images of flattened or scrolled PEEG, inset: corresponding SAED pattern. Two arrows pointing in opposite directions indicate the thickness of PEEG that was on the top of the copper grid.

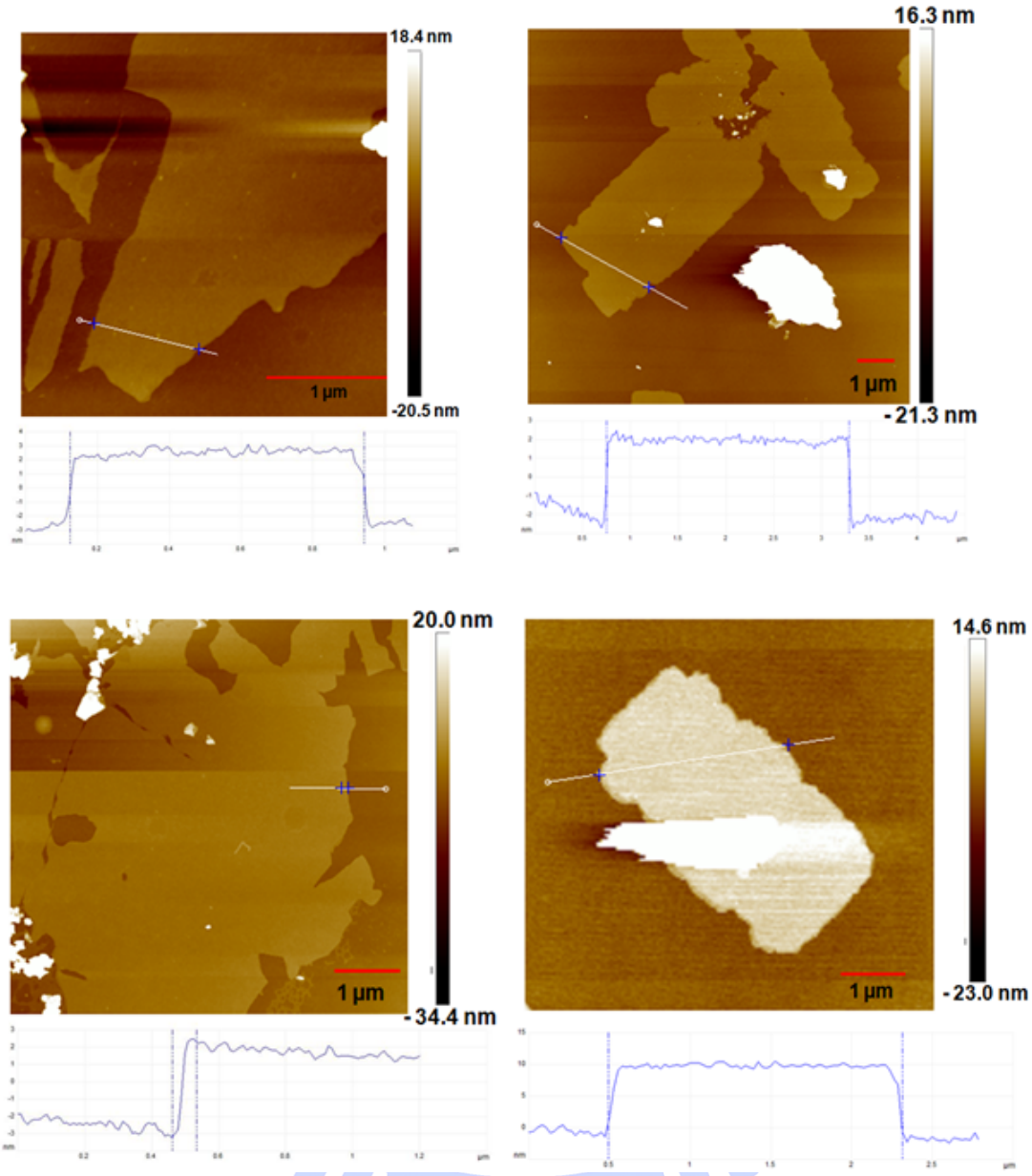

Figure 4-6. AFM images and height profile of a PEEG sample deposited on a Si/SiO_2 substrate.

Fig. 4-3 presents SEM and TEM images of the HG and PEEG samples that were collected after filtration with PVDF film and dispersed in NMP, respectively;

they indicate a dramatic change in morphology in the prepared samples. The HG comprised thick, bulk graphite flakes that transformed into thinner nanometer-scale platelets after after plasma-assisted electrochemical exfoliation process. We also observed scrolled graphene sheets, as indicates by the arrows in Fig. 4-4 and Fig. 4-5, where in the folded regions, the thickness of layers could be approximately determined (see high-magnification images of the folded regions in Fig. 4-4 and Fig. 4-5). Image analyses based on PEEG sheets revealed that the average lateral dimensions was approximately 2.5 μm with a thickness of approximately 10–30 nm, close to the dimensions of a nanoplatelet;[16,89] based on cross-sectional imaging of the folded edges of PEEG after tilting the sample from 0 to 25°; furthermore, Fig.4-6 shows the AFM image of the samples prepared from a diluted solution, revealing in a lateral dimension of approximately 0.5–2.5 μm and a thickness of approximately 2.5 nm, corresponding to approximately seven layers of graphene, based on an interlayer spacing of 0.34 nm, confirming the formation of graphene sheets. The exfoliated graphite flakes have a tendency to aggregate and stack on each other after drying on the surface of Si/SiO_2 substrate and copper grid when they are used for SEM and TEM observation, resulting in different thickness values obtained using SEM/TEM and AFM imaging.

Table 4-2. Comparison between graphene sheets produced with plasma-assisted and conventional electrochemical exfoliation methods

Electrochemical method	Experimental conditions KOH (5%, 200 mL) and $(NH_4)_2SO_4$ (2.5%, 40 mL), 80˚C, 5 min	Average graphene sheet diameter (μm)	Thickness of a single nanoplatelet (nm)	Potential applied	Yield of product (filtrated with 200nm PVDF)
Plasma-assisted	HG tip cathode barely above the surface of electrolyte. HG rod anode submerged in electrolyte.	2.5	2.5	–60 V (I ~ 1.2 A)	32 mg
Conventional	HG rod submerged in electrolyte.	2.0	3.5	9.3 V (I ~ 3.1 A)	5 mg

Table 4-2 displays a comparison between the PEEG that were produced with the plasma-assisted electrochemical method and a conventional electrochemical method and indicates the production rate of graphene sheets is six times as fast as that obtained from the conventional electrochemical method, 32mg vs. 5mg in five minutes. Moreover, the PEEG produced are larger and thinner than that fabricated by the conventional electrochemical method (see Fig. 4-7), suggesting that the plasma-assisted electrochemical exfoliation method appears to be a very efficient means of synthesizing graphene sheets.

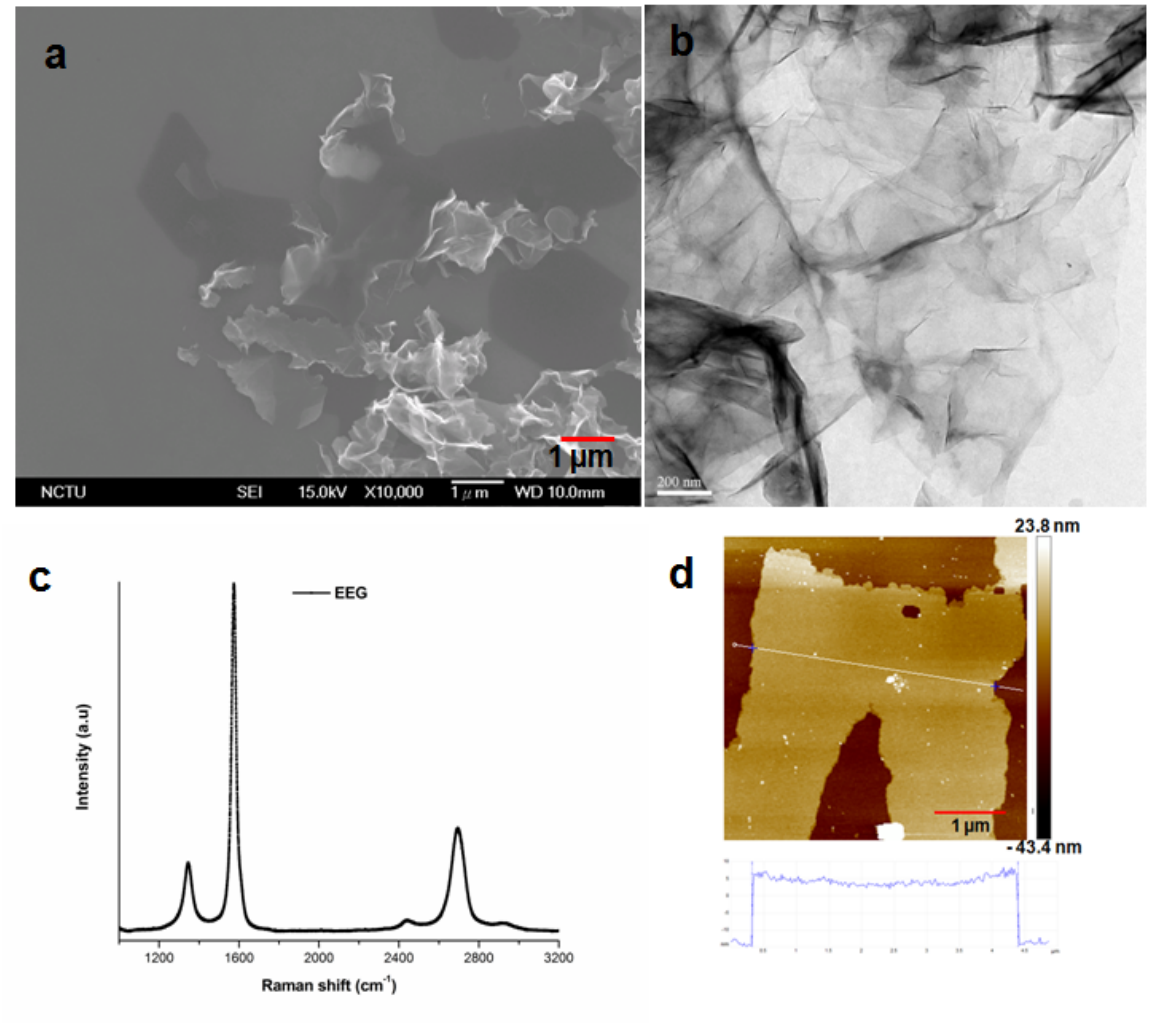

Figure 4-7. (a) SEM high-magnification and (b) TEM images of electrochemically exfoliated graphene sheets (EEG), (c) Raman spectra of EEG, and (d) AFM image and height profile of a EEG sample deposited on a Si/SiO_2 substrate.

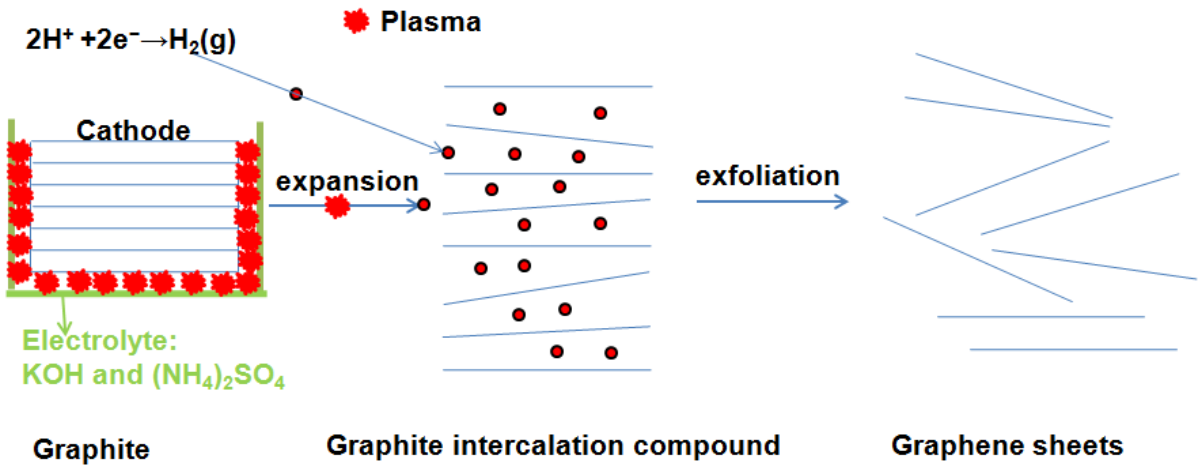

Figure 4-8. Proposed mechanisms for the formation of PEEG.

Fig. 4-8 depicts the mechanism of the formation of graphene sheets from graphite. We suspect that rapid hydrogen bubble evolution (hydrolysis of water) in the cathode played a role in the exfoliation of the graphite as depicted in Fig 4-8: first, a violent release of hydrogen gas on the tip of the HG surface cathode results in opened up the edge sheets of the its surface and facilitated the intercalation of hydrogen gas into the graphite layers, forming graphite intercalation compounds, as a result of these expansion processes, the van der Waals forces between the graphitic sheets weakened. Second, in the plasma the temperature could instantaneously reach above 2000 °C within a short period of time (e.g., $<10^{-6}$ s)[35] on the HG tip surface during discharging, thermo-mechanical stresses occurred on this surface. A combination of these two factors induces the expansion and sequential exfoliation of the surface layer of the thick graphite cathode into smaller and thinner graphene sheets. Furthermore, electrochemical reactions on the surface of anode could induce exfoliation directly from graphite electrode, producing a small portion of graphene sheets from the starting graphite. Thus, our

method is a new route toward the production of graphene sheets from both electrodes simultaneously in a basic electrolyte medium.

4-3. Conclusion

Graphene sheets with good dispersion in solvents can be prepared through plasma-assisted electrochemical exfoliation process at moderate temperatures without the need for acidic media. This method is quite promising because of its simple setup, environmentally benign, and rapid throughput.

Chapter 5: The influence of electrolytic concentration on morphological and structural properties of plasma-electrochemically exfoliated graphene

5-1. Introduction

As follows from the previous chapter, electrochemical methods are considered as cheap, scalable product and can be operated under mild conditions. However, the electrochemical exfoliation of graphite to form graphene sheets by the insertion of bulky ions from electrolytes to the anode and the process is expected to be time-consuming, using harsh chemicals (acid electrolyte) or expensive ionic-based electrolytes. Thus, the development of efficient, facile and practical processing methods is essential and urgent.

Previously,[105,106] I adopted a highly efficient cathodic plasma (CP) process in which the vapor plasma envelope calorific effect provides instant oxidation and expansion of graphite for producing plasma-expanded graphite oxides or graphene sheets from recycled graphite electrodes or high purity graphite, within a reaction time of 10 min without the need for strong oxidants or concentrated acids —a first green step toward the mass production of graphene sheets. However the effect of processing parameters on plasma-assited electrochemical exfoliation of graphite such as the influence of electrolytic concentration on morphological and structural properties of the as-prepared graphene has not yet been properly investigated. Therefore, it is critical to study systematically these issues for identifying how plasma contributes to exfoliation and applies this knowledge for producing of other nanomaterials, such us, MoS_2, TiS_2.

5-2. Experimental

5-2.1 Preparation of plasma- electrochemically exfoliated graphene (PEEG)

The electrolytic solution, comprising KOH (5%, 10%, 15%, 20%, 200 mL) and $(NH_4)_2SO_4$ (5%, 25 mL) at a pH of approximately 14 was preheated to an initial temperature of 70 °C. A cylindrical high-purity graphite rod (HG) was used as the cathode connected to a voltage supply unit (negative voltage output); the cathode diameter and length were 6 and 100 mm, respectively. Another HG rod (diameter: 6 mm; length: 150 mm) was used as the anode in the electrochemical system for the plasma-assisted electrochemical exfoliation process (PEEP). The HG tip surface cathode was placed about 1 mm above the surface of the electrolytic solution, while the anode was submerged in the electrolytic solution. Both electrodes were connected to a regulated DC power supply with the bias voltage increased gradually to 60 V, resulting in discharging plasma in the area adjacent to the HG tip surface cathode and the electrolytic solution. The temperature of the solution within the beaker was measured during the process using a conventional mercury thermometer; it was maintained at approximately 70–80 °C. To enhance exfoliation and the homogeneity of the reaction, a magnetic stirrer was placed in the beaker with its rate of spinning maintained at 200 rpm. When a sufficiently high potential of 60 V was applied across the two electrodes, electrochemical oxidation reactions were triggered with the simultaneous release of gases on the surface of anode and the generation of plasma on the HG tip surface cathode (see movie in SI); as a result, the surface of the graphite electrodes slowly disintegrated into micrometer-sized sheets and dispersed into the electrolyte. The tip position of the cathode was lowered to maintain an approximate current range from 0.6 to 1.7 A. The length of time in which the samples experienced simultaneous treatment was 5 min. Fig. 4-1a provides a schematic representation of the equipment setup. After cooling to room temperature, the resulting exfoliated graphite flakes were collected through vacuum filtration of the solution through PVDF membranes (average pore size: 0.2 μm) supported on a fritted glass holder.

The prepared products were washed with DI water and dried at 50 °C under vacuum for 24 h. After peeling off the PVDF membrane, the powder prepared from PEEP, described herein as plasma-electrochemically exfoliated graphene (PEEG) was stored in a drying box at 50 °C until required for use. The as-prepared sample from varied concentration KOH (5%, 10%, 15%, 20%, 200 mL) is named PEEG 5, 10, 15, 20, respectively.

5-2.2 Preparation of PEEG dispersion

The obtained PEEGs (20 mg) was added to *N*,*N*-dimethylformamide (DMF, 20 mL) to create PEEG dispersion (1 mg/mL) when treated with an ultrasonic cleaning bath, operated at 20 kHz and a power of 130 W for 20 min.

5-2.3 Measurements and Characterization

Raman spectra of these samples were recorded using a high-resolution confocal Raman microscope (HOROBA, Lab RAM HR) and a 514.5 nm Ar laser source. High-resolution transmission electron microscopy (HRTEM) images were recorded using a JEOL 2100F apparatus operated at 200 kV; for HRTEM measurement, a few drops of the HG or PEEG dispersion were placed on a Cu grid presenting an ultrathin holey C film. Scanning electron microscopy (SEM) was performed using a JEOL JSM-6500F scanning electron microscope operated at 15 kV. For preparation of the SEM sample, a PEEG dispersion was filtered through an AAO membrane (Anodisc; diameter: 47 mm; nominal pore size: 0.02 μm); the solids were then dipped in EtOH to remove residual DMF; the flakes that floated on the surface of the EtOH were collected on a Si substrate for SEM measurement. XPS were performed using the facilities at National Synchrotron Radiation Research Center, Hsinchu, Taiwan. The photoelectron spectroscopy experiments were performed at the 09A2 U5-spectroscopy beamline for XPS. Photon with fixed

energy of 620 eV was used for C1s throughout the XPS experiments. The total energy resolution, including the beamline and energy analyzer, was estimated to be 0.1 eV for C 1s. For preparation of the Raman and XPS samples, PEEG dispersion was dropped-casting on the surface of Si/SiO_2 substrate, followed drying in vacuum at 80 °C for 24h.

5-3. Results and discussion

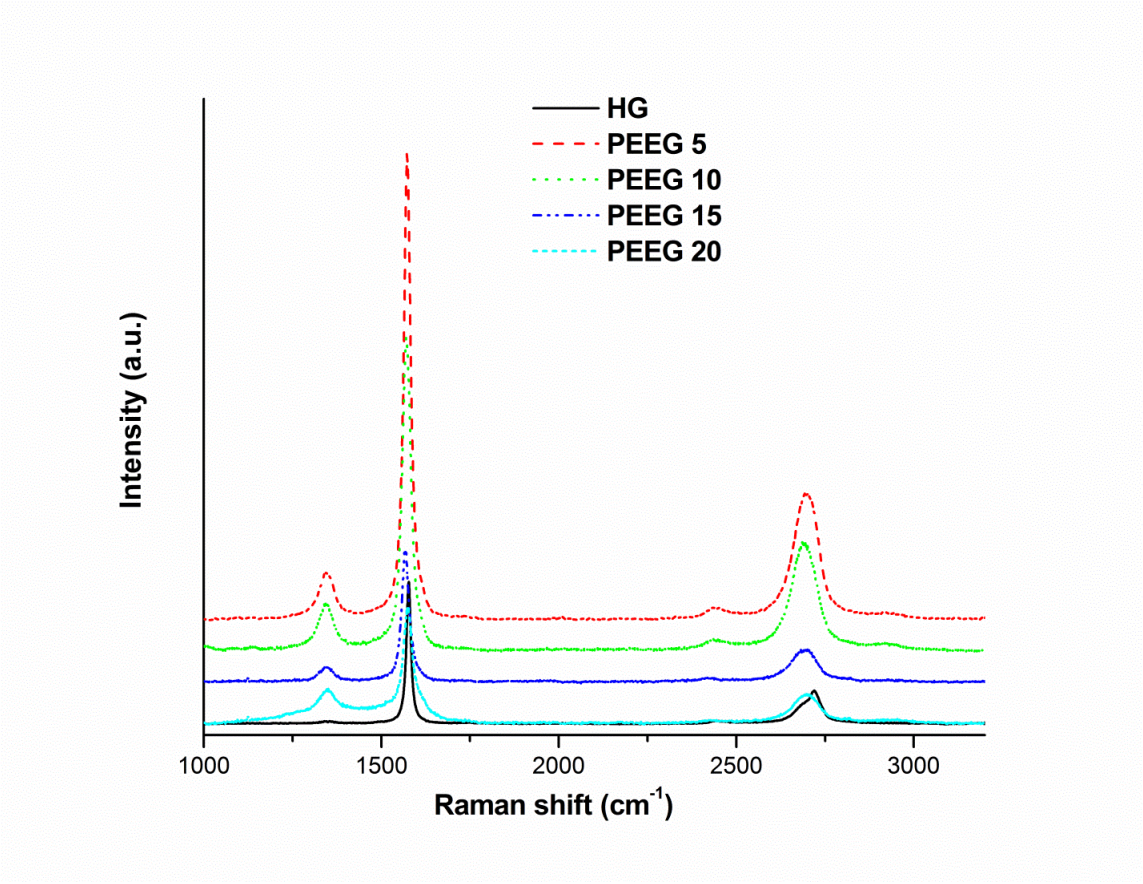

Figure 5-1. Raman spectra of HG and PEEG at different concentrations of KOH

Fig.5-1 displays Raman spectra of HG, and PEEGs at different concentration of KOH, revealing their D (defect), G (graphite), and 2D (doubly generated G) bands at 1342, 1572, and 2695 cm^{-1}, respectively. [83,84] The intensity D band of the PEEGs

is enhanced compare to that of HG, implying that defects or structural disorder had occurred in the graphitic lattice of PEEG, probably due to the reduction in size of the in-plane sp2 domains caused by the oxidation during plasma processing. Moreover, the intensity of the G band was significantly higher than that of the D band for the PEEG 5 and PEEG 10, suggesting a high quality of as-prepared graphene. In addition, the 2D band appears on all PEEGs sample but their intensity significantly changes from PEEG 5 to PEEG 20. Clearly, the 2D of PEEG 15 and PEEG 20 is hardly distinguishable from that of HG while the intensity of their G bands was significantly lower than that of PEEG 5 and PEEG 10. Notably, the 2D band of PEEG5 and PEEG 10 had shifted to a lower frequency with a significant increase in intensity relative to that of HG, particularly with PEEG5, indicating the formation of graphene structures in these samples.[24,95,99,102,103] These observations suggest that the plasma-assisted electrochemical exfoliation of graphite into graphene sheets is likely efficient at PEEG 5 and PEEG 10. We consider that increase concentration of KOH could cause the pitting/corroding of cathodic surface (HG tip), as will be discussed in SEM/TEM images and XPS C1s spectra.

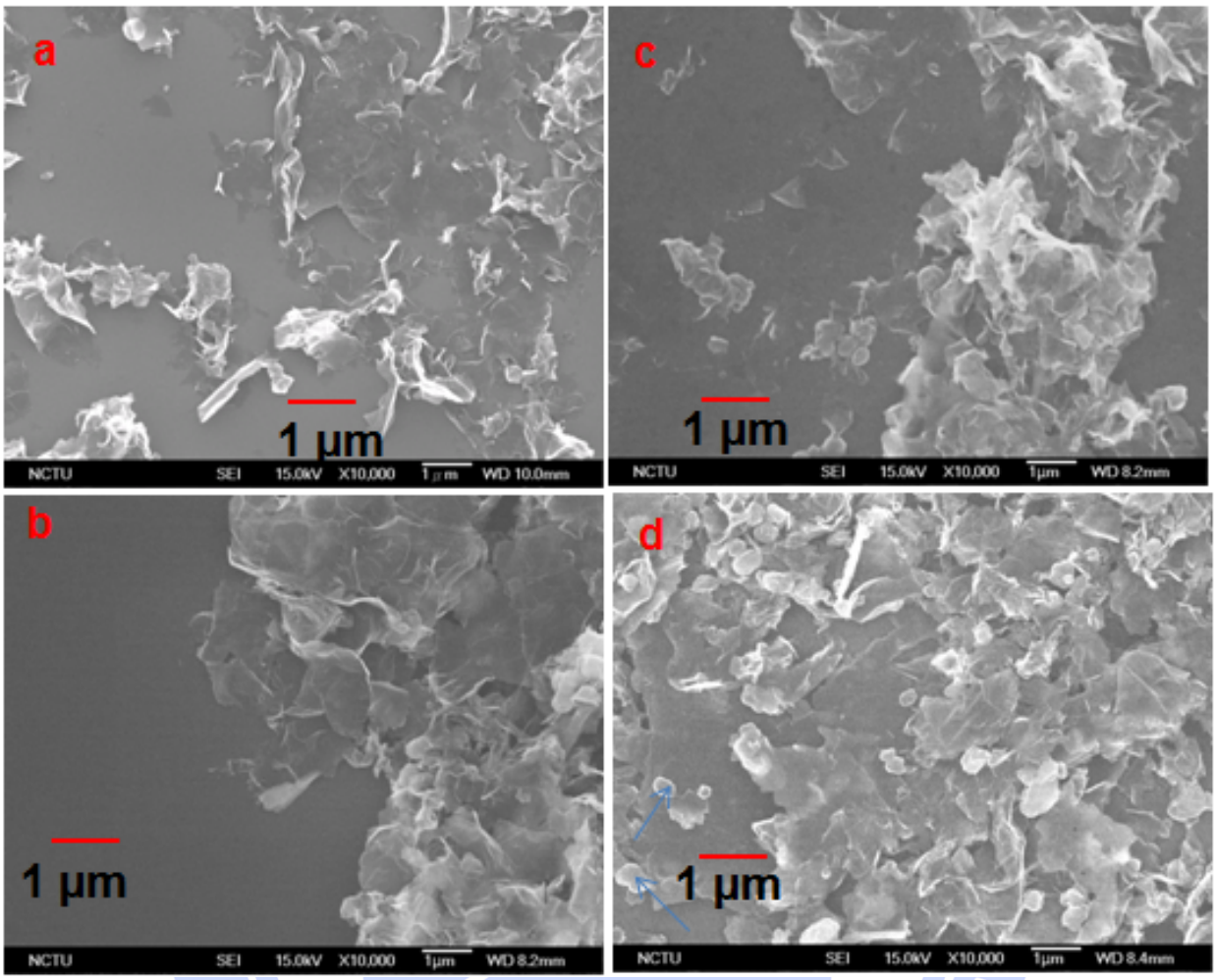

Figure 5-2. SEM images of the (a) PEEG5, (b) PEEG 10, (c) PEEG 15, and (d) PEEG 20

Fig.5-2 presents scanning electron microscopy (SEM) images of the PEEGs at different concentrations of KOH revealing their significantly different morphology. Fig. 5-2a and 2b displays a translucent sheet-like structure with a lateral dimension of approximately 0.5–2.5 μm, and one can easily see the thin sheets of them in these images. Fig.5-2b, 2c reveals that the PEEG 15 and PEEG 20 consisted largely of multilayered graphite clusters and featured a heterogeneous surface, as indicates by the arrows in Fig. 5-2d and Fig.5-3d, which is likely

attributed to the fast quenching in the vicinity of the spaces between the graphene sheets in the VPE-encompassed HG tip when increase concentration of KOH.

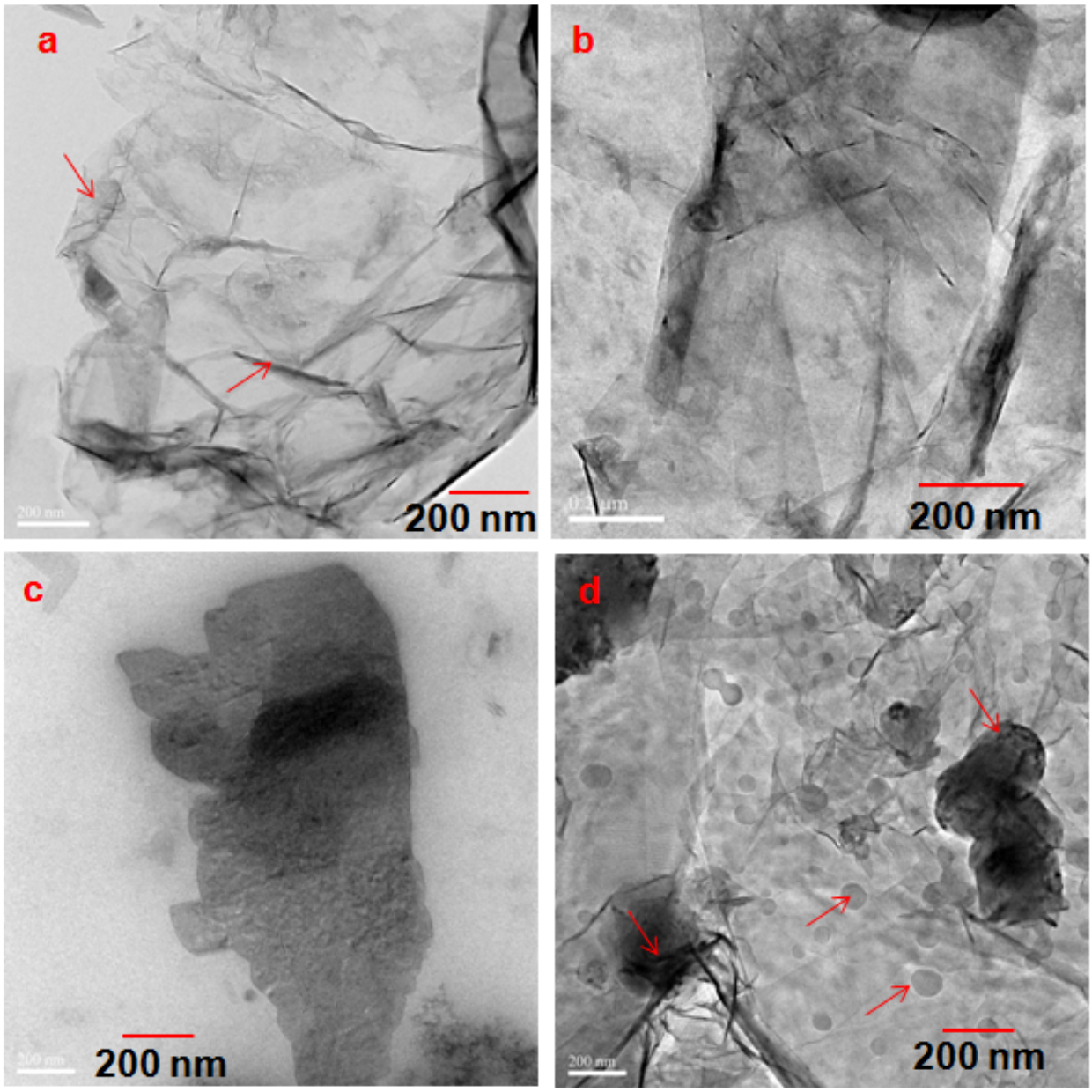

Fig. 5-3. TEM images of the (a) PEEG5, (b) PEEG 10, (c) PEEG 15, and (d) PEEG 20

Fig. 5-3 presents TEM images of the PEEG samples that were collected after filtration with PVDF film and dispersed in DMF, respectively; they indicate a

dramatic change in morphology in the prepared samples. The TEM image of PEEG 5 shows a translucent layer by layer morphology with the lateral size of the flakes is around a few micrometers. We also observed scrolled PEEG5 (Fig. 5-3a) as reported previously.[106] Notably, the color contrast of images changes considerably from PEEG 5 to PEEG 20, and is visible to naked eye, suggesting a thicker thickness of PEEG 15 and PEEG 20, consistent with AFM images and Raman spectra. We suspect that a violent gas release opened up the edge sheets of the HG rod cathode surface and facilitated the intercalation of hydrogen, as well as both oxygen and nitrogen functionalities into the graphite layers, forming graphite intercalation compounds;[97,107] as a result of these intercalation, the van der Waals forces between the graphitic sheets weakened. When a critical level of stress was reached on their outer surfaces, these graphite layers were peeled off effectively, thereby forming graphene sheets from the starting graphite. We briefly consider that the key issue in this exfoliation process is to create a suitable intercalation/oxidation of the graphite to reduce the van der Waals forces between the graphitic sheets weakened while generate a sufficiently strong external force via a violent release of hydrogen gas on the tip of the HG surface cathode as well as thermo-mechanical stresses occurred on this surface to peel off only the oxidized outer side-surfaces of the graphite layers. Therefore, it will be necessary to control the ratio of the surface area between anode and cathode, optimal concentration of the electrolyte and the optimal bias voltage range to ensure the best combination of intercalation and rate of peeling/exfoliating. A combination of these as-mentioned factors induces the expansion and sequential exfoliation of the surface layer of the thick graphite cathode into smaller and thinner graphene sheets.

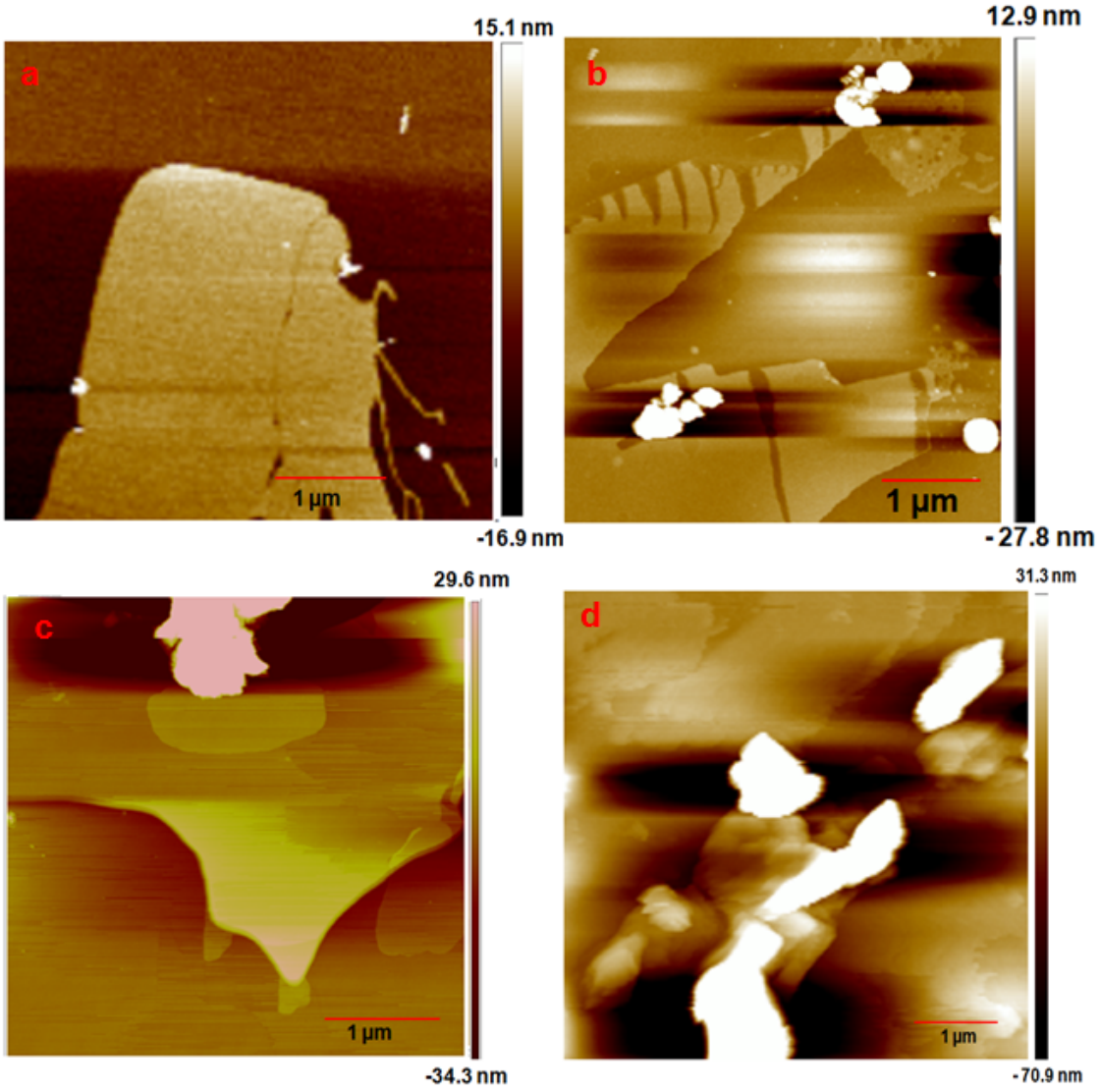

Figure 5-4. AFM images of the (a) PEEG5, (b) PEEG 10, (c) PEEG 15, and (d) PEEG 20

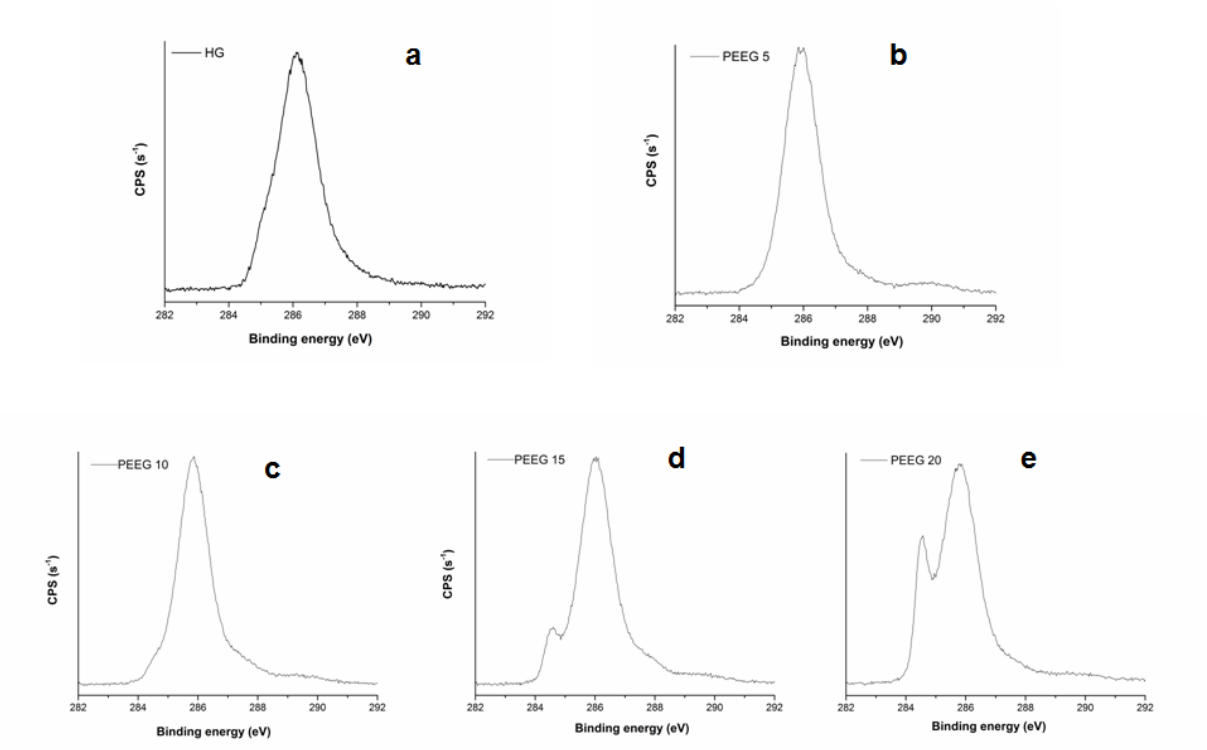

Figure 5-5. XPS spectra C 1s signal of (a) PEEG 5, (b) PEEG 10, (c) PEEG 15, and (d) PEEG 20

Fig. 5-5 displays the C 1s XPS spectrum of HG and PEEGs. To fully realize the influence of electrolytic concentration on morphological and structural properties of plasma-electrochemically exfoliated graphene, a carefully analyze XPS data should be combined with an accurately measure the temperature in the plasma region and the spectrum of the emitting light from it using optical emission spectroscopy (OES) technique together with a high speed rate camera. The process to complete these tasks is underway.

5-4. Conclusions

The results showed that plasma electrochemical exfoliation processing can be effectively used for producing graphene in controllable manner. The exfoliation of graphite into graphene takes places by combination of intercalation and peeling/exfoliating via control the ratio of the surface area between anode and cathode, optimal concentration of the electrolyte and the optimal bias voltage.

Chapter 6: Production of few-layer MoS_2 nanosheets through exfoliation of liquid N_2–quenched bulk MoS_2

Although a wide range of two-dimensional layered materials can generally be prepared using the chapter 2-mentioned methods, but control morphology of product, inclusion of secondary phases and impurities, achieving throughput speed and cost-effective are still big challenge.[41,44] It is still intriguing to search new and effective approaches for producing two-dimensional layered materials from available source material, simple and low cost equipments, and rapid throughput processing. In this chapter, we employed and developed further cracking/quenching phenomenon for the production of few-layer MoS_2 nanosheets through exfoliation of bulk MoS_2 compounds through quenching in liquid N_2. This method also based on breaking van der Waals force similar to exfoliation of graphite, as presented in previous chapter.

6-1. Introduction

MoS_2 nanosheets comprising S–Mo–S layers separated by relatively large van der Waals gaps have attracted considerable attention in the field of two-dimensional materials because of their peculiar structural characteristics and potential applications.[40-42,108-114] Several methods have been developed recently for the preparation of MoS_2 nanosheets, including Scotch tape–based mechanical exfoliation,[115-117] liquid-based exfoliation,[44,118-121] and chemical vapor deposition growth.[16-19,122-126] Among them, controllable solution-based exfoliation through Li^+ ion intercalation and subsequent ultrasonication and exfoliation of the Li^+-intercalated compounds in water or EtOH is one of the most common approaches for the production of MoS_2 nanosheets.[108,127] This method is extremely sensitive to environmental conditions and requires special care during handling, thereby

limiting the scalability of the product. Thus, the challenge remains to develop a facile and efficient approach for the production of high-quality MoS_2 nanosheets in large yield. Herein, we describe a highly efficient, green, and facile approach—involving a quenching process and subsequent ultrasonication—for the synthesis of few-layer MoS_2 nanosheets from MoS_2 powder.

Quenching is one of the most fundamental yet complex processes in the heat treatment of metals; it involves the surface of a sample being suddenly cooled in a solution medium, such as oil or liquid N_2. The instant cooling on the surface induces quenching cracks because of different quenching stresses between the surface and the interior of the sample. In MoS_2, each layer of Mo atoms is sandwiched between two layers of hexagonally close-packed S atoms, with the adjacent layers, bound by weak van der Waals interactions, readily exfoliating into individual MoS_2 nanosheets upon quenching with liquid N_2 and ultrasonication; as a result, we suspected that the quenching cracks phenomenon might be involved in breaking van der Waals force bonded MoS_2 layers in the bulk state to produce MoS_2 nanosheets. Recently, high-quality single and few-layer graphene sheets have been synthesized through rapid quenching of hot bulk highly ordered pyrolytic graphite (HOPG) and expandable graphite (EG) in aqueous solutions of 1.0 wt % NH_4HCO_3 and hydrazine hydrate, respectively.[128,129] These processes involve rapid expansion of HOPG/EG at high temperature to weaken van der Waals forces and then rapid quenching of the heated samples in appropriate quenching media to form graphenes. To the best of our knowledge, the quenching approach has not been adopted previously for the production of MoS_2 nanosheets.

In the present study, we stirred a mixture of MoS_2 and KOH at 80 °C for 24 h and then quenched the sample in a matter of a few seconds to low temperature in liquid N_2. The stresses generated from the sudden, large temperature gradient

between the surface and the interior of the sample during this quenching process disrupted the van der Waals forces binding these MoS_2 layers and resulted in MoS_2 nanosheets. The resulting liquid N_2–quenched MoS_2 served as a precursor for the production of MoS_2 nanosheets through solution-based exfoliation (see detailed experimental conditions). Unlike previously employed quenching-based methods, this approach does not require either a rapid heating process or a special quenching medium. Thus, the major advantages when using this quenching approach for the production of MoS_2 nanosheets from MoS_2 powder are: (i) MoS_2 nanosheets can be derived from commercially available MoS_2 powder without the need for Li^+ intercalation prior to ultrasonication, (ii) environmental friendliness, (iii) and facile operation open to the atmosphere.

6-2. Exprimental

6-2.1. Preparation of exfoliated MoS_2 nanosheets

MoS_2 (500 mg) and KOH (5 g) were added to DI water (100 mL) to create a MoS_2 dispersion (5 mg/mL). The mixture was stirred and maintained at 80 °C for 24 h and then it was rapidly quenched to low temperature in liquid N_2. After quenching, the dispersion was subjected to exfoliation for 180 min in an ultrasonication bath maintained at 20 kHz under a power of 130 W. The resulting exfoliated MoS_2 powder was collected through vacuum filtration through PVDF membranes (average pore size: 0.2 μm) supported on a fritted glass holder. The as-prepared product was washed with DI water and then dried at 50 °C under vacuum for 24 h. After peeling off the PVDF membrane, the resulting MoS_2 powder, described herein as exfoliated MoS_2, was stored in a drying box at 50 °C until required for use.

6-2.2. Preparation of exfoliated MoS_2 dispersion

The exfoliated MoS_2 (50 mg) was added to $CHCl_3$ (100 mL) to create a dispersion (0.5 mg/mL), which was subjected to treatment for 30 min in an ultrasonication bath maintained at 20 kHz under a power of 130 W.

6-2.3. Measurements and Characterization

Raman spectra of the raw MoS_2 and exfoliated MoS_2 powder were recorded using a high-resolution confocal Raman microscope (HOROBA, Lab RAM HR) and a 632-nm He–Ne laser source. SAED patterns and HRTEM images were recorded using a JEOL 2100F instrument equipped with an Oxford Instruments EDS apparatus operated at 200 kV; for HRTEM measurement, a few drops of the diluted dispersion of exfoliated MoS_2 were placed on a standard holey C-covered Cu TEM micro grid. AFM images were recorded using a Digital Instruments Nanoscope III apparatus equipped with a NANOSENSORS Si tip, operated in the tapping mode with a resonance frequency of 130 kHz. AFM and Raman samples were prepared by spin-coating the dispersions onto the surfaces of Si/SiO_2 substrates and then drying in air.

6.3 Results and discussion

Figure 6-1 compares the Raman spectra of the exfoliated MoS_2 with that of bulk MoS_2. The spectrum of the bulk MoS_2 displays bands at 376 and 403.2 cm^{-1} representing the A_{1g} and E_{2g} modes, respectively, while that of the exfoliated MoS_2 features these bands at 383.8 and 405.2 cm^{-1}, respectively; the frequency difference for of the latter (21.4 cm^{-1}) is smaller than that for the former (27.2 cm^{-1}), consistent with the Raman signature of MoS_2 nanosheets comprising two to four layers.[115,122]

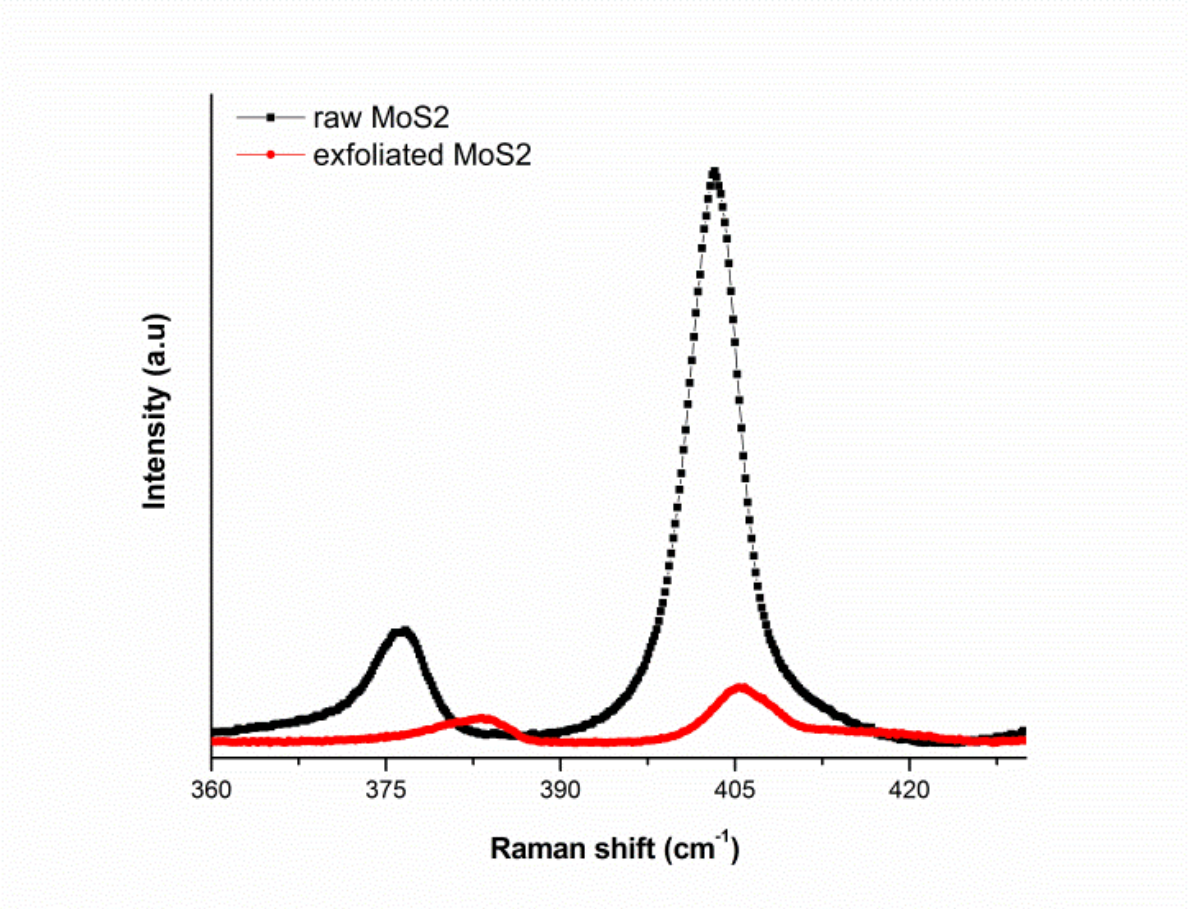

Figure 6-1. Raman spectra of bulk MoS_2 and exfoliated MoS_2 nanosheets processed using the liquid N_2–exfoliation process.

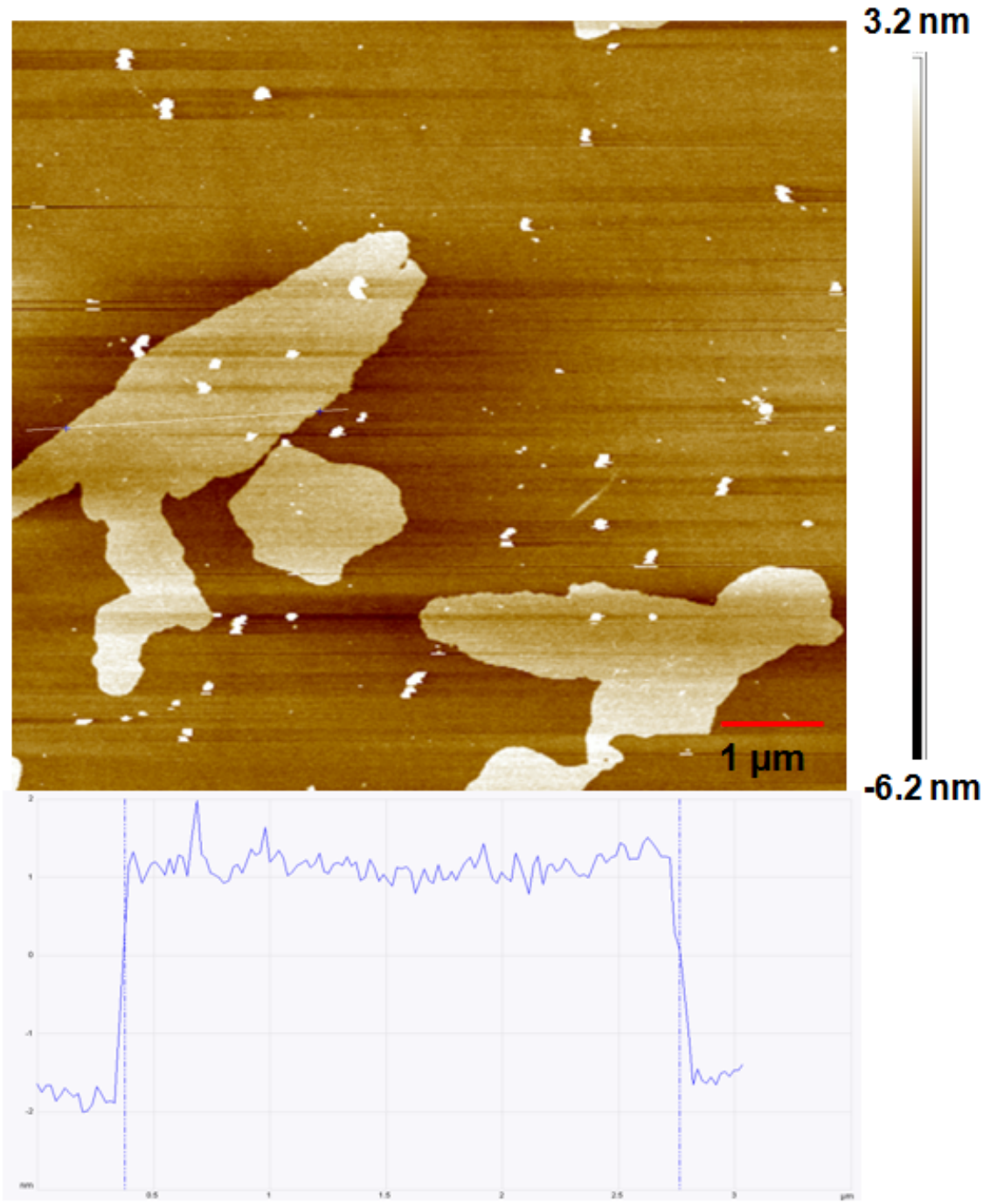

Figure 6-2. AFM image and height profile of MoS_2 samples processed from a dispersion of exfoliated MoS_2.

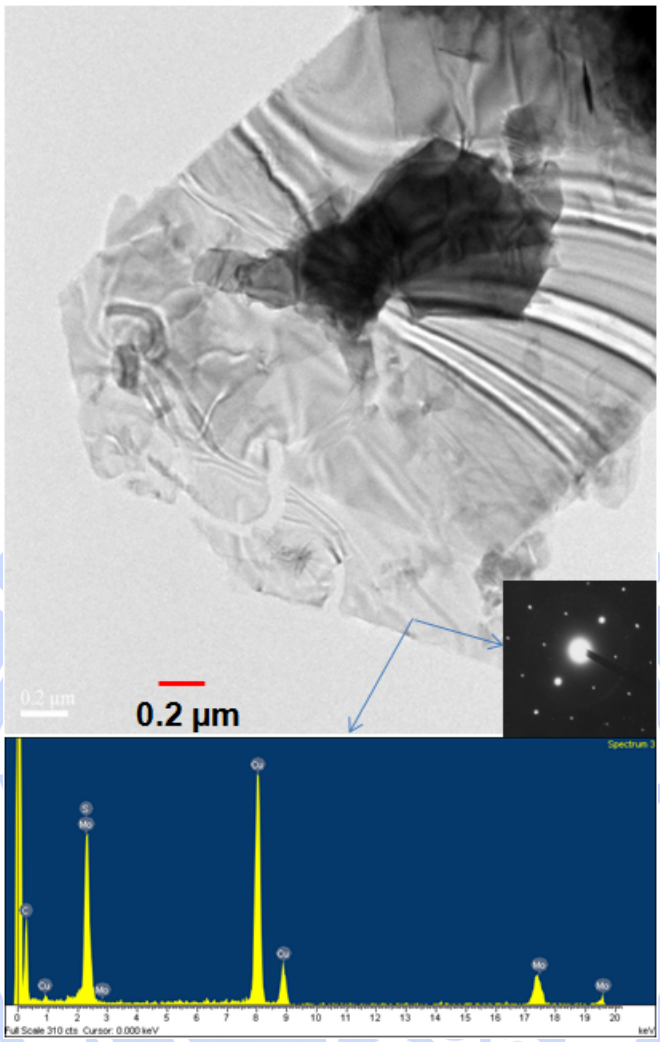

Figure 6-3. TEM image of a MoS_2 sample processed from a dispersion of exfoliated MoS_2; inset: SAED pattern and EDS spectrum of the in situ–recorded area. The Cu signal arose from the TEM support grid.

Fig. 6-2 presents an AFM image of a sample prepared by spin-coating a diluted solution (0.05 wt%) of exfoliated MoS_2 onto the surfaces of a Si/SiO_2 substrate and then drying in air. The lateral dimension of this exfoliated nanosheet was approximately 3.0 µm; its thickness was approximately 1.5 nm, corresponding to approximately two layers, based on the thickness of a single MoS_2 layer being 0.7 nm—again, consistent with our production of few-layer MoS_2 nanosheets.

AFM images of other individual nanosheets (see SI) revealed that the thickness varied from 1.5 to 3.5 nm and the lateral dimensions from 0.5 to 3.5 μm. For further examination of an individual sheet-like nanostructure, Fig.6-3 presents a TEM image of an exfoliated MoS_2 product. It indicates that the sheets were flat, folded, and slightly transparent to the electron beam. A selected-area electron diffraction pattern (SAED) of the flat area of the nanosheet (inset to Fig.6-3) reveals the typical six-fold symmetry of MoS_2, indicating that the MoS_2 sheets obtained using this method had good crystallinity; furthermore, point energy dispersive X-ray spectroscopy (EDS) from the same area revealed the presence of Mo and S atoms in a 1:2 ratio, further confirming the formation of MoS_2 nanosheets.

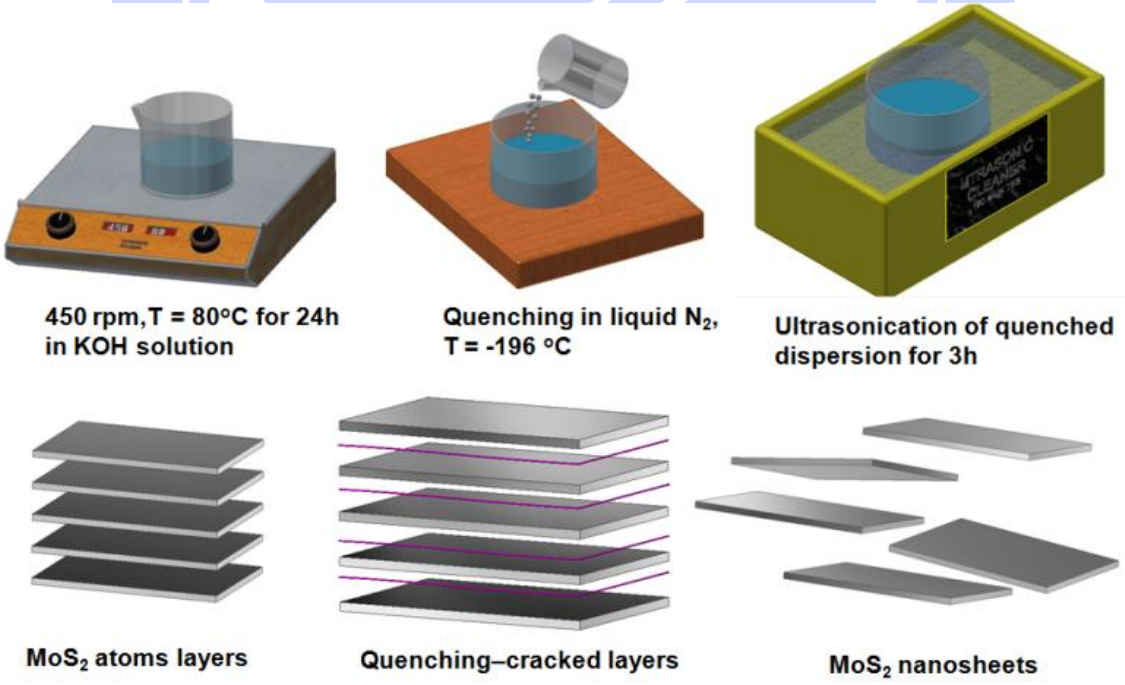

Figure 6-4. Suggested mechanism for the formation of exfoliated MoS_2 through quenching and exfoliation processes.

Table 6-1. Exfoliation of solutions with and without quenching treatment

Exfoliation	Results	
	With quenching	Without quenching
Solution of MoS_2 in DI water	Large amounts of exfoliated sheets having a thickness of 3 nm; difference in frequency between the A_{1g} and E_{2g} signals of ca. 22.2 cm^{-1}, but not uniform among sheets.	Small amounts of exfoliated sheets having a thickness of 5 nm; difference in frequency between the A_{1g} and E_{2g} signals of ca. 25.4 cm^{-1}. Flake-like MoS_2 particles did not fully exfoliate and remained on the surfaces of the sheets. Obtained sheets were relatively thick, with a lack of uniformity among them.
KOH-based MoS_2 solution	Large amounts of uniformly exfoliated sheets having a thickness of 2 nm; difference in frequency between the A_{1g} and E_{2g} signals was ca. 21.4 cm^{-1}.	Small amounts of exfoliated sheets having a thickness of 5 nm; difference in frequency between the A_{1g} and E_{2g} signals was ca. 25.8 cm^{-1}. Obtained sheets were relatively thick, with a lack of uniformity among them.

We consider a possible two-step mechanism for the exfoliation of the liquid N_2–quenched MoS_2 powder, as shown in Fig.6-4. The first step of the quenching process involved gradual heating of the bulk MoS_2 powder at a moderate temperature (80 °C, 24 h), resulting in a uniform dispersion of MoS_2 flakes. The hot flake-like MoS_2 particles were then cooled rapidly to low temperature in liquid N_2. Because the surfaces of the hot flake-like MoS_2 particles cooled faster than

their interiors, quenching stresses occurred instantly upon contact with the liquid N_2, leading to cracking of bonds between the layers of weakly bonded MoS_2 layers, instantly freezing the cracks within the liquid N_2 medium. The interaction between the hot flake-like MoS_2 particles and the liquid N_2 quenching medium resulted in quenching-cracked layers that allow further ultrasonic-facilitated exfoliation. Then, detachment of MoS_2 layers preferentially at these quenching-cracked layers via ultrasonication and subsequent re-dispersion in chloroform. To further identify the mechanism behind this quenching approach, we exfoliated MoS_2 solutions in both DI water and in aqueous KOH with and without the quenching process. The MoS_2 nanosheets prepared from exfoliation of bulk MoS_2 in DI water with and without quenching are termed MoS_2-DIQ and MoS_2-DI, respectively, and the MoS_2 nanosheets prepared from exfoliation of bulk MoS_2 in aqueous KOH with and without quenching are termed MoS_2-KOHQ and MoS_2-KOH, respectively. Tables 6-1, Fig. 6-4, and Fig.6-5 provide details of the experimental methods and the obtained results. We observed that exfoliation of MoS_2 in aqueous KOH was greater than that in DI water. We suspect that aqueous KOH created better conditions for uniform dispersion of the flake-like MoS_2 particles than did DI water, leading to more-uniform quenching on the surfaces of the hot flake-like MoS_2 particles. One possible reason for the more uniform dispersion of flake-like MoS_2 in the presence of KOH is that KOH can dissociate into K^+ and OH^- ions, and K^+ ion might intercalate into the layered MoS_2 in bulk, which facilitates exfoliation. Furthermore, chemical reactions between KOH solutions with MoS_2 powder for long time could induce exfoliation directly from MoS_2 flakes, producing a small portion of MoS_2 nanosheets from the starting MoS_2. The detailed chemistry and mechanism of exfoliation associated with these reactions seem very exciting and further work is necessary along this direction.

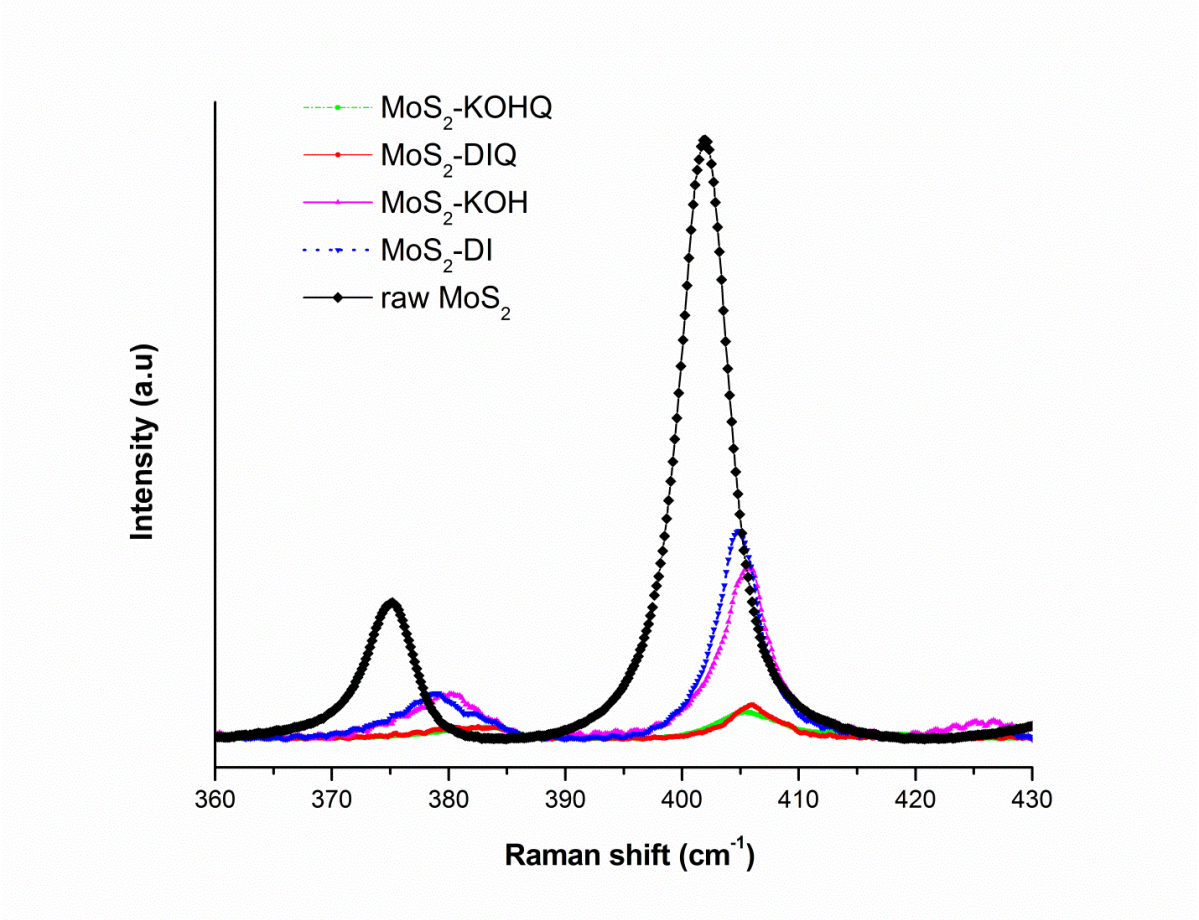

Figure 6-5. Raman spectra of raw MoS_2 (bulk MoS_2) and exfoliated MoS_2 samples processed from solutions of MoS_2 in DI water and aqueous KOH.

MoS_2-DI: Exfoliation of solution of MoS_2 in DI water, without quenching.

MoS_2-DIQ: Exfoliation of solution of MoS_2 in DI water, with quenching.

MoS_2-KOH: Exfoliation of solution of MoS_2 in aqueous KOH, without quenching.

MoS_2-KOHQ: Exfoliation of solution of MoS_2 in aqueous KOH, with quenching.

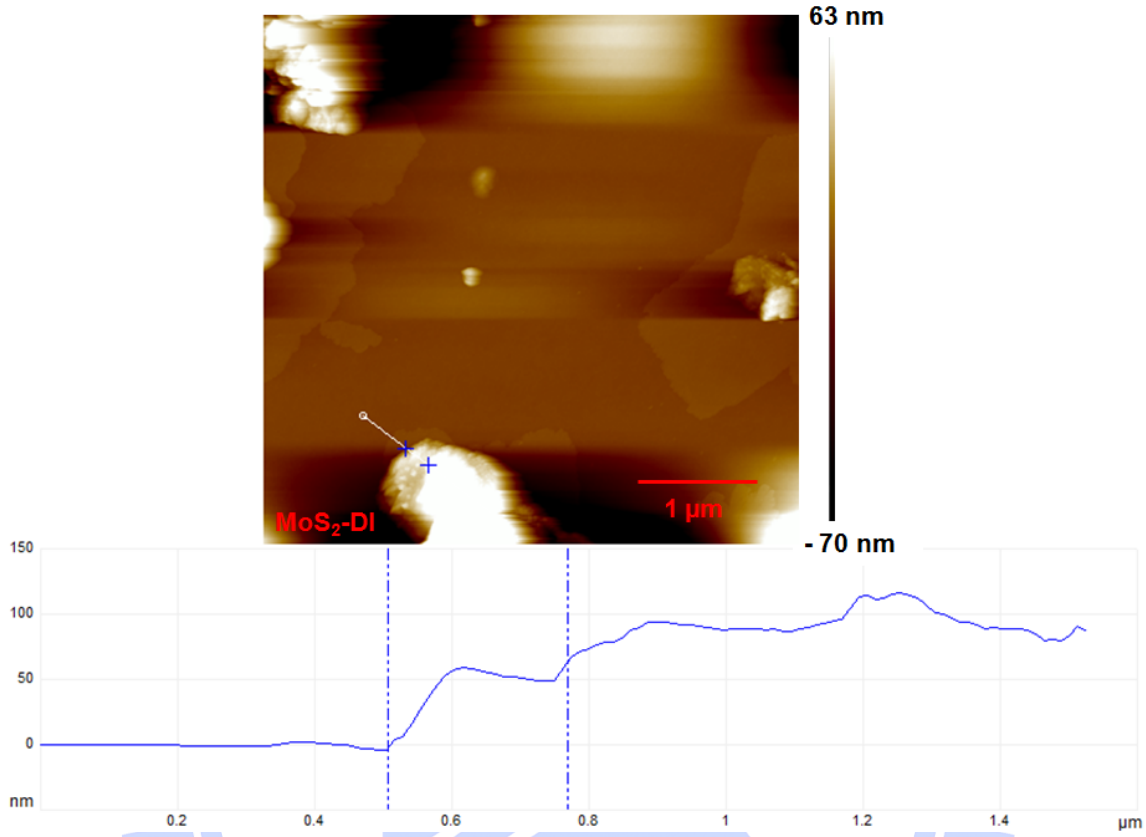

Figure 6-6a. AFM images and height profiles of MoS_2-DI.

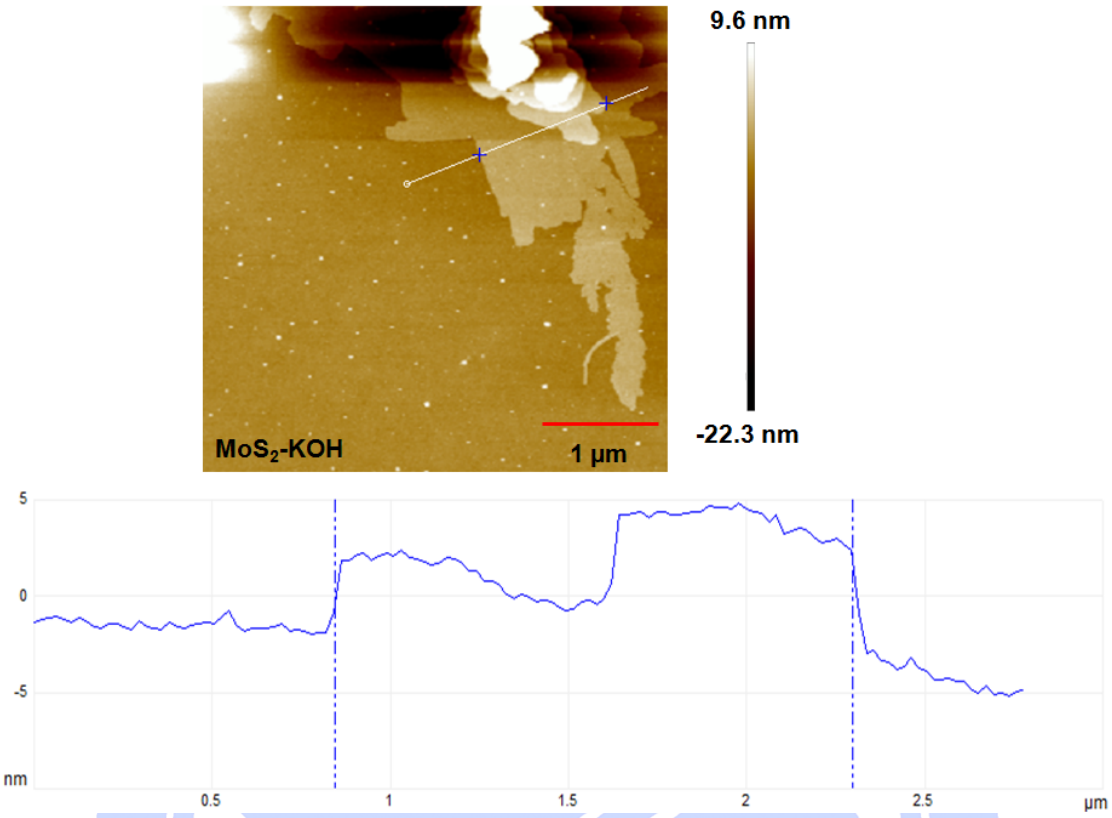

Figure 6- 6b. AFM images and height profiles of MoS2-KOH.

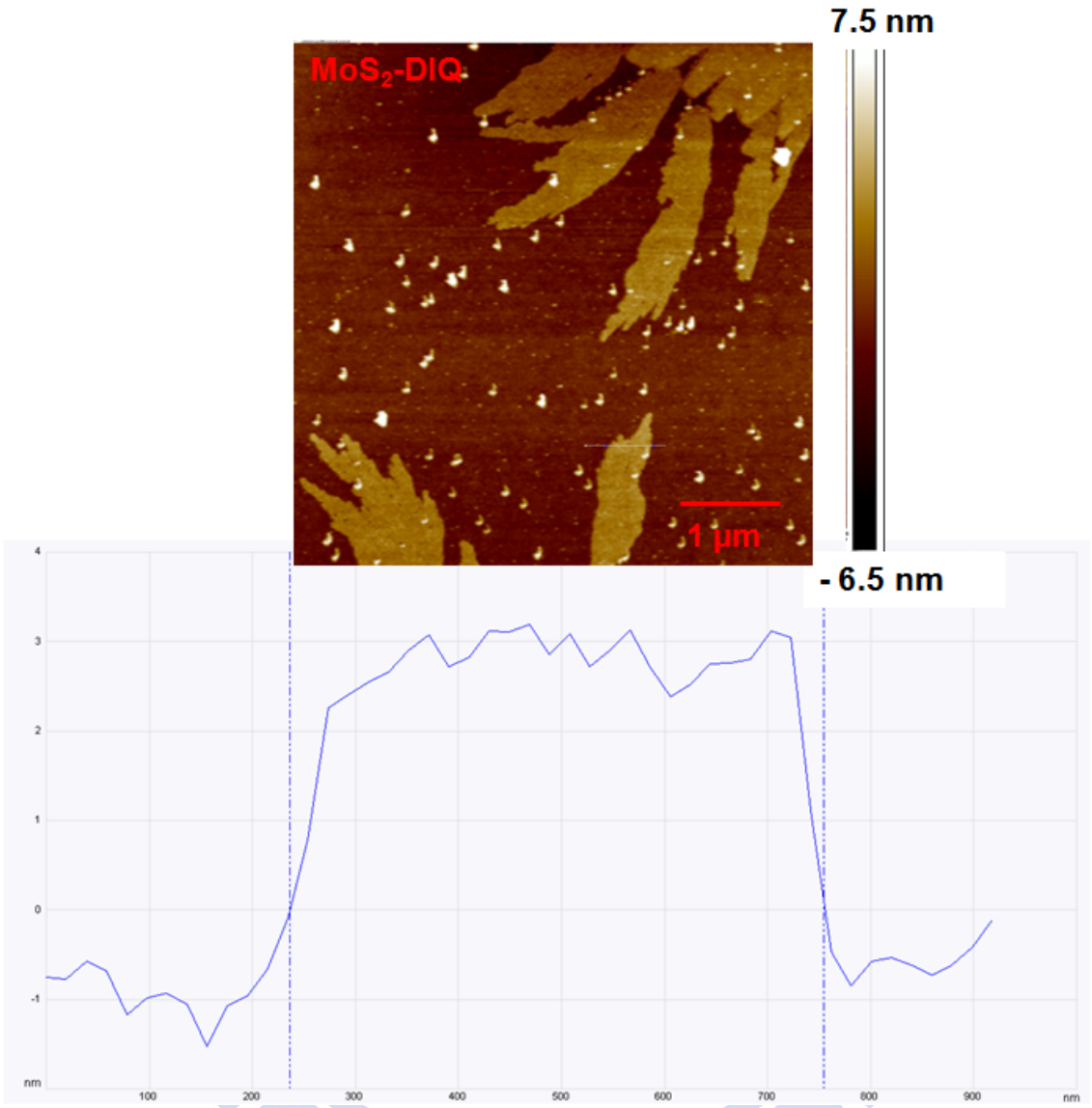

Figure 6-6c. AFM images and height profiles of MoS2-DIQ.

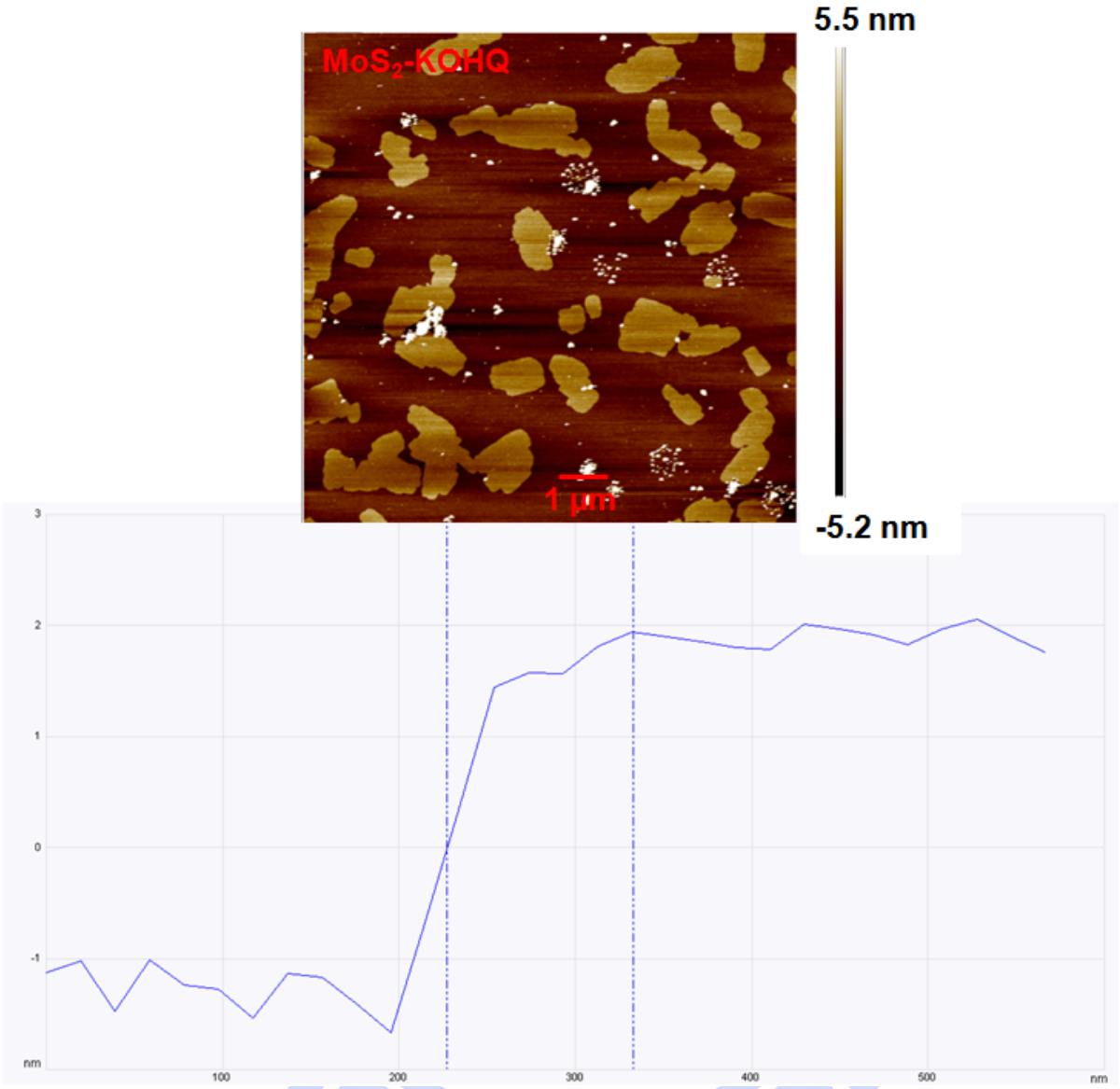

Figure 6-6d. AFM images and height profiles of MoS_2-KOHQ.

6-4. Conclusion

In conclusion, we have synthesized MoS_2 nanosheets from commercially available bulk MoS_2 through a two-step process involving quenching in liquid N_2 and subsequent exfoliation through sonication. To the best of our knowledge, this paper provides the first example of the use of quenching technology for the preparation of MoS_2 nanosheets at low temperature and under atmospheric

pressure. This method is quite promising because of its highly efficient, green, and facile operation.

Chapter 7: Conclusions and outlook

7-1. Conclusion

In summary, we have demonstrated a hybrid process of plasma electrolysis and electrochemical processing, we termed plasma electrochemical processing, in which we have taken advantage of the vapor plasma envelope calorific effect of the efficient CP process to provide thermal energy for the oxidation of the GEs/HG to plasma-expanded graphite oxide or exfoliation them into plasma-electrochemically exfoliated graphene sheets depend on changing ratio of the surface area of the cathode to that of the anode or electrolytic concentration, respectively. The result shown that the morphology and structures of as-prepared samples can be tuned via a fast and controlled electrochemical exfoliation of graphite in a basic electrolyte solution in a short-reaction time with regards of environmental friendliness, energy/time saving, and low cost. X-ray diffraction, X-ray photoelectron spectroscopy and Raman spectroscopy confirmed the dramatic structural change from GEs or HG to graphite oxides after the CP process. Furthermore, scanning electron microscopy and transmission electron microscopy revealed that the graphite oxide possessed a spheroidal morphology, with dimensions of 1–3 μm, as a result of melting and subsequent quenching during the plasma electrolysis process.

We also used plasma-expanded graphite oxide as precursors for the preparation of graphite nanoplatelets by exfoliating it in N-methyl-2-pyrrolidone and sequential centrifugation resultant dispersion. We further employed spheroidal graphite oxide particles as effective adsorbents for the removal of pollutants (e.g., Methylene Blue) from aqueous solutions.

Additionally, we have developed a facile and efficient plasma-assisted electrochemical exfoliation method, involving a plasma-generated graphite cathode and a graphite anode, for the production of graphene sheets from graphite electrodes in a basic electrolyte solution in a short reaction time. The AFM image of the samples prepared from a diluted solution, revealing in a lateral dimension of approximately 0.5–2.5 μm and a thickness of approximately 2.5 nm, corresponding to approximately seven layers of graphene, based on an interlayer spacing of 0.34 nm. To further identify the mechanism behind this exfoliation, we have investigated the influence of electrolytic concentration on morphological and structural properties of the as-prepared graphene. The results indicated that there is an efficient electrolytic concentration at which exfoliation of graphite into graphene could occur.

Finally, we developed and employed further the exfoliated mechanism in chapter 3-4 for the production of few-layer MoS_2 nanosheets through exfoliation of bulk MoS_2 compounds through quenching in liquid N_2. AFM images of individual nanosheets revealed that the thickness varied from 1.5 to 3.5 nm and the lateral dimensions from 0.5 to 3.5 μm.

7-2. Outlook for future work

The received results indicated that, graphene sheets with good dispersion in solvents can be prepared through plasma-assisted electrochemical exfoliation process at moderate temperatures without the need for acidic media. This method has several advantages such its simple setup, environmentally benign, and rapid throughput when compared to previously reported techniques and methods. However, as-prepared graphene/MoS_2 films could have been compressed during vacuum-assisted filtration, resulting in re-agglomeration of the films and need for

re-dispersion before processing for a wide range of applications, if not carried out in situ. In addition, to realize the mechanism of this process, a accurately measure the temperature in the plasma region or the spectrum of the emitting light from the plasma in order to identify the species involving the reaction and perform a quantitative investigation of the prepared samples using various other characterization tools should be performed using optical emission spectroscopy (OES) technique together with a high speed rate camera (HRS). These clues provided by OES/HSR will further identify how plasma contributes to exfoliation and apply this knowledge to the development of novel and effective approaches for producing 2d layered materials and to increase field of its application. Furthermore, a better control and further understanding of processing will be necessary for reducing the number of graphene layers as well as MoS_2. The results also showed that there is a great potential for researching of capacities of our method aimed to improve effectiveness of the plasma electrolysis processing and to increase field of its application, for example, development of plasma technology for in situ-plasma electrochemical polymerization of a water-soluble polymer–graphene composite.

References

(1) Lee, C.; Wei, X.; Kysar, J. W.; Hone, J.: Measurement of the Elastic Properties and Intrinsic Strength of Monolayer Graphene. *Science* **2008**, *321*, 385-388.

(2) Balandin, A. A.; Ghosh, S.; Bao, W.; Calizo, I.; Teweldebrhan, D.; Miao, F.; Lau, C. N.: Superior Thermal Conductivity of Single-Layer Graphene. *Nano Letters* **2008**, *8*, 902-907.

(3) Bolotin, K. I.; Sikes, K. J.; Jiang, Z.; Klima, M.; Fudenberg, G.; Hone, J.; Kim, P.; Stormer, H. L.: Ultrahigh electron mobility in suspended graphene. *Solid State Communications* **2008**, *146*, 351-355.

(4) Stoller, M. D.; Park, S.; Zhu, Y.; An, J.; Ruoff, R. S.: Graphene-Based Ultracapacitors. *Nano Letters* **2008**, *8*, 3498-3502.

(5) Wang, J.; Manga, K. K.; Bao, Q.; Loh, K. P.: High-Yield Synthesis of Few-Layer Graphene Flakes through Electrochemical Expansion of Graphite in Propylene Carbonate Electrolyte. *Journal of the American Chemical Society* **2011**, *133*, 8888-8891.

(6) Parvez, K.; Li, R.; Puniredd, S. R.; Hernandez, Y.; Hinkel, F.; Wang, S.; Feng, X.; Müllen, K.: Electrochemically Exfoliated Graphene as Solution-Processable, Highly Conductive Electrodes for Organic Electronics. *ACS Nano* **2013**, *7*, 3598-3606.

(7) Fan, H.; Wang, L.; Zhao, K.; Li, N.; Shi, Z.; Ge, Z.; Jin, Z.: Fabrication, Mechanical Properties, and Biocompatibility of Graphene-Reinforced Chitosan Composites. *Biomacromolecules* **2010**, *11*, 2345-2351.

(8) Wu, Y.; Wang, B.; Ma, Y.; Huang, Y.; Li, N.; Zhang, F.; Chen, Y.: Efficient and large-scale synthesis of few-layered graphene using an arc-discharge method and conductivity studies of the resulting films. *Nano Res.* **2010**, *3*, 661-669.

(9) Knieke, C.; Berger, A.; Voigt, M.; Taylor, R. N. K.; Röhrl, J.; Peukert, W.: Scalable production of graphene sheets by mechanical delamination. *Carbon* **2010**, *48*, 3196-3204.

(10) Antisari, M. V.; Montone, A.; Jovic, N.; Piscopiello, E.; Alvani, C.; Pilloni, L.: Low energy pure shear milling: A method for the preparation of graphite nano-sheets. *Scripta Materialia* **2006**, *55*, 1047-1050.

(11) Chen, G.; Weng, W.; Wu, D.; Wu, C.; Lu, J.; Wang, P.; Chen, X.: Preparation and characterization of graphite nanosheets from ultrasonic powdering technique. *Carbon* **2004**, *42*, 753-759.

(12) He, F.; Lau, S.; Chan, H. L.; Fan, J.: High Dielectric Permittivity and Low Percolation Threshold in Nanocomposites Based on Poly(vinylidene fluoride) and Exfoliated Graphite Nanoplates. *Advanced Materials* **2009**, *21*, 710-715.

(13) Chen, G.; Wu, D.; Weng, W.; Wu, C.: Exfoliation of graphite flake and its nanocomposites. *Carbon* **2003**, *41*, 619-621.

(14) Li, J.; Vaisman, L.; Marom, G.; Kim, J.-K.: Br treated graphite nanoplatelets for improved electrical conductivity of polymer composites. *Carbon* **2007**, *45*, 744-750.

(15) Cai, M.; Thorpe, D.; Adamson, D. H.; Schniepp, H. C.: Methods of graphite exfoliation. *Journal of Materials Chemistry* **2012**, *22*, 24992-25002.

(16) Stankovich, S.; Dikin, D. A.; Piner, R. D.; Kohlhaas, K. A.; Kleinhammes, A.; Jia, Y.; Wu, Y.; Nguyen, S. T.; Ruoff, R. S.: Synthesis of graphene-based nanosheets via chemical reduction of exfoliated graphite oxide. *Carbon* **2007**, *45*, 1558-1565.

(17) Wang, G.; Yang, J.; Park, J.; Gou, X.; Wang, B.; Liu, H.; Yao, J.: Facile Synthesis and Characterization of Graphene Nanosheets. *The Journal of Physical Chemistry C* **2008**, *112*, 8192-8195.

(18) Shen, J.; Hu, Y.; Shi, M.; Lu, X.; Qin, C.; Li, C.; Ye, M.: Fast and Facile Preparation of Graphene Oxide and Reduced Graphene Oxide Nanoplatelets. *Chemistry of Materials* **2009**, *21*, 3514-3520.

(19) Stankovich, S.; Piner, R. D.; Chen, X.; Wu, N.; Nguyen, S. T.; Ruoff, R. S.: Stable aqueous dispersions of graphitic nanoplatelets via the reduction of exfoliated graphite oxide in the presence of poly(sodium 4-styrenesulfonate). *Journal of Materials Chemistry* **2006**, *16*, 155-158.

(20) Bonaccorso, F.; Lombardo, A.; Hasan, T.; Sun, Z.; Colombo, L.; Ferrari, A. C.: Production and processing of graphene and 2d crystals. *Materials Today* **2012**, *15*, 564-589.

(21) Noel, M.; Santhanam, R.: Electrochemistry of graphite intercalation compounds. *Journal of Power Sources* **1998**, *72*, 53-65.

(22) Low, C. T. J.; Walsh, F. C.; Chakrabarti, M. H.; Hashim, M. A.; Hussain, M. A.: Electrochemical approaches to the production of graphene flakes and their potential applications. *Carbon* **2013**, *54*, 1-21.

(23) Wang, G.; Wang, B.; Park, J.; Wang, Y.; Sun, B.; Yao, J.: Highly efficient and large-scale synthesis of graphene by electrolytic exfoliation. *Carbon* **2009**, *47*, 3242-3246.

(24) Liu, N.; Luo, F.; Wu, H.; Liu, Y.; Zhang, C.; Chen, J.: One-Step Ionic-Liquid-Assisted Electrochemical Synthesis of Ionic-Liquid-Functionalized Graphene Sheets Directly from Graphite. *Advanced Functional Materials* **2008**, *18*, 1518-1525.

(25) Su, C.-Y.; Lu, A.-Y.; Xu, Y.; Chen, F.-R.; Khlobystov, A. N.; Li, L.-J.: High-Quality Thin Graphene Films from Fast Electrochemical Exfoliation. *ACS Nano* **2011**, *5*, 2332-2339.

(26) Sirisaksoontorn, W.; Adenuga, A. A.; Remcho, V. T.; Lerner, M. M.: Preparation and Characterization of a Tetrabutylammonium Graphite Intercalation Compound. *Journal of the American Chemical Society* **2011**, *133*, 12436-12438.

(27) Zhong, Y. L.; Swager, T. M.: Enhanced Electrochemical Expansion of Graphite for in Situ Electrochemical Functionalization. *Journal of the American Chemical Society* **2012**, *134*, 17896-17899.

(28) Lu, X.; Zhao, C.: Controlled electrochemical intercalation, exfoliation and in situ nitrogen doping of graphite in nitrate-based protic ionic liquids. *Physical Chemistry Chemical Physics* **2013**, *15*, 20005-20009.

(29) Viculis, L. M.; Mack, J. J.; Mayer, O. M.; Hahn, H. T.; Kaner, R. B.: Intercalation and exfoliation routes to graphite nanoplatelets. *Journal of Materials Chemistry* **2005**, *15*, 974-978.

(30) Brownson, D. A. C.; Kampouris, D. K.; Banks, C. E.: Graphene electrochemistry: fundamental concepts through to prominent applications. *Chemical Society Reviews* **2012**, *41*, 6944-6976.

(31) Singh, V. V.; Gupta, G.; Batra, A.; Nigam, A. K.; Boopathi, M.; Gutch, P. K.; Tripathi, B. K.; Srivastava, A.; Samuel, M.; Agarwal, G. S.; Singh, B.; Vijayaraghavan, R.: Greener Electrochemical Synthesis of High Quality Graphene Nanosheets Directly from Pencil and its SPR Sensing Application. *Advanced Functional Materials* **2012**, *22*, 2352-2362.

(32) *Fabrication of*

nanostructures by plasma electrolysis; Rouhaghdam, M. A. a. A. S., Ed., 2010.

(33) Aliofkhazraei, M.; Rouhaghdam, A. S.; Gupta, P.: Nano-Fabrication by Cathodic Plasma Electrolysis. *Critical Reviews in Solid State and Materials Sciences* **2011**, *36*, 174-190.

(34) Gupta, P.; Tenhundfeld, G.; Daigle, E. O.; Ryabkov, D.: Electrolytic plasma technology: Science and engineering—An overview. *Surface and Coatings Technology* **2007**, *201*, 8746-8760.

(35) Yerokhin, A. L.; Nie, X.; Leyland, A.; Matthews, A.; Dowey, S. J.: Plasma electrolysis for surface engineering. *Surface and Coatings Technology* **1999**, *122*, 73-93.

(36) Gupta, P.; Tenhundfeld, G.; Daigle, E. O.; Schilling, P. J.: Synthesis and characterization of hard metal coatings by electro-plasma technology. *Surface and Coatings Technology* **2005**, *200*, 1587-1594.

(37) Nie, X.; Tsotsos, C.; Wilson, A.; Yerokhin, A. L.; Leyland, A.; Matthews, A.: Characteristics of a plasma electrolytic nitrocarburising treatment for stainless steels. *Surface and Coatings Technology* **2001**, *139*, 135-142.

(38) Paulmier, T.; Bell, J. M.; Fredericks, P. M.: Deposition of nano-crystalline graphite films by cathodic plasma electrolysis. *Thin Solid Films* **2007**, *515*, 2926-2934.

(39) Campos, C. S.; Spada, E. R.; de Paula, F. R.; Reis, F. T.; Faria, R. M.; Sartorelli, M. L.: Raman and XRD study on brookite–anatase coexistence in cathodic electrosynthesized titania. *Journal of Raman Spectroscopy* **2012**, *43*, 433-438.

(40) Laursen, A. B.; Kegnaes, S.; Dahl, S.; Chorkendorff, I.: Molybdenum sulfides-efficient and viable materials for electro - and photoelectrocatalytic hydrogen evolution. *Energy & Environmental Science* **2012**, *5*, 5577-5591.

(41) Butler, S. Z.; Hollen, S. M.; Cao, L.; Cui, Y.; Gupta, J. A.; Gutiérrez, H. R.; Heinz, T. F.; Hong, S. S.; Huang, J.; Ismach, A. F.; Johnston-Halperin, E.; Kuno, M.; Plashnitsa, V. V.; Robinson, R. D.; Ruoff, R. S.; Salahuddin, S.; Shan, J.; Shi, L.; Spencer, M. G.; Terrones, M.; Windl, W.; Goldberger, J. E.: Progress, Challenges, and Opportunities in Two-Dimensional Materials Beyond Graphene. *ACS Nano* **2013**, *7*, 2898-2926.

(42) Coleman, J. N.; Lotya, M.; O'Neill, A.; Bergin, S. D.; King, P. J.; Khan, U.; Young, K.; Gaucher, A.; De, S.; Smith, R. J.; Shvets, I. V.; Arora, S. K.; Stanton, G.; Kim, H.-Y.; Lee, K.; Kim, G. T.; Duesberg, G. S.; Hallam, T.; Boland, J. J.; Wang, J. J.; Donegan, J. F.; Grunlan, J. C.; Moriarty, G.; Shmeliov, A.; Nicholls, R. J.; Perkins, J. M.; Grieveson, E. M.; Theuwissen, K.; McComb, D. W.;

Nellist, P. D.; Nicolosi, V.: Two-Dimensional Nanosheets Produced by Liquid Exfoliation of Layered Materials. *Science* **2011**, *331*, 568-571.

(43) Lee, Y.-H.; Zhang, X.-Q.; Zhang, W.; Chang, M.-T.; Lin, C.-T.; Chang, K.-D.; Yu, Y.-C.; Wang, J. T.-W.; Chang, C.-S.; Li, L.-J.; Lin, T.-W.: Synthesis of Large-Area MoS2 Atomic Layers with Chemical Vapor Deposition. *Advanced Materials* **2012**, *24*, 2320-2325.

(44) Mitzi, D. B.: Solution Processing of Chalcogenide Semiconductors via Dimensional Reduction. *Advanced Materials* **2009**, *21*, 3141-3158.

(45) Geim, A. K.; Novoselov, K. S.: The rise of graphene. *Nat Mater* **2007**, *6*, 183-191.

(46) Luo, J.; Jang, H. D.; Huang, J.: Effect of Sheet Morphology on the Scalability of Graphene-Based Ultracapacitors. *ACS Nano* **2013**, *7*, 1464-1471.

(47) Pumera, M.: Graphene-based nanomaterials for energy storage. *Energy & Environmental Science* **2011**, *4*, 668-674.

(48) Wen, Z.; Wang, X.; Mao, S.; Bo, Z.; Kim, H.; Cui, S.; Lu, G.; Feng, X.; Chen, J.: Crumpled Nitrogen-Doped Graphene Nanosheets with Ultrahigh Pore Volume for High-Performance Supercapacitor. *Advanced Materials* **2012**, *24*, 5610-5616.

(49) Wu, Z.-S.; Sun, Y.; Tan, Y.-Z.; Yang, S.; Feng, X.; Müllen, K.: Three-Dimensional Graphene-Based Macro- and Mesoporous Frameworks for High-Performance Electrochemical Capacitive Energy Storage. *Journal of the American Chemical Society* **2012**, *134*, 19532-19535.

(50) Tjong, S. C.: Polymer nanocomposite bipolar plates reinforced with carbon nanotubes and graphite nanosheets. *Energy & Environmental Science* **2011**, *4*, 605-626.

(51) Stankovich, S.; Dikin, D. A.; Dommett, G. H. B.; Kohlhaas, K. M.; Zimney, E. J.; Stach, E. A.; Piner, R. D.; Nguyen, S. T.; Ruoff, R. S.: Graphene-based composite materials. *Nature* **2006**, *442*, 282-286.

(52) Pang, S.; Hernandez, Y.; Feng, X.; Müllen, K.: Graphene as Transparent Electrode Material for Organic Electronics. *Advanced Materials* **2011**, *23*, 2779-2795.

(53) Hsu, C.-L.; Lin, C.-T.; Huang, J.-H.; Chu, C.-W.; Wei, K.-H.; Li, L.-J.: Layer-by-Layer Graphene/TCNQ Stacked Films as Conducting Anodes for Organic Solar Cells. *ACS Nano* **2012**, *6*, 5031-5039.

(54) Huang, X.; Zeng, Z.; Fan, Z.; Liu, J.; Zhang, H.: Graphene-Based Electrodes. *Advanced Materials* **2012**, *24*, 5979-6004.

(55) Hong, T.-K.; Lee, D. W.; Choi, H. J.; Shin, H. S.; Kim, B.-S.: Transparent, Flexible Conducting Hybrid Multilayer Thin Films of Multiwalled Carbon Nanotubes with Graphene Nanosheets. *ACS Nano* **2010**, *4*, 3861-3868.

(56) Hong, A. J.; Song, E. B.; Yu, H. S.; Allen, M. J.; Kim, J.; Fowler, J. D.; Wassei, J. K.; Park, Y.; Wang, Y.; Zou, J.; Kaner, R. B.; Weiller, B. H.; Wang, K. L.: Graphene Flash Memory. *ACS Nano* **2011**, *5*, 7812-7817.

(57) Ji, Y.; Lee, S.; Cho, B.; Song, S.; Lee, T.: Flexible Organic Memory Devices with Multilayer Graphene Electrodes. *ACS Nano* **2011**, *5*, 5995-6000.

(58) Liu, J.; Yin, Z.; Cao, X.; Zhao, F.; Wang, L.; Huang, W.; Zhang, H.: Fabrication of Flexible, All-Reduced Graphene Oxide Non-Volatile Memory Devices. *Advanced Materials* **2013**, *25*, 233-238.

(59) Chen, T.-Y.; Loan, P. T. K.; Hsu, C.-L.; Lee, Y.-H.; Tse-Wei Wang, J.; Wei, K.-H.; Lin, C.-T.; Li, L.-J.: Label-free detection of DNA hybridization using transistors based on CVD grown graphene. *Biosensors and Bioelectronics* **2013**, *41*, 103-109.

(60) Lin, J.; Teweldebrhan, D.; Ashraf, K.; Liu, G.; Jing, X.; Yan, Z.; Li, R.; Ozkan, M.; Lake, R. K.; Balandin, A. A.; Ozkan, C. S.: Gating of Single-Layer Graphene with Single-Stranded Deoxyribonucleic Acids. *Small* **2010**, *6*, 1150-1155.

(61) Brownson, D. A. C.; Banks, C. E.: Graphene electrochemistry: Fabricating amperometric biosensors. *Analyst* **2011**, *136*, 2084-2089.

(62) Lin, C.-T.; Loan, P. T. K.; Chen, T.-Y.; Liu, K.-K.; Chen, C.-H.; Wei, K.-H.; Li, L.-J.: Label-Free Electrical Detection of DNA Hybridization on Graphene using Hall Effect Measurements: Revisiting the Sensing Mechanism. *Advanced Functional Materials* **2013**, *23*, 2301-2307.

(63) Reina, A.; Jia, X.; Ho, J.; Nezich, D.; Son, H.; Bulovic, V.; Dresselhaus, M. S.; Kong, J.: Large Area, Few-Layer Graphene Films on Arbitrary Substrates by Chemical Vapor Deposition. *Nano Letters* **2008**, *9*, 30-35.

(64) Wei, D.; Wu, B.; Guo, Y.; Yu, G.; Liu, Y.: Controllable Chemical Vapor Deposition Growth of Few Layer Graphene for Electronic Devices. *Accounts of Chemical Research* **2012**, *46*, 106-115.

(65) Su, C.-Y.; Lu, A.-Y.; Wu, C.-Y.; Li, Y.-T.; Liu, K.-K.; Zhang, W.; Lin, S.-Y.; Juang, Z.-Y.; Zhong, Y.-L.; Chen, F.-R.; Li, L.-J.: Direct Formation of Wafer Scale Graphene Thin Layers on Insulating Substrates by Chemical Vapor Deposition. *Nano Letters* **2011**, *11*, 3612-3616.

(66) Parvez, K.; Li, R.; Puniredd, S. R.; Hernandez, Y.; Hinkel, F.; Wang, S.; Feng, X.; Müllen, K.: Electrochemically Exfoliated Graphene as Solution-Processable, Highly Conductive Electrodes for Organic Electronics. *ACS Nano* **2013**.

(67) Hernandez, Y.; Nicolosi, V.; Lotya, M.; Blighe, F. M.; Sun, Z.; De, S.; McGovern, I. T.; Holland, B.; Byrne, M.; Gun'Ko, Y. K.; Boland, J. J.; Niraj, P.; Duesberg, G.; Krishnamurthy, S.; Goodhue, R.; Hutchison, J.; Scardaci, V.; Ferrari, A. C.; Coleman, J. N.: High-yield production of graphene by liquid-phase exfoliation of graphite. *Nat Nano* **2008**, *3*, 563-568.

(68) Choi, E.-K.; Jeon, I.-Y.; Bae, S.-Y.; Lee, H.-J.; Shin, H. S.; Dai, L.; Baek, J.-B.: High-yield exfoliation of three-dimensional graphite into two-dimensional graphene-like sheets. *Chemical Communications* **2010**, *46*, 6320-6322.

(69) Shin, H.-J.; Kim, K. K.; Benayad, A.; Yoon, S.-M.; Park, H. K.; Jung, I.-S.; Jin, M. H.; Jeong, H.-K.; Kim, J. M.; Choi, J.-Y.; Lee, Y. H.: Efficient Reduction of Graphite Oxide by Sodium Borohydride and Its Effect on Electrical Conductance. *Advanced Functional Materials* **2009**, *19*, 1987-1992.

(70) Sui, Z.; Zhang, X.; Lei, Y.; Luo, Y.: Easy and green synthesis of reduced graphite oxide-based hydrogels. *Carbon* **2011**, *49*, 4314-4321.

(71) Staudenmaier, L.: Verfahren zur Darstellung der Graphitsäure. *Berichte der deutschen chemischen Gesellschaft* **1898**, *31*, 1481-1487.

(72) Hofmann, U.; König, E.: Untersuchungen über Graphitoxyd. *Zeitschrift für anorganische und allgemeine Chemie* **1937**, *234*, 311-336.

(73) Hummers, W. S.; Offeman, R. E.: Preparation of Graphitic Oxide. *Journal of the American Chemical Society* **1958**, *80*, 1339-1339.

(74) Poh, H. L.; Sanek, F.; Ambrosi, A.; Zhao, G.; Sofer, Z.; Pumera, M.: Graphenes prepared by Staudenmaier, Hofmann and Hummers methods with consequent thermal exfoliation exhibit very different electrochemical properties. *Nanoscale* **2012**, *4*, 3515-3522.

(75) Marcano, D. C.; Kosynkin, D. V.; Berlin, J. M.; Sinitskii, A.; Sun, Z.; Slesarev, A.; Alemany, L. B.; Lu, W.; Tour, J. M.: Improved Synthesis of Graphene Oxide. *ACS Nano* **2010**, *4*, 4806-4814.

(76) Hudson, M. J.; Hunter-Fujita, F. R.; W. Peckett, J.; Smith, P. M.: Electrochemically prepared colloidal, oxidised graphite. *Journal of Materials Chemistry* **1997**, *7*, 301-305.

(77) Bowling, R.; Packard, R. T.; McCreery, R. L.: Mechanism of electrochemical activation of carbon electrodes: role of graphite lattice defects. *Langmuir* **1989**, *5*, 683-688.

(78) Dai, H.-P.; Shiu, K.-K.: Voltammetric studies of electrochemical pretreatment of rotating-disc glassy carbon electrodes in phosphate buffer. *Journal of Electroanalytical Chemistry* **1996**, *419*, 7-14.

(79) Jeong, H.-K.; Lee, Y. P.; Lahaye, R. J. W. E.; Park, M.-H.; An, K. H.; Kim, I. J.; Yang, C.-W.; Park, C. Y.; Ruoff, R. S.; Lee, Y. H.: Evidence of Graphitic AB Stacking Order of Graphite Oxides. *Journal of the American Chemical Society* **2008**, *130*, 1362-1366.

(80) Cai, D.; Song, M.: Preparation of fully exfoliated graphite oxide nanoplatelets in organic solvents. *Journal of Materials Chemistry* **2007**, *17*, 3678-3680.

(81) Mottaleb, M. A.; Yang, J. S.; Kim, H.-J.: ELECTROLYTE-AS-CATHODE GLOW DISCHARGE (ELCAD)/GLOW DISCHARGE ELECTROLYSIS AT THE GAS-SOLUTION INTERFACE. *Applied Spectroscopy Reviews* **2002**, *37*, 247-273.

(82) Thagard, S. M.; Takashima, K.; Mizuno, A.: Chemistry of the Positive and Negative Electrical Discharges Formed in Liquid Water and Above a Gas–Liquid Surface. *Plasma Chem Plasma Process* **2009**, *29*, 455-473.

(83) Tuinstra, F.; Koenig, J. L.: Raman Spectrum of Graphite. *The Journal of Chemical Physics* **1970**, *53*, 1126-1130.

(84) Ferrari, A. C.; Meyer, J. C.; Scardaci, V.; Casiraghi, C.; Lazzeri, M.; Mauri, F.; Piscanec, S.; Jiang, D.; Novoselov, K. S.; Roth, S.; Geim, A. K.: Raman Spectrum of Graphene and Graphene Layers. *Physical Review Letters* **2006**, *97*, 187401.

(85) Lu, Y.; Zhu, Z.; Liu, Z.: Carbon-encapsulated Fe nanoparticles from detonation-induced pyrolysis of ferrocene. *Carbon* **2005**, *43*, 369-374.

(86) Lenski, D. R.; Fuhrer, M. S.: Raman and optical characterization of multilayer turbostratic graphene grown via chemical vapor deposition. *Journal of Applied Physics* **2011**, *110*, 013720-4.

(87) Chen, L.; Hernandez, Y.; Feng, X.; Müllen, K.: From Nanographene and Graphene Nanoribbons to Graphene Sheets: Chemical Synthesis. *Angewandte Chemie International Edition* **2012**, *51*, 7640-7654.

(88) Shahil, K. M. F.; Balandin, A. A.: Graphene–Multilayer Graphene Nanocomposites as Highly Efficient Thermal Interface Materials. *Nano Letters* **2012**, *12*, 861-867.

(89) Li, B.; Zhong, W.-H.: Review on polymer/graphite nanoplatelet nanocomposites. *J Mater Sci* **2011**, *46*, 5595-5614.

(90) Chang, Y.-H.; Lin, C.-T.; Chen, T.-Y.; Hsu, C.-L.; Lee, Y.-H.; Zhang, W.; Wei, K.-H.; Li, L.-J.: Highly Efficient Electrocatalytic Hydrogen Production by MoSx Grown on Graphene-Protected 3D Ni Foams. *Advanced Materials* **2013**, *25*, 756-760.

(91) Rao, C. N. R.; Sood, A. K.; Subrahmanyam, K. S.; Govindaraj, A.: Graphene: The New Two-Dimensional Nanomaterial. *Angewandte Chemie International Edition* **2009**, *48*, 7752-7777.

(92) Brownson, D. A. C.; Banks, C. E.: Fabricating graphene supercapacitors: highlighting the impact of surfactants and moieties. *Chemical Communications* **2012**, *48*, 1425-1427.

(93) Kim, J.-Y.; Lee, W. H.; Suk, J. W.; Potts, J. R.; Chou, H.; Kholmanov, I. N.; Piner, R. D.; Lee, J.; Akinwande, D.; Ruoff, R. S.: Chlorination

of Reduced Graphene Oxide Enhances the Dielectric Constant of Reduced Graphene Oxide/Polymer Composites. *Advanced Materials* **2013**, n/a-n/a.

(94) Xue, Y.; Liu, J.; Chen, H.; Wang, R.; Li, D.; Qu, J.; Dai, L.: Nitrogen-Doped Graphene Foams as Metal-Free Counter Electrodes in High-Performance Dye-Sensitized Solar Cells. *Angewandte Chemie International Edition* **2012**, *51*, 12124-12127.

(95) Geng, J.; Kong, B.-S.; Yang, S. B.; Jung, H.-T.: Preparation of graphene relying on porphyrin exfoliation of graphite. *Chemical Communications* **2010**, *46*, 5091-5093.

(96) Compton, O. C.; Jain, B.; Dikin, D. A.; Abouimrane, A.; Amine, K.; Nguyen, S. T.: Chemically Active Reduced Graphene Oxide with Tunable C/O Ratios. *ACS Nano* **2011**, *5*, 4380-4391.

(97) Wei, D.; Grande, L.; Chundi, V.; White, R.; Bower, C.; Andrew, P.; Ryhanen, T.: Graphene from electrochemical exfoliation and its direct applications in enhanced energy storage devices. *Chemical Communications* **2012**, *48*, 1239-1241.

(98) Zhou, M.; Tang, J.; Cheng, Q.; Xu, G.; Cui, P.; Qin, L.-C.: Few-layer graphene obtained by electrochemical exfoliation of graphite cathode. *Chemical Physics Letters* **2013**, *572*, 61-65.

(99) Lin, T.; Chen, J.; Bi, H.; Wan, D.; Huang, F.; Xie, X.; Jiang, M.: Facile and economical exfoliation of graphite for mass production of high-quality graphene sheets. *Journal of Materials Chemistry A* **2013**, *1*, 500-504.

(100) Erable, B.; Duteanu, N.; Kumar, S. M. S.; Feng, Y.; Ghangrekar, M. M.; Scott, K.: Nitric acid activation of graphite granules to increase the

performance of the non-catalyzed oxygen reduction reaction (ORR) for MFC applications. *Electrochemistry Communications* **2009**, *11*, 1547-1549.

(101) Mao, M.; Wang, M.; Hu, J.; Lei, G.; Chen, S.; Liu, H.: Simultaneous electrochemical synthesis of few-layer graphene flakes on both electrodes in protic ionic liquids. *Chemical Communications* **2013**, *49*, 5301-5303.

(102) Zeng , F.; Sun, Z.; Sang, X.; Diamond, D.; Lau, K. T.; Liu, X.; Su, D. S.: In Situ One-Step Electrochemical Preparation of Graphene Oxide Nanosheet-Modified Electrodes for Biosensors. *ChemSusChem* **2011**, *4*, 1587-1591.

(103) Malard, L. M.; Pimenta, M. A.; Dresselhaus, G.; Dresselhaus, M. S.: Raman spectroscopy in graphene. *Physics Reports* **2009**, *473*, 51-87.

(104) D. V. Thanh, H. C. C., L. J. Li, C. W. Chu, K. H Wei: *RSC Advances* **2013**.

(105) Thanh, D. V.; Chen, H.-C.; Li, L.-J.; Chu, C.-W.; Wei, K.-H.: Plasma electrolysis allows the facile and efficient production of graphite oxide from recycled graphite. *RSC Advances* **2013**, *3*, 17402-17410.

(106) Van Thanh, D.; Li, L.-J.; Chu, C.-W.; Yen, P.-J.; Wei, K.-H.: Plasma-assisted electrochemical exfoliation of graphite for rapid production of graphene sheets. *RSC Advances* **2014**, *4*, 6946-6949.

(107) Lu, J.; Yang, J.-x.; Wang, J.; Lim, A.; Wang, S.; Loh, K. P.: One-Pot Synthesis of Fluorescent Carbon Nanoribbons, Nanoparticles, and Graphene by the Exfoliation of Graphite in Ionic Liquids. *ACS Nano* **2009**, *3*, 2367-2375.

(108) Huang, X.; Zeng, Z.; Zhang, H.: Metal dichalcogenide nanosheets: preparation, properties and applications. *Chemical Society Reviews* **2013**, *42*, 1934-1946.

(109) Chen, T.-Y.; Chang, Y.-H.; Hsu, C.-L.; Wei, K.-H.; Chiang, C.-Y.; Li, L.-J.: Comparative study on MoS2 and WS2 for electrocatalytic water splitting. *International Journal of Hydrogen Energy* **2013**, *38*, 12302-12309.

(110) Chang, Y.-H.; Wu, F.-Y.; Chen, T.-Y.; Hsu, C.-L.; Chen, C.-H.; Wiryo, F.; Wei, K.-H.; Chiang, C.-Y.; Li, L.-J.: Three-Dimensional Molybdenum Sulfide Sponges for Electrocatalytic Water Splitting. *Small* **2013**, n/a-n/a.

(111) Stephenson, T.; Li, Z.; Olsen, B.; Mitlin, D.: Lithium ion battery applications of molybdenum disulfide (MoS2) nanocomposites. *Energy & Environmental Science* **2014**, *7*, 209-231.

(112) Lv, X.-J.; She, G.-W.; Zhou, S.-X.; Li, Y.-M.: Highly efficient electrocatalytic hydrogen production by nickel promoted molybdenum sulfide microspheres catalysts. *RSC Advances* **2013**, *3*, 21231-21236.

(113) Chou, S. S.; De, M.; Kim, J.; Byun, S.; Dykstra, C.; Yu, J.; Huang, J.; Dravid, V. P.: Ligand Conjugation of Chemically Exfoliated MoS2. *Journal of the American Chemical Society* **2013**, *135*, 4584-4587.

(114) Zheng, J.; Zhang, H.; Dong, S.; Liu, Y.; Tai Nai, C.; Suk Shin, H.; Young Jeong, H.; Liu, B.; Ping Loh, K.: High yield exfoliation of two-dimensional chalcogenides using sodium naphthalenide. *Nat Commun* **2014**, *5*.

(115) Lee, C.; Yan, H.; Brus, L. E.; Heinz, T. F.; Hone, J.; Ryu, S.: Anomalous Lattice Vibrations of Single- and Few-Layer MoS2. *ACS Nano* **2010**, *4*, 2695-2700.

(116) Zhang, Y.; Ye, J.; Matsuhashi, Y.; Iwasa, Y.: Ambipolar MoS2 Thin Flake Transistors. *Nano Letters* **2012**, *12*, 1136-1140.

(117) Li, H.; Zhang, Q.; Yap, C. C. R.; Tay, B. K.; Edwin, T. H. T.; Olivier, A.; Baillargeat, D.: From Bulk to Monolayer MoS2: Evolution of Raman Scattering. *Advanced Functional Materials* **2012**, *22*, 1385-1390.

(118) Park, S.-K.; Yu, S.-H.; Woo, S.; Ha, J.; Shin, J.; Sung, Y.-E.; Piao, Y.: A facile and green strategy for the synthesis of MoS2 nanospheres with excellent Li-ion storage properties. *CrystEngComm* **2012**, *14*, 8323-8325.

(119) Yao, Y.; Tolentino, L.; Yang, Z.; Song, X.; Zhang, W.; Chen, Y.; Wong, C.-p.: High-Concentration Aqueous Dispersions of MoS2. *Advanced Functional Materials* **2013**, *23*, 3577-3583.

(120) Zhou, K.-G.; Mao, N.-N.; Wang, H.-X.; Peng, Y.; Zhang, H.-L.: A Mixed-Solvent Strategy for Efficient Exfoliation of Inorganic Graphene Analogues. *Angewandte Chemie International Edition* **2011**, *50*, 10839-10842.

(121) Ibrahem, M. A.; Lan, T.-w.; Huang, J. K.; Chen, Y.-Y.; Wei, K.-H.; Li, L.-J.; Chu, C. W.: High quantity and quality few-layers transition metal disulfide nanosheets from wet-milling exfoliation. *RSC Advances* **2013**, *3*, 13193-13202.

(122) Liu, K.-K.; Zhang, W.; Lee, Y.-H.; Lin, Y.-C.; Chang, M.-T.; Su, C.-Y.; Chang, C.-S.; Li, H.; Shi, Y.; Zhang, H.; Lai, C.-S.; Li, L.-J.: Growth of Large-Area and Highly Crystalline MoS2 Thin Layers on Insulating Substrates. *Nano Letters* **2012**, *12*, 1538-1544.

(123) Wang, X.; Feng, H.; Wu, Y.; Jiao, L.: Controlled Synthesis of Highly Crystalline MoS2 Flakes by Chemical Vapor Deposition. *Journal of the American Chemical Society* **2013**, *135*, 5304-5307.

(124) Yu, Y.; Li, C.; Liu, Y.; Su, L.; Zhang, Y.; Cao, L.: Controlled Scalable Synthesis of Uniform, High-Quality Monolayer and Few-layer MoS2 Films. *Sci. Rep.* **2013**, *3*.

(125) Zhan, Y.; Liu, Z.; Najmaei, S.; Ajayan, P. M.; Lou, J.: Large-Area Vapor-Phase Growth and Characterization of MoS2 Atomic Layers on a SiO2 Substrate. *Small* **2012**, *8*, 966-971.

(126) Lee, K.; Gatensby, R.; McEvoy, N.; Hallam, T.; Duesberg, G. S.: High Performance Sensors Based on Molybdenum Disulfide Thin Films. *Advanced Materials* **2013**, n/a-n/a.

(127) Zeng, Z.; Yin, Z.; Huang, X.; Li, H.; He, Q.; Lu, G.; Boey, F.; Zhang, H.: Single-Layer Semiconducting Nanosheets: High-Yield Preparation and Device Fabrication. *Angewandte Chemie International Edition* **2011**, *50*, 11093-11097.

(128) Jiang, B.; Tian, C.; Wang, L.; Xu, Y.; Wang, R.; Qiao, Y.; Ma, Y.; Fu, H.: Facile fabrication of high quality graphene from expandable graphite: simultaneous exfoliation and reduction. *Chemical Communications* **2010**, *46*, 4920-4922.

(129) Tang, Y. B.; Lee, C. S.; Chen, Z. H.; Yuan, G. D.; Kang, Z. H.; Luo, L. B.; Song, H. S.; Liu, Y.; He, Z. B.; Zhang, W. J.; Bello, I.; Lee, S. T.: High-Quality Graphenes via a Facile Quenching Method for Field-Effect Transistors. *Nano Letters* **2009**, *9*, 1374-1377.

Publication List

1. ***D.V. Thanh***, H.-C. Chen, L.-J. Li, C.-W. Chu, K.-H. Wei, "Plasma electrolysis allows the facile and efficient production of graphite oxide from recycled graphite", *RSC Advances.*, 2013, *3*, 17402.

2. ***D.V. Thanh***, L.-J. Li, C.-W. Chu, Po-Jen Yen, K.-H. Wei, "Plasma-assisted electrochemical exfoliation of graphite for rapid production of graphene sheets", *RSC Advances*., 2014, 4, 6946.

3. ***D.V. Thanh***, Chien-Chung Pan, C.-W. Chu, K.-H. Wei, "Production of few-layer MoS_2 nanosheets through exfoliation of liquid N_2–quenched bulk MoS_2", *RSC Advances* **2014**, *4*, 15586-15589.

Patents

1. "Graphite oxide and/or graphene preparation method", **approved** for copyright in Taiwan, 13(專) A213, A213=102171TWI.

2. Graphene preparation method using Plasma electrolysis", submitted application for United States patent and trademark office, US 13/960,028, 13(專) A029, 102171USI.